AD-A074 799 ENVIRONMENTAL RESEARCH INST OF MICHIGAN ANN ARBOR IN--ETC F/G 17/5
STUDY AND INVESTIGATION OF INFRARED MULTISPECTRAL TARGET CUEING--ETC(U)
JUN 79 S R STEWART, J L BEARD DAAK70-77-C-0203
UNCLASSIFIED ERIM-131500-9-F NL

1 OF 2
AD
AD A074 799

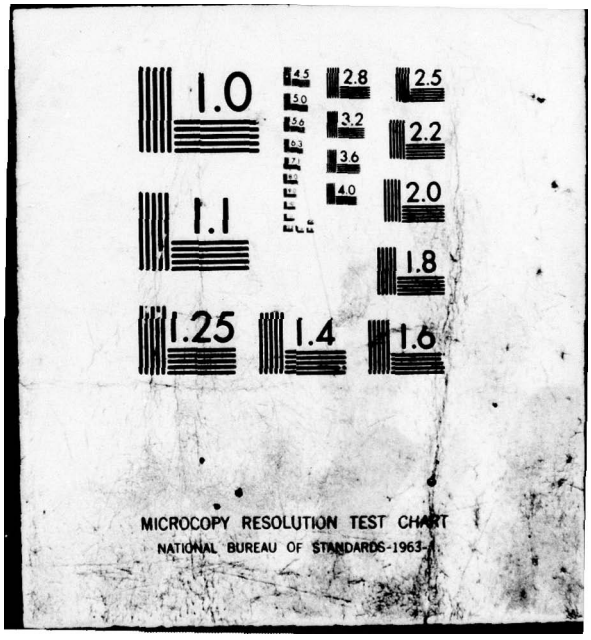
1.0
1.1
1.25
1.4
1.6
1.8
2.0
2.2
2.5
2.8
3.2
3.6
4.0
4.5
5.0
5.6
MICROCOPY RESOLUTION TEST CHART
NATIONAL BUREAU OF STANDARDS-1963-A

LEVEL II

131500-9-F

AD A074799

Final Report

STUDY AND INVESTIGATION OF INFRARED MULTISPECTRAL TARGET CUEING TECHNIQUES

STEPHEN R. STEWART and JERRY L. BEARD
Infrared and Optics Division

JUNE 1979

Night Vision Laboratory
Mobility Equipment Research
and Development Command
Ft. Belvoir, Va.

ORIGINAL CONTAINS COLOR PLATES: ALL DDC REPRODUCTIONS WILL BE IN BLACK AND WHITE.

ENVIRONMENTAL
RESEARCH INSTITUTE OF MICHIGAN
BOX 8618 • ANN ARBOR • MICHIGAN 48107

NOTICES

Sponsorship. The work reported herein was conducted by the Environmental Research Institute of Michigan for the Night Vision Laboratory, Mobility Equipment Research & Development Command, Ft Belvoir, Virginia, under contract DAAK70-77-C-0203. Mr. G. David Singer served as Technical Monitor for the Night Vision Laboratory.

UNCLASSIFIED

SECURITY CLASSIFICATION OF THIS PAGE (When Data Entered)

REPORT DOCUMENTATION PAGE

READ INSTRUCTIONS BEFORE COMPLETING FORM

1. REPORT NUMBER: ERIM-131500-9-F	2. GOVT ACCESSION NO
3. RECIPIENT'S CATALOG NUMBER	
4. TITLE (and Subtitle): Study and Investigation of Infrared Multispectral Target Cueing Techniques.	5. TYPE OF REPORT & PERIOD COVERED: Final rept. 22 Feb-Oct 78
6. PERFORMING ORG. REPORT NUMBER	
7. AUTHOR(s): Stephen R. Stewart and Jerry L. Beard	8. CONTRACT OR GRANT NUMBER(s): DAAK70-77-C-0203
9. PERFORMING ORGANIZATION NAME AND ADDRESS: Infrared and Optics Division, Environmental Research Institute of Michigan, P.O. Box 8618, Ann Arbor, Michigan	10. PROGRAM ELEMENT, PROJECT, TASK AREA & WORK UNIT NUMBERS
11. CONTROLLING OFFICE NAME AND ADDRESS: Night Vision Laboratory, Mobility Equipment Research & Development Command, Ft. Belvoir, Va.	12. REPORT DATE: June 1979
	13. NUMBER OF PAGES: 162
14. MONITORING AGENCY NAME AND ADDRESS (if different from Controlling Office) 161	15. SECURITY CLASS (of this report): Unclassified
	15a. DECLASSIFICATION/DOWNGRADING SCHEDULE

16. DISTRIBUTION STATEMENT (of this Report)

This document has been approved for public release and sale; its distribution is unlimited.

17. DISTRIBUTION STATEMENT (of the abstract entered in Block 20, if different from Report)

18. SUPPLEMENTARY NOTES

19. KEY WORDS (Continue on reverse side if necessary and identify by block number)

Multispectral scanning
Spatial target cueing
IR data collection
Temperature calibration
Multispectral pattern recognition

20. ABSTRACT (Continue on reverse side if necessary and identify by block number)

This report presents the results of a study to analyze and evaluate multispectral infrared target cueing algorithms using an infrared data base (in the 1 - 14 μm region) of tactical targets against real backgrounds. Using ERIM's modified M7 line scanner, simultaneous multispectral imagery of five bands in the 1 - 14 μm region were collected over several classes of tactical targets at the Camp A.P. Hill, VA, test site for later analysis.

DD FORM 1 JAN 73 1473 EDITION OF 1 NOV 65 IS OBSOLETE

UNCLASSIFIED

SECURITY CLASSIFICATION OF THIS PAGE (When Data Entered)

408 259

20. ABSTRACT (Cont'd)

A description of the collected infrared data base is given including discussions of ~~(1)~~ the motivating factors in determining the spectral regions employed and ~~(2)~~ target and background optical properties. Also, M7 system performance characteristics are examined. Finally, a preliminary evaluation of two different approaches to multispectral target cueing using the collected data base was accomplished. The results of both approaches, the first involving classical maximum likelihood classification using in-scene training and the second involving unsupervised spectral/spatial clustering followed by discrimination based upon size are reported.

CONTENTS

CONTENTS (Continued)

LIST OF FIGURES

LIST OF FIGURES (Continued)

LIST OF TABLES

LIST OF TABLES (Continued

PREFACE

This final report summarizes a fourteen month program of infrared data collection and infrared multispectral target cueing analysis. The research was carried out for the Night Vision Laboratory (NVL) of the Army's Mobility Equipment Research and Development Command (MERDC) at Ft. Belvoir. The basic objectives of this effort were to generate a multispectral infrared data base of tactical targets against real backgrounds in the 1-14 μm region and to use these data to develop, analyze, and evaluate multispectral target cueing algorithms. The motivation behind the effort lay in the potential aid to new generation imagers that infrared multispectral pattern recognition technology may add to already developed spatial and 3-D cueing techniques. The scope of the program included: hardware modification of an optical/mechanical line scanner to provide high spatial resolution imagery; test plan development and scanner performance characterization, airborne infrared multispectral data acquisition at Fort A.P. Hill; digital reformatting of the raw data to computer compatible tapes; and initiation of limited analysis of the data to investigate the utility of multispectral classification cueing techniques.

The research described in this report was performed under Contract DAAK70-77-C-0203 and covers the period 22 September 1978 through 6 December 1978. Mr. G. David Singer served as Technical Monitor for NVL. The program was directed by Richard R. Legault, Vice President of the Environmental Research Institute of Michigan (ERIM) and Max Bair, Head of the Infrared and Optics Division Program Office. The principal investigator for this program was Stephen R. Stewart. The ERIM number for this report is 131500-9-F.

The authors wish to acknowledge the technical contributions provided by J. Ladd, W. Juodawlkis, and H. Doss in the data collection effort and K. Nalepka and R. Horvath for their valuable comments and suggestions during the writing of this report. The authors also thank C. Conley and F. Elliott for their help in preparation of reports.

1.0
INTRODUCTION

Studies conducted over several years by the Environmental Research Institute of Michigan (ERIM) and others have contributed to the development of advanced spatial and 3-dimensional target cueing techniques. These improved image processing methods have reached the stage where inclusion of automatic cueing technology in new generation imagers now appears feasible. The Army's Night Vision Laboratory (NVL) at Ft. Belvoir has been assessing the state-of-the-art of these current techniques through several image processing study contracts. These studies have indicated that, although thermal (8-14 μm) spatial cueing algorithms and multispectral (MS) pattern recognition techniques in the visible and near-infrared region (.4 to 2.6 μm) have been developed which independently provide successful target cueing, none have considered the utility of the entire infrared spectrum from 1 to 14 μm simultaneously. Not only was there a void in the target cueing technology development in this respect, a suitable data base sufficient for a thorough study did not exist.

Because of the potential of multispectral pattern recognition as applied to the entire 1 to 14 μm spectral region to supplement other cueing techniques already under investigation, NVL and ERIM undertook a two-phase program which:

- Provided, in the 1 to 14 μm region, an airborne MS data base of tactical targets against real backgrounds from which MS cueing techniques could be evaluated; and
- Performed a cursory analysis of the above data to determine the potential utility of classical MS techniques for thermal target cueing.

This final report presents the results of that effort.

Phase I consisted of test plan development, scanner hardware modifications, data collection, and data reformatting and comprised most of the total program effort. Since this infrared data base was intended to be

used in the evaluation of various MS cueing techniques, an emphasis was placed on the acquisition of a complete and representative data matrix (in terms of time of data collection, classes of tactical targets, and backgrounds/clutter variability) as well as a comprehensive characterization of the scanner used to collect the data. Section 2 of this report presents a brief description of the infrared data base collected, including an outline of the mission plan and data collection scenario as well as documentation of the data matrix. More detailed information concerning the data collection effort has been reported under separate cover [1]. The performance of ERIM's M-7 multispectral scanner is documented in Section 3. Only those performance figures which are unique to this mission and pertinent to the analysis of the imagery are reported. A general description of the scanner's operation is given in Appendix A. Additional performance tests and a discussion of techniques for radiometric calibration of the data are described in Appendices B and C respectively.

Phase II of the program consisted of analysis of the MS data. The emphasis placed on collection of the data base itself severely limited processing and subsequent evaluation of classical multispectral "training set" classification techniques. The results of the analyses accomplished are presented in Section 4. There are, however, several other techniques (such as multispectral clustering, pulse height and pulse width analysis, and MS classification combined with spatial filtering) which offer potential utility in target cueing and which should be evaluated against these data. Recommendation for additional target cueing technique evaluation as well as a summary of the conclusions drawn from the limited MS analysis is reported in Section 5.

---

[1] Stewart, Steve, MS Cueing Techniques Program, Mission Report for Night Vision Laboratory Program, Camp A.P. Hill Virginia Test Site, March 28, 29, 30, 1978, Environmental Research Institute of Michigan, Ann Arbor, Mi., Report No. 131500-8-P, May 1978.

2.0

DESCRIPTION OF INFRARED MS DATA BASE

2.1 INTRODUCTION

Multispectral data obtained to date have been used primarily to evaluate multispectral pattern recognition technology applied to agricultural, mineral exploration, water quality and land use problems. For such applications, night-time operation is typically not required, and targets of interest to tactical military scenarios are not involved. Therefore, virtually all multispectral data collection efforts thus far have been directed at the evaluation of multispectral pattern recognition techniques in non-military applications using the reflective (0.3 to 3 μm) portion of the spectrum. Hence, there has been a basic deficiency of multispectral imagery involving military targets in tactical military environments.

The deficiency goes farther than just the lack of targets and backgrounds, however. For military applications, there are potential target cues which occur in the mid and far infrared region (3 to 14 μm) which have not been exploited with today's available multispectral imagers. At wavelengths beyond 3 μm, the primary source of infrared energy is the thermal self-radiation produced by the target and it is the fact that this IR radiant energy source is internalized to the target that opens a new dimension of possibilities for multispectral pattern recognition techniques.

For example, the identification, composition, and material properties of both man-made and natural scene objects can often be inferred by applying qualitative knowledge of how different objects respond thermally to various environmental driving forces. Since the radiometric temperature of an object depends upon its surface optical characteristics and temperature and since different materials possess different optical characteristics and thermal properties, material type and structural differences are often indicated by different temperature responses under equivalent environmental driving forces. In addition these material properties (e.g. emissivity)

are a function of wavelength and thus objects of the same surface temperature but with a spectrally different material properties can exhibit completely different IR radiometric temperatures when observed in different spectral regions. It is this variation in radiometric response as a function of material type, spectral IR properties, and a given environmental condition that can be exploited by multispectral pattern recognition techniques in the infrared region.

There are other IR cues which have yet to be fully exploited in the military application. Consider the fact that the temperature of an object responding only to normal environmental driving forces will be different from that of a like object within which heat is being generated, or upon which anomalous heat is externally applied. Thus, a motor casing is hotter when the motor runs (internal heat generation), and an exhaust deflector is hotter when exhaust is present (external heat application). It is a fact that some targets are recognizable by virtue only of their "hot spot" distribution while others have "warmer areas" on the target surface rather than hot spots because of conductive or convective heat redistribution. Infrared image exploitation of this nature utilizes the qualitative spatial characteristics of objects within a scene. Only the existence of contrasts and not their temperature inferences is directly relevant to this spatial exploitation. Hence, night-time IR imagery, with no requirement for natural illumination and with familiar spatial representation of targets can substitute for visible imagery under low light level conditions.

Also, infrared shadows, while not enjoying a direct spatial relationship with a target, can still provide useful cueing information. The magnitude of the IR shadow contrast is a function of how long the target or background object producing the shadow is stationary. This is one case wherein both the thermal IR and reflective signals are positively correlated. When used in conjunction with spatial processing the length and width of the shadow may provide information about target height or provide other inferences about the object producing the shadow.

Investigation of the utility of the IR target cues suggested in the previous paragraphs in discriminating military vehicular targets from background in a tactical military environment requires a data base of multispectral imagery of the appropriate targets and background which can be used to evaluate not only the significance of the spectral signatures but also the variation in scene spatial distribution encountered under a variety of environmental conditions, vehicle types and operating modes, and background types. The generation of a suitable data matrix which takes into consideration all these factors was considered a major responsibility of the data collection effort. The salient features of the data matrix are discussed in the following sections.

2.2 SPECTRAL CONSIDERATIONS

Paramount to the successful application of any multispectral cueing technique (visible or IR) is the choice of wavelengths to use and the associated spectral differences in target/background optical and thermal characteristics encountered in the chosen wavelength regions. Obviously, if wavelength regions are chosen where little difference in target and background optical cueing properties exist, then any multispectral cueing technique based on spectral signatures alone, is doomed to failure. In like manner, if the regions are chosen without regard for 1) the effect of spectral absorption and scattering within the intervening atmosphere and 2) the detector spectral operating characteristics then differences in target/background optical properties may be masked by noise. Hence, the spectral band requirements for the multispectral data base were based upon the following criteria:

(1) Atmospheric Transmission
(2) Target/Background Optical Properties
(3) Detector Noise Considerations

As shown in Figure 1, there are several broadband regions in the 1 to 14 μm region that can be considered from an atmospheric transmission standpoint. These are:

ATMOSPHERIC TRANSMISSION

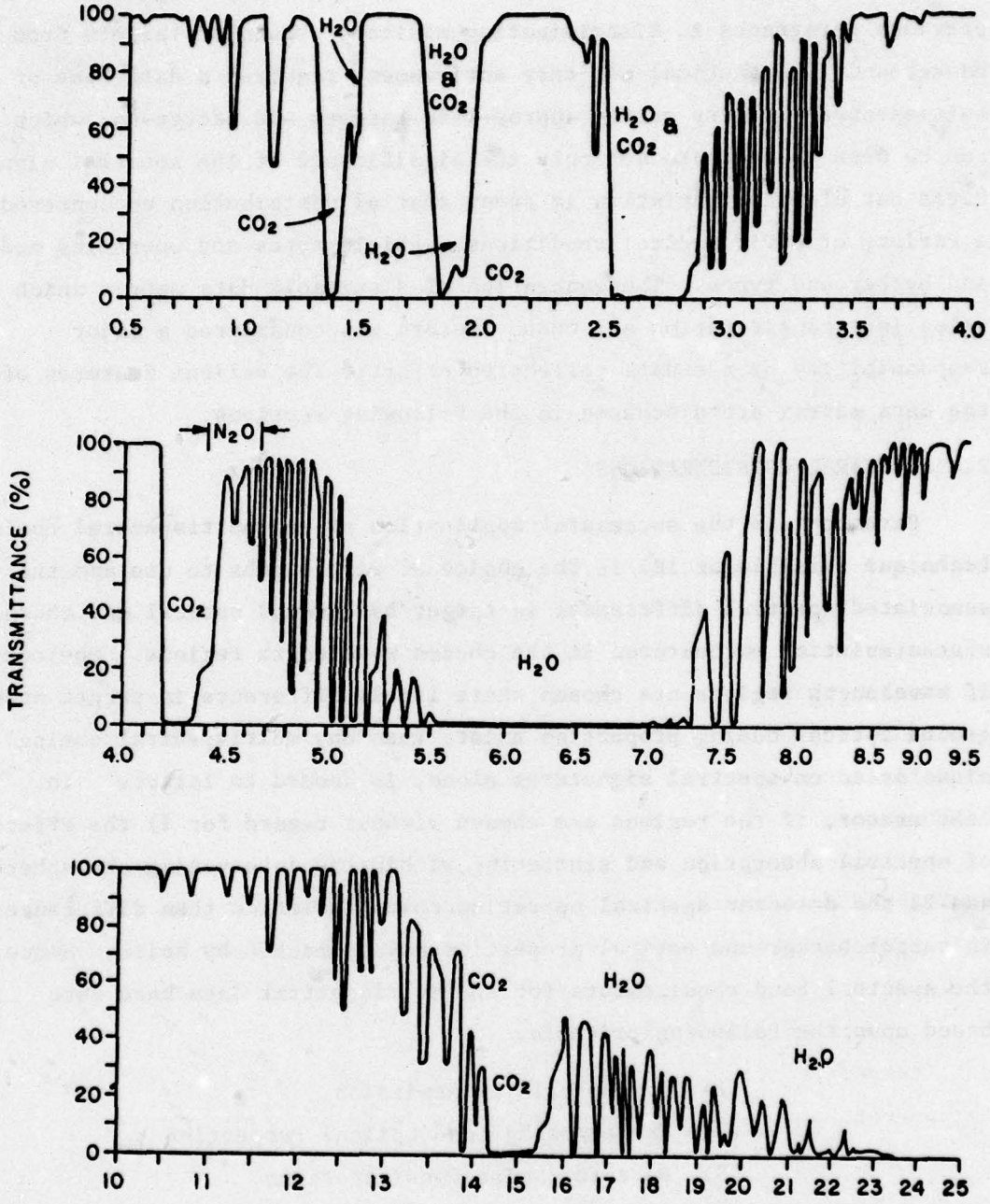

FIGURE 1

Transmission of 1000 foot horizontal air path at sea level, 5.7 mm precipitable water, 79°F temperature.
(Reprinted with permission of Santa Barbara Research Center)

(a) 1 to 1.1 μm
(b) 1.1 to 1.4 μm
(c) 1.5 to 1.8 μm
(d) 2 to 2.6 μm
(e) 3 to 4.2 μm
(f) 4.5 to 5.5 μm
and (g) 8 to 14 μm spectral bands.

Any application (military or other) of multispectral processing techniques to infrared imagery of the earth viewed through the atmosphere in the 1 to 14 μm spectral region is limited to these broad spectral bands; outside of these bands, the atmosphere becomes the prime source of the IR radiant energy observed in the imagery.

Of these seven (7) broadbands, the first four are considered reflective bands and the last two emissive bands. Figure 2 shows the spectral dependence of the reflected solar and self-emitted radiant energy for an object with a spectrally constant reflectance of 20%, an emissivity of 80% and no atmospheric effects. As can be seen, the spectral region where these two radiant energy components are equal is in the 3 to 4 μm region. Hence, band five as defined by the atmospheric limits above can be classified neither totally reflective nor totally emissive as though in the absence of any solar energy. The target radiance observed in this band (though admittedly low in magnitude) is primarily self-emission. Figure 3 shows this effect more clearly. Spectral apparent temperature measurements in the 3.3 to 14 μm region were obtained from bare soil on a clear (.1 cloud cover) and and overcast day [Ref. 2]. The increase in apparent soil temperature in the 3 to 4 μm region on the clear day (top graph) is due entirely to reflected solar energy. No increase is observed in this

---

[2] Spectral and Polarization Characteristics of Selected Targets and Backgrounds: Instrumentation and Measured Results (3.3 - 14.0 μm), D. Faulkner, R. Horvath, J.P. Ulrich, E. Work, Willow Run Laboratories, The University of Michigan, Technical Report No. AFAL-TR-71-199, August 1971.

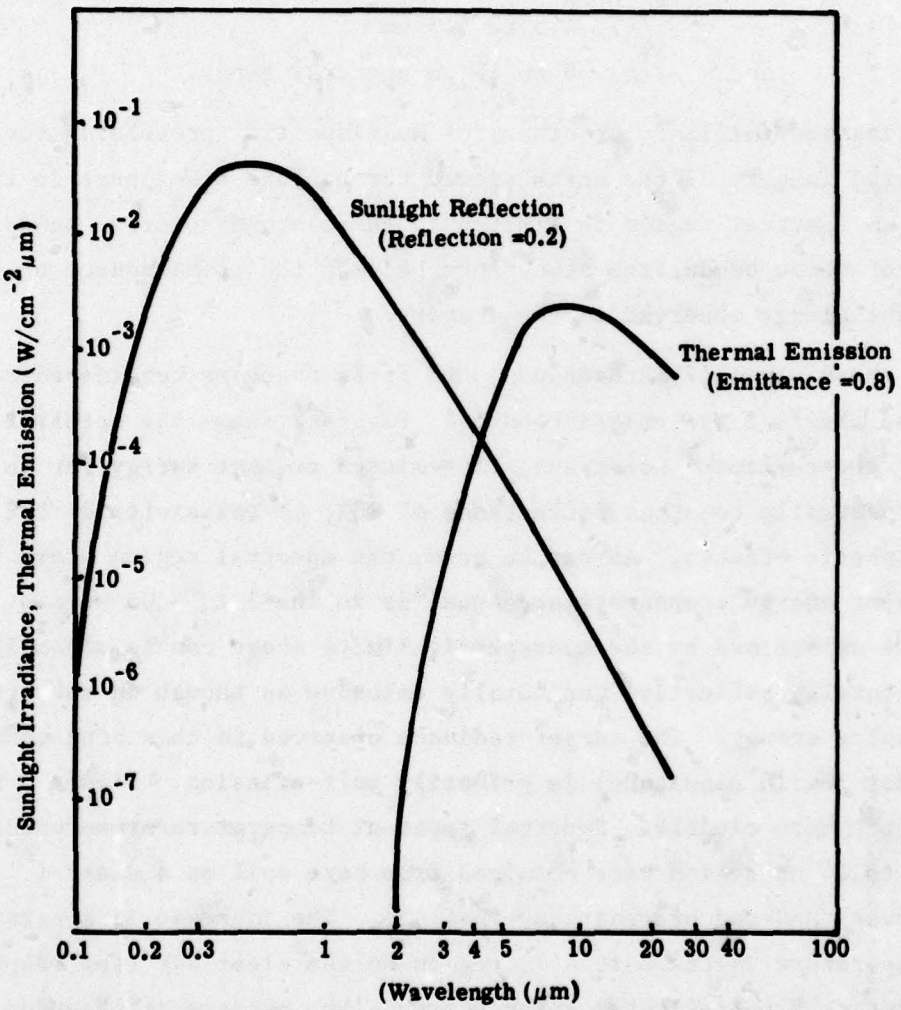

FIGURE 2. SOLAR (6000°K) REFLECTED AND THERMALLY EMITTED RADIANCE (ρ=0.8, ϵ=0.2) NEGLECTING ATMOSPHERIC EFFECTS

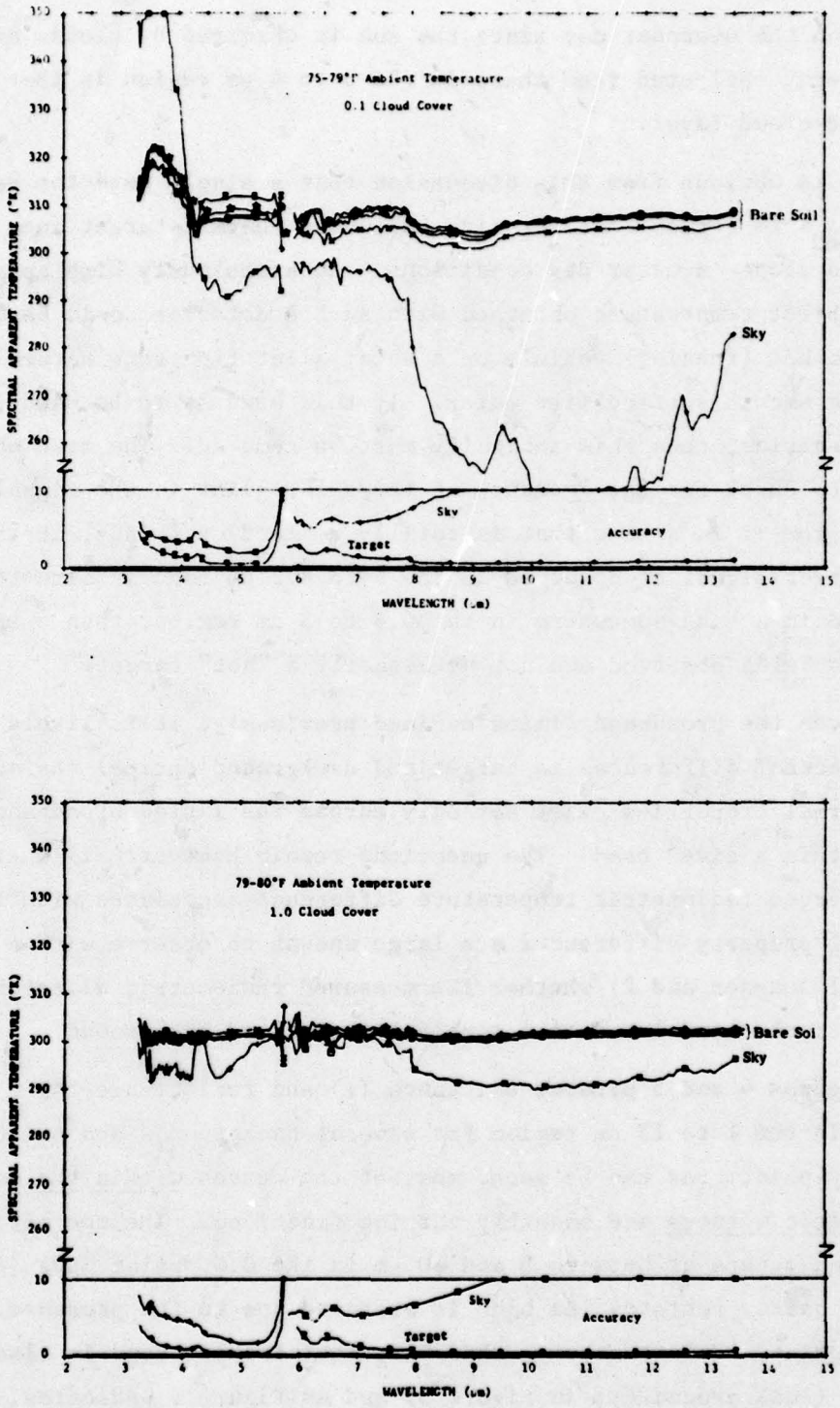

FIGURE 3. BARE SOIL AND SKY SPECTRAL APPARENT TEMPERATURE

region on the overcast day since the sun is obscured by clouds and the only energy reflected from these in the 3 to 4 μm region is that coming from the cloud layer.

It is obvious from this discussion that a single detector band covering the 3 to 4 μm region could provide ambiguous thermal target cues when operated alone in clear day conditions. An anamolously high apparent scene object temperature obtained with such a detector could be due to either a hot (running) vehicle or a solar glint from some naturally occuring smooth surface like water. If this band is to be used in daytime scenarios, then this ambiguity must be removed. The most obvious way is to check for the presence of the solar glint in the signal by looking for it in a band that is totally reflective. Thus, if the same high target signal as observed in the 3 to 4.2 μm band is simultaneously observed in a band somewhere in the 0.4 to 3 μm region, then a solar glint is being observed and not necessarily a "hot" target.

Given the broadband limits defined previously, it is likely that some spectral differences in target and background optical characteristics and thermal properties exist not only across the listed broadbands but also within a given band. The questions remain however: 1) whether the observed radiometric temperature difference associated with the material property differences are large enough to observe with a multispectral scanner and 2) whether the measured radiometric difference can be positively correlated to a specific target and background.

Figures 4 and 5 present emittance (ε) and reflectance ($\approx 1 - \varepsilon$) curves in the 1 to 15 μm region for several backgrounds and one O.D. military paint. As can be seen, most of the curves within the defined atmospheric windows are smoothly varying functions. The one obvious exception occurs at between 9 and 10 μm in the O.D. paint data (Figure 4) where a narrow reststrahlen band is observed due to the presence of SiO_2 in the paint. Unfortunately, this SiO_2 reststrahlen band is also present in soil (look around 9 μm in Figure 3) and as Figure 3 indicates, the magnitude is dependent upon the degree of cloud cover. Because of this

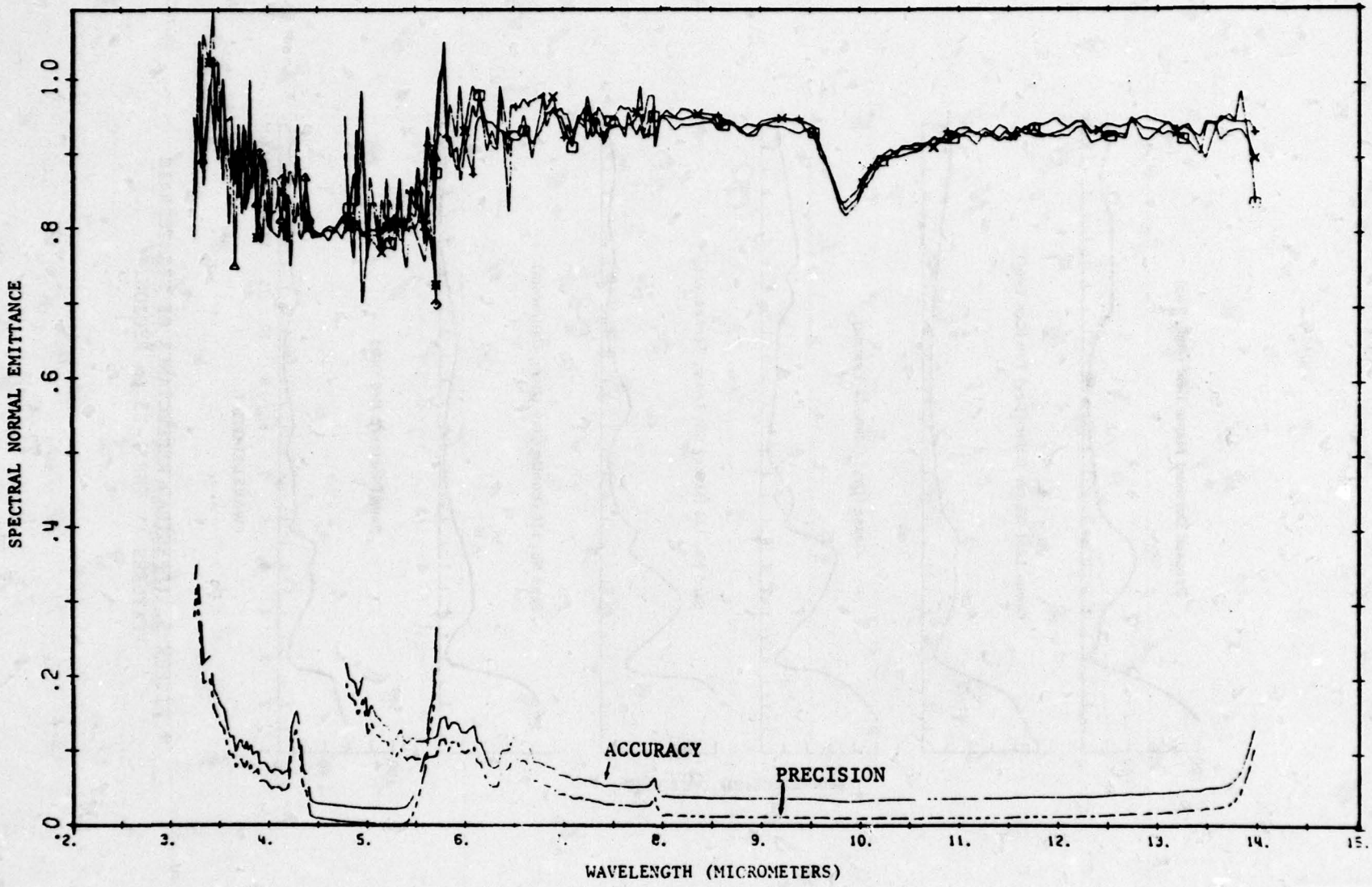

FIGURE 4. SPECTRAL NORMAL EMITTANCE OF O.D. (x34087) LUSTERLESS ACRYLIC
(ALUMINUM SUBSTRATE, MIL-C-5541 SURFACE PREPARATION, MIL-C-8514 WASH PRIMER, MIL-P-23377A PRIMER)

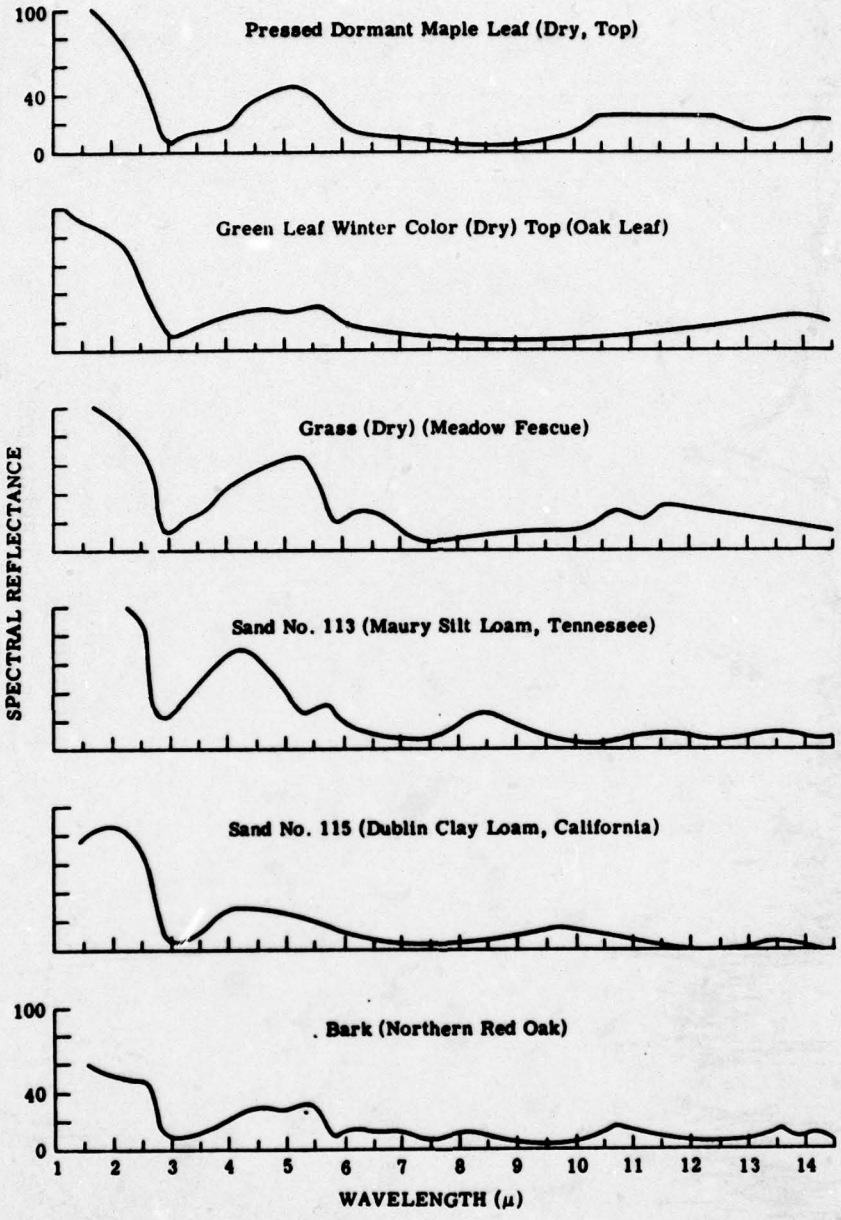

FIGURE 5. SPECTRAL REFLECTANCE OF SIX TERRAIN FEATURES IN THE 1-15 μm REGION.

environmental dependence and because many military paints do not contain SiO_2, there is no unambiguous technique employing a SiO_2 reststrahlen band detector to determine the presence of painted metal. Other than the reststrahlen band phenomena, military paints in general do not show rapidly varying spectral reflectance and/or spectral emittance characteristics in the 1 to 14 μm spectral region [3]. Because of the above factors and adding the additional fact that, except for the 8 to 14 μm spectral band, consideration of more than two independent sub-bands within each of the atmospheric window regions is precluded by detector signal-to-noise considerations, multiple sub-bands within any of the broad atmospheric windows were not considered for the proposed effort.

Shown in Table 1 are the spectral bands chosen for this MS data base along with a summary of each band's utility. The first band in Table 1 corresponds to the 1 to 1.1 μm band described earlier. Detector signal to noise considerations dictated a 0.8 μm cut-on instead of 1 μm. The 1.1 to 1.4 μm and 1.5 to 1.8 μm bands were not included because of detector hardware limitations in the collecting sensor. However, significant amounts of background data have been collected in these bands in recent years on non-military programs although no known vehicular data exists.

2.3 TARGET AND BACKGROUND CONSIDERATION

The choice of spectral bands for the multispectral data collection and cueing evaluation effort was made somewhat objectively. However, consideration of targets and backgrounds was much more subjective in that many different tactical environments can be presented to a sensor, depending upon battlefield scenario and season. Obviously, not all target vehicle and background combinations need be considered since some combinations occur too infrequently to warrant significant effort or the combination lends itself to conventional, visible cueing techniques (e.g. O.D. painted

---

[3] Handbook of Military Infrared Technology, William L. Wolfe, Editor, The University of Michigan, 1965, Sponsored by Office of Naval Research, Department of the Navy, Washington, D.C.

TABLE 1. NOMINAL MS DATA BASE SPECTRAL BANDS

Channel	Nominal Band Limits	Reason
1	0.8 to 1.1	Solar glint discriminator plus reflective multispectral
2	2 to 2.6*	Solar glint discriminator plus reflective multispectral
3	3 to 4.0*	Reflective multispectral, emissive multispectral, and thermal temperature
4	4.5 to 5.5*	Thermal temperature plus emissive multispectral
5	8 to 14	Thermal temperature plus emissive multispectral

*3-element detector

tank in the desert). Even without these, however, the number of combinations remaining is still much too large to attempt a data collection effort involving all possibilities. Hence, for this particular program a decision was made in the interest of time and money, to limit the target/background combinations to one which was of the most interest of the sponsor -- namely, an Eastern European-like scenario.

The site selected by the sponsor for this experiment was the test facility located at Camp A.P. Hill, Virginia. The backgrounds available at the time of data collection flights were primarily baresoil in open fields, tree stands of leafless deciduous and coniferous trees (types unknown) and forest carpet of leaves, broken limbs, and soil. Although this site's latitude is approximately 15° south of the latitude of Germany, variety of backgrounds encountered here were thought to be reasonably representative of what might be found in some spring-time European scenarios.

This was based in part on the presumption that pine tree canopies, leafless tree trunks, and spring-time forest carpets presumably don't exhibit significantly different thermal spectrums over the many varieties in existence at these latitudes. While it is quite likely that more northernly latitudes do have different soil mixtures and types of hardwood and coniferous tree stands than present at this site, it is equally likely that variations exist at a given latitude as a function of longitude so that one may question how good a European simulation any U.S. site is. Since this particular site had the "kinds" of spring-time backgrounds expected in Europe and since the facilities existed to supply the tactical targets and other logistical ground support, the site was used. (Figure 6 shows an airborne photograph of the target site.)

Eleven targets were made available for the data collection exercise. These included the following:

(1) M-60 Tank (3, 2 running [1 diesel, 1 gas] and 1 static)

(2) M-113 APC (2 diesel, 2 gas, all running)

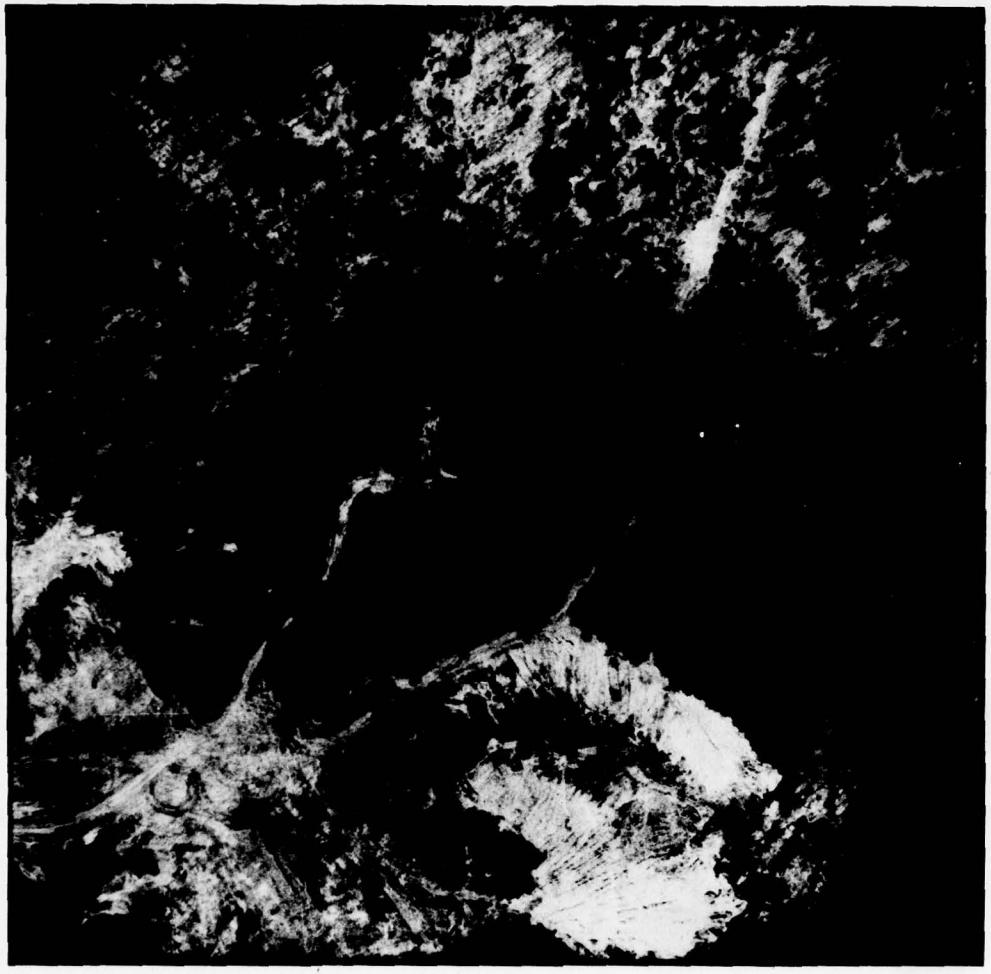

FIGURE 6. AERIAL PHOTOGRAPH OF TARGET SITE(TARGETS IN POSITION)
3/30/78,PASS#5. 1830

(3) 3/4, 2 1/2 and 5 Ton Trucks (all running)

(4) Jeep (running)

The targets were started up about one-half hour before the overflight and kept running throughout the period of data collection. The targets were positioned in one of the twelve target locations shown in Figure 7 and, after each data collection pass, were moved to the next available target position. This permitted each class of vehicle to be placed in a background of varying clutter and/or cover while maintaining a vehicle operating temperature consistent with those that might be encountered in an operational tactical scenario. A summary of the backgrounds at each target location is shown in Table 2. The data matrix of target positions for each flight is shown in Tables 3 through 6.

The data collection mission took place over the period from 28 March through 1 April 1978. ERIM's M-7 scanner and associated boresighted camera were the principal sensors flown in our C-47 aircraft. The instrumentation configuration is depicted in Figure 3. Four flights were planned so that data could be collected under conditions producing maximum and minimum scene contrasts: 0930, 1330, 1830, and 2330 hours. The general profile for each of the four missions consisted of a total of ten (1) passes ranging in altitude from 6400 ft. to 800 ft. This provided ground resolutions for the normal nadir viewing which range from 1.6 ft. square to 12.8 ft. square. The only exception to this occurred during the 0930 flight when four additional passes at low altitude were completed which utilized slightly different spectral bands and a forward tilt of the scanner of 55° (35° depression angle). These passes were flown to provide data which could be used for additional spectral analysis and which would represent a scene aspect more typical of those viewed by forward looking air-to-ground sensors. Table 7 and 8 show the altitude, time of day and spectral bands for each of the passes flown during the four flights.

The data base just described, consisting of data from all forty-four (44) data collection passes over the A.P. Hill site, is now resident on a set of 14 computer compatible tapes (CCTs). Each file of these tapes contains five channels of spectral data as described in Table 9.

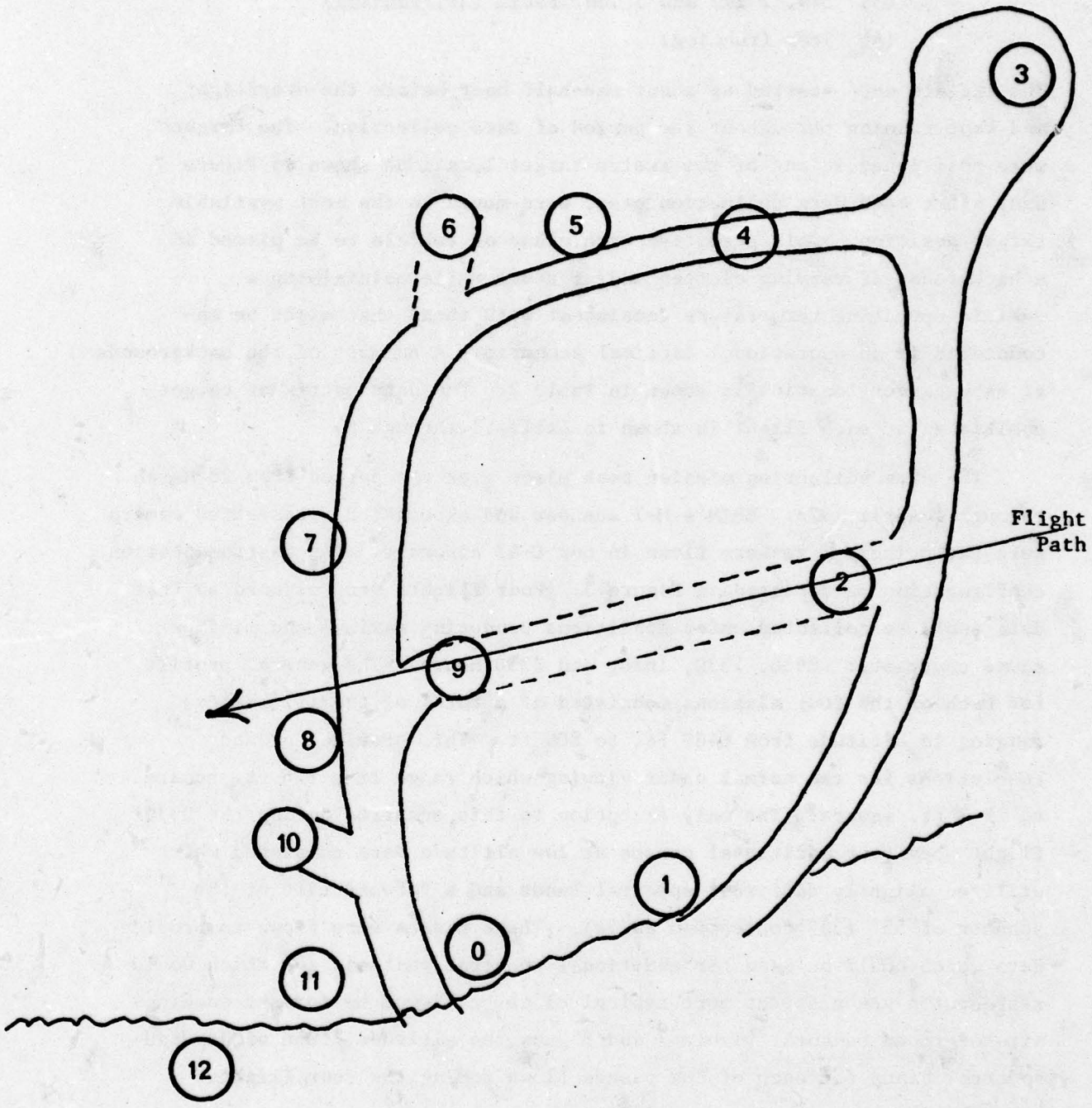

FIGURE 7. DRAWING OF VEHICLE POSITIONS AT CAMP A.P. HILL TEST SITE

TABLE 2. DESCRIPTION OF BACKGROUND AT TARGET LOCATIONS

Target Position	Background Description
0	Open soil mixed with sparsely populated pine trees. Completely open on one side. Approximately 15% obscuration.
1	Open soil cut out of dense stand of pine trees. Open soil on one side -- no overhead obscurations.
2	Forest carpet surrounded closely on three sides by dense pine tree stand -- 50% overhead obscuration.
3	Forest carpet loosely bounded by dense pine tree stand on one side and mixture of pine trees and leafless deciduous trees on other -- no overhead obscurations.
4	Narrow dird road boardered closely on both sides by dense pine trees -- 5% obscuration.
5	Forest carpet loosely surrounded by leafless, deciduous trees and pine trees -- no overhead obscurations.
6	Forest carpet within tree stand of pines and leafless deciduous - 15% overhead obscuration.
7	Forest carpet in small pine tree stand -- not very dense -- 25% obscuration.
8	Forest carpet in sparsely populated, leafless deciduous tree stand -- 10% overhead obscuration.
9	Open forest carpet cut out of dense pine tree stand -- no obscuration
10	Forest carpet loosely located between small pine tree stand on one side and sparsely populated leafless deciduous trees on other -- no obscuration.

TABLE 2. DESCRIPTION OF BACKGROUND AT TARGET LOCATIONS (Continued)

Target Position	Background Description
11	Open soil bounded lossely on one side by small stand of pine trees -- no obscuration.
12	Open soil bounded closely on one side by small stand of pine trees -- 5% obscuration.

TABLE 3. MATRIX OF VEHICLE POSITIONS DURING 3/28/78, 2330 HOURS
DC-3 DATA PASSES OVER SITE

Vehicle Position No.	Pass #1	#2	#3	#4	#5	#6	#7	#8	#9	#10
0	-	-	APC	Tank	APC	2 1/2	Tank	3/4	5T	APC
1	-	APC	Tank	APC	2 1/2	Tank	3/4	5T	APC	APC
2	APC	Tank	APC	2 1/2	Tank	3/4	5T	APC	APC	Jeep
3	Tank	APC	2 1/2	Tank	3/4	5T	APC	APC	Jeep	-
4	APC	2 1/2	Tank	3/4	5T	APC	APC	Jeep	-	-
5	2 1/2	Tank	3/4	5T	APC	APC	Jeep	-	-	APC
6	Tank	3/4	5T	APC	APC	Jeep	-	-	APC	Tank
7	3/4	5T	APC	APC	Jeep	-	-	APC	Tank	APC
8	5T	APC	APC	Jeep	-	-	APC	Tank	APC	2 1/2
9	APC	APC	Jeep	-	-	APC	Tank	APC	2 1/2	Tank
10	APC	Jeep	-	-	APC	Tank	APC	2 1/2	Tank	3/4
11	Jeep	-	-	APC	Tank	APC	2 1/2	Tank	3/4	5T
12	← Cold Tank →									

TABLE 4. MATRIX OF VEHICLE POSITIONS DURING 3/29/78, 1830 HOURS FLIGHT
DC-3 DATA PASSES OVER SITE

Vehicle Position No.	Pass # 1	Pass # 2	#3	#4	#5	#6	#7	#8	#9	#10
0	APC	-	-	5T	APC	Jeep	Tank	APC	2 1/2	3/4
1	-	-	5T	APC	Jeep	Tank	APC	2 1/2	3/4	APC
2	-	5T	APC	Jeep	Tank	APC	2 1/2	3/4	APC	APC
3	Tank	Tank	Tank	Tank Jeep	Tank Jeep	Tank Jeep	Tank Jeep	Tank Jeep	Tank Jeep	Tank Jeep
4	5T	APC	Jeep	Tank	APC	2 1/2	3/4	APC	APC	-
5	APC	Jeep	Tank	APC	2 1/2	3/4	APC	APC	-	-
6	Jeep	Tank	APC	2 1/2	3/4	APC	APC	-	-	5T
7	Tank	APC	2 1/2	3/4	APC	APC	-	-	5T	APC
8	2 1/2	3/4	APC	APC	-	-	5T	APC	Jeep	Tank
9	APC	2 1/2	3/4	APC	APC	-	-	5T	APC	Jeep
10	3/4	APC	APC	-	-	5T	APC	Jeep	Tank	APC
11	APC	APC	-	-	5T	APC	Jeep	Tank	APC	2 1/2
12	Cold Tank									

Note: On this flight (1) The tank in Position #3 lost a tread. It remained in this position with engine running for the entire test. By the 4th run a jeep had been taken to the position to aid in the repair where it remained for the rest of the test. (2) Most of the signs marking the sites had been knocked down. Since Site #9 is farther down the road then #8, the rotational sequence was reversed by the first drivers and those following kept this new sequence.

TABLE 5. MATRIX OF VEHICLE POSITIONS DURING 3/30/78, 0930 HOURS FLIGHT
DC-3 DATA PASSES OVER SITE

Vehicle Position No.	Pass #1	Pass #2	#3	#4	#5	#6	#7	#8	#9	#10
0	-	-	APC	Tank	APC	2 1/2	Tank	3/4	5T	APC
1	-	APC	Tank	APC	2 1/2	Tank	3/4	5T	APC	APC
2	APC	Tank	APC	2 1/2	Tank	3/4	5T	APC	APC	Jeep
3	Tank	APC	2 1/2	Tank	3/4	5T	APC	APC	Jeep	-
4	APC	2 1/2	Tank	3/4	5T	APC	APC	Jeep	-	-
5	2 1/2	Tank	3/4	5T	APC	APC	Jeep	-	-	APC
6	Tank	3/4	5T	APC	APC	Jeep	-	-	APC	Tank
7	3/4	5T	APC	APC	Jeep	-	-	APC	Tank	APC
8	5T	APC	APC	Jeep	-	-	APC	Tank	APC	2 1/2
9	APC	APC	Jeep	-	-	APC	Tank	APC	2 1/2	Tank
10	APC	Jeep	-	-	APC	Tank	APC	2 1/2	Tank	3/4
11	Jeep	-	-	APC	Tank	APC	2 1/2	Tank	3/4	5T
12	← Cold Tank →									

TABLE 6. MATRIX OF VEHICLE POSITIONS DURING 3/30/78, 1330 HOURS

DC-3 DATA PASSES OVER SITE

Vehicle Position No.	Pass #1	#2	#3	#4	#5	#6	#7	#8	#9	#10
0	APC	APC	-	-	-	APC	Tank	APC	2 1/2	Tank
1	APC	-	-	-	APC	Tank	APC	2 1/2	Tank	3/4
2	Jeep	Jeep	Jeep	APC Jeep	Tank Jeep	APC Jeep	2 1/2 Jeep	Tank Jeep	3/4 Jeep	5T Jeep
3	-	-	APC	Tank	APC	2 1/2	Tank	3/4	5T	APC
4	-	APC	Tank	APC	2 1/2	Tank	3/4	5T	APC	APC
5	APC	Tank	APC	2 1/2	Tank	3/4	5T	APC	APC	-
6	Tank	APC	2 1/2	Tank	3/4	5T	APC	APC	-	-
7	APC	2 1/2	Tank	3/4	5T	APC	APC	-	-	-
8	2 1/2	Tank	3/4	5T	APC	APC	-	-	-	APC
9	Tank	3/4	5T	APC	APC	-	-	-	APC	Tank
10	3/4	5T	APC	APC	-	-	-	APC	Tank	APC
11	5T	APC	APC	-	-	-	APC	Tank	APC	2 1/2
12	← Cold Tank →									

Note: This flight was started with the vehicles in the same positions as the final run from Flight #3. The jeep in Position #2 began to leak oil on the first run and was shut off and moved slightly out of position where it remained for the rest of the passes.

TABLE 7. ALTITUDES, TIMES, AND BANDS DURING EVENING MISSIONS

Pass #	Alt. (ft.)	3/29/78 Local Time	3/29/78 Local Time	Spectral Bands	
1	6400	0022	1908	4.3-5.3 μm	8.4-13.7 μm
2	3200	0034	1916	"	"
3	1600	0041	1922	"	"
4	800	0046	1927	"	"
5	800	0051	1932	"	"
6	800	0055	1936	"	"
7	800	0059	1947	"	"
8	3200	0107	1950	"	"
9	1600	0114	1956	"	"
10	800	0119	2002	"	"

TABLE 8. ALTITUDES, TIMES, AND SPECTRAL BANDS DURING DAYTIME MISSIONS

Pass #	Alt. (ft.)	3/30/78 Local Time	3/29/78 Local Time	Spectral Bands (μm)
1	6400	1025	1357	.86-1.04; 1.9-2.55; 2.9-3.9; 4.3-5.3;
2	3200	1033	1403	8.4-13.7;
3	1600	1039	1408	" " " "
4	800	1043	1412	" " " "
5	800	1047	1418	" " " "
6	800	1051	1421	" " " "
7	800	1055	1425	" " " "
8	3200	1102	1431	" " " "
9	1600	1108	1436	" " " "
10	800	1112	1440	" " " "
11*	800	1119		" " " "
12**	500	1137		" " " "
13**	900	1142		" " " "
14**	900	1149		.86-1.04; 3.5-4.0; 3.9-4.7; 8.4-13.7;
15**	900	1156		.86-1.04; 2.0-2.6; 3.5-4.0; 3.9-4.7;

* Did not cover target site

** Scanner tilted 35° down fron horizon

TABLE 9. CCT TAPE CHANNEL-SPECTRAL REGION DOCUMENTATION

Tape No.	Nominal Spectral Region for Each Tape Channel (μm)				
	Channel 1	Channel 2	Channel 3	Channel 4	Channel 5
NVL001A	.78-1.1	2 - 2.6	3 - 4.0	4.5 - 5.5	8 - 13.5
2A	"	"	"	"	"
3A	"	"	"	"	"
4A	"	"	"	"	"
5	"	"	"	"	"
6	"	"	"	"	"
7	"	"	"	"	"
8	"	"	"	"	"
9	"	"	"	"	"
10	"	"	"	"	"
11 (Run 14)	"	-	3.9 - 4.7	3.5 - 3.9	"
11 (Run 15)	"	2 - 2.6	"	"	-
12	"	"	3 - 4.0	4.5 - 5.5	8 - 13.5
13	"	"	"	"	"
14	"	"	"	"	"

The CCTs contain 132 images of M-60 tank-types, 176 images of M-113 APC-type, 176 images of truck-type targets. The flight parameters associated with each of the aircraft overpasses are described in detail in Reference [4.4].

Further documentation of the organization of the data base is provided in Table 10. For those interested in using this data base to test target cueing techniques, the tape format is described in Appendix D.

TABLE 10. DOCUMENTATION FOR COMPUTER COMPATIBLE TAPES

Tape	Tape File No.	Date of Data Collection	Take-off Time	Run No.	No. of Scan Lines	No. of Pixels	Target Area			
							L_{min}	L_{max}	P_{min}	P_{max}
NVL001A	1	3/28/78	2330	2	1000	1000	250	750	300	800
	2	3/28/78	2330	3	1000	1000	250	750	300	800
	3	3/28/78	2330	5	1000	1000	250	750	350	850
	4	3/28/78	2330	6	530*	1000	20	530	250	750
NVL002A	1	3/28/78	2330	1	1000	968	100	600	250	750
	2	3/28/78	2330	4	650	968	1	500	150	650
	3	3/28/78	2330	6	530	968	20	530	250	750
	4	3/28/78	2330	7	600	968	100	600	200	700
	5	3/28/78	2330	8	700	968	100	600	350	850
NVL003A	1	3/28/78	2330	9	700	968	50	550	360	860
	2	3/28/78	2330	10	700	968	50	550	180	680

$L_{(\ )}$ = line number (maximum or minimum)

$P_{(\ )}$ = pixel number (maximum or minimum)

*Note header record on tape indicates 1000 lines but there are only 530 lines.

TABLE 10. DOCUMENTATION FOR COMPUTER COMPATIBLE TAPES (Con't.)

Tape	Tape File No.	Date of Data Collection	Take-off Time	Run No.	No. of Scan Lines	No. of Pixels	Target Area			
							L_{min}	L_{max}	P_{min}	P_{max}
NVL004A	1	3/29/78	1830	1	1000	968	1	500	230	730
	2	3/29/78	1830	2	1000	968	75	575	350	850
	3	3/29/78	1830	3	1000	968	250	750	250	750
NVL005A	4	3/29/78	1830	4	1000	968	40	540	250	750
	5	3/29/78	1830	5	700	968	50	550	250	750
	6	3/29/78	1830	6	700	968	100	600	250	750
	7	3/29/78	1830	7	700	968	100	600	200	700
NVL006A	8	3/29/78	1830	8	700	968	100	600	200	700
	9	3/29/78	1830	9	700	968	100	600	330	830
	10	3/29/78	1830	10	700	968	100	600	300	800

$L_{( )}$ = line number (maximum or minimum)

$P_{( )}$ = pixel number (maximum or minimum)

TABLE 10. DOCUMENTATION FOR COMPUTER COMPATIBLE TAPES (Con't.)

Tape	Tape File No.	Date of Data Collection	Take-off Time	Run No.	No. of Scan Lines	No. of Pixels	Target Area			
							L_{min}	L_{max}	P_{min}	P_{max}
NVL007A	1	3/30/78	9:30	1	1000	968	270	770	130	630
	2	3/30/78	9:30	2	1000	968	120	620	70	570
	3	3/30/78	9:30	3	1000	968	220	720	140	640
NVL008A	1	3/30/78	9:30	4	1000	968	270	770	100	600
	2	3/30/78	9:30	5	700	968	110	610	130	630
	3	3/30/78	9:30	6	700	968	100	600	160	660
	4	3/30/78	9:30	7	700	968	110	610	150	650
NVL009A	1	3/30/78	9:30	8	700	968	110	610	80	580
	2	3/30/78	9:30	9	700	968	110	610	140	640
	3	3/30/78	9:30	10	700	968	110	610	170	670

$L_{(\ )}$ = line number (maximum or minimum)

$P_{(\ )}$ = pixel number (maximum or minimum)

TABLE 10. DOCUMENTATION FOR COMPUTER COMPATIBLE TAPES (Con't.)

Tape	Tape File No.	Date of Data Collection	Take-off Time	Run No.	No. of Scan Lines	No. of Pixels	Target Area			
							L_{min}	L_{max}	P_{min}	P_{max}
NVL010A	1	3/30/78	9:30	12	1000	968	250	750	140	640
	2	3/30/78	9:30	13	1000	968	250	750	100	600
NVL011A	1	3/30/78	9:30	14	1000	968	250	750	100	600
	2	3/30/78	9:30	15	1000	968	250	750	60	560
NVL012A	1	3/30/78	13:30	1	1001	968	250	750	250	750
	2	3/30/78	13:30	2	1002	968	250	750	150	650
	3	3/30/78	13:30	3	1003	968	250	750	130	630
NVL013A	1	3/30/78	13:30	4	1004	968	250	750	140	640
	2	3/30/78	13:30	5	705	968	100	600	170	670
	3	3/30/78	13:30	6	706	968	100	600	110	610
NVL014A	1	3/30/78	13:30	7	707	968	100	600	90	590
	2	3/30/78	13:30	8	708	968	100	600	60	560
	3	3/30/78	13:30	9	709	968	100	600	140	640
	4	3/30/78	13:30	10	710	968	100	600	110	610

$L_{(\ )}$ = line number (maximum or minimum)

$P_{(\ )}$ = pixel number (maximum or minimum)

3.0

M-7 SYSTEM PERFORMANCE CHARACTERIZATION

In order that the information contained in the data base be maximally useful, it is important that the user be familiar with the performance characteristics of the sensor system. We provide discussions of these characteristics in this section. This information, along with that contained in the appendices, completely documents the operation and performance of the sensor employed to generate the data base.

3.1 BACKGROUND

The airborne line scanner used on the data collection task was modified to meet the requirements specified for the data set by the Sponsor. The modifications included the following:

(1) Increasing the scan rate of the scanner to obtain contiguous ground coverage for minimum ground resolution (.5 m);

(2) The purchase and installation of a 3-element detector array to obtain spatially registered multispectral data for the near IR (2.0 to 2.6 μm) and mid IR (3.0 to 5.5 μm) spectral regions; and

(3) Interfacing a high data rate digital recorder to the modified M-7 scanner.

The results of these modifications were to alter the M-7's performance characteristics from its nominal configuration, a general description of which is given in Appendix A.

In the following text, the results of the laboratory tests documenting the performance of the M-7 scanner configured for the A.P. Hill mission are summarized. Only a limited discussion is given on the majority of procedures used. Further detail on the M-7 scanner and some of the

characterization tests can be found in Appendix B. Nominal operating characteristics of the system as it was flown for the program are shown in Table 11.

3.2 SYSTEM SPECTRAL RESPONSIVITY

Figures 8 through 11 show the actual relative spectral response of the five detector/filter combinations used in the NVL configuration. Spectral data for the near infrared band was obtained by actual measurement of the M-7 spectrometer using a monochrometer at the focal plane of a laboratory collimator. The mid-IR spectral responsibities were measured by the vendor supplying the InSb 3-element array. A curve for the long wave IR band was generated from the detector spectral responsibity measured by the detector vendor and a spectral cut-on filter transmission measured at ERIM. Except for the near IR band which was measured through the entire scanner, these data represent the spectral response of only two elements in the optical chain, i.e., narrow band spectral filter and the detector. However, since these are the major components in determining spectral responsivity, the other components in the optical path such as the scanning mirror and focusing optics can be neglected without introducing significant error.

The 50% spectral response points as depicted in Figures 4 through 6 are listed below:

(1) .86 - 1.04
(2) 1.9 - 2.55
(3) 2.9 - 3.9
(4) 4.3 - 5.3
(5) 8.4 - 13.7

3.3 SPATIAL REGISTRATION

Figures 12 and 13 show the spatial registration of the five (5) spectral channels by viewing a point target of appeoximately 2 1/2 mr size with the M-7 scanner placed on a laboratory collimator. As the figures show, two of the channels are not in registration in the cross-track dimension. These

TABLE 11. M-7 SCANNER PERFORMANCE CHARACTERISTICS
(A.P. Hill Configuration)

- 5 Spectral Bands in the Near, Mid, and Far IR Regions
- 90° External FOV (± 45° from nadir)
- 2.0 mrad Spatial Resolution
- 0.2°C Nominal (mid and far IR) Thermal Resolution
- 5 Inch Diameter Collector Optics
- 100 Scans/Sec
- DC to 150 KHz Electonic Bandwidth
- Roll-Stabilized Imagery
- 8-Bit Airborne High Density Digital Recording (10 K bits/inch)

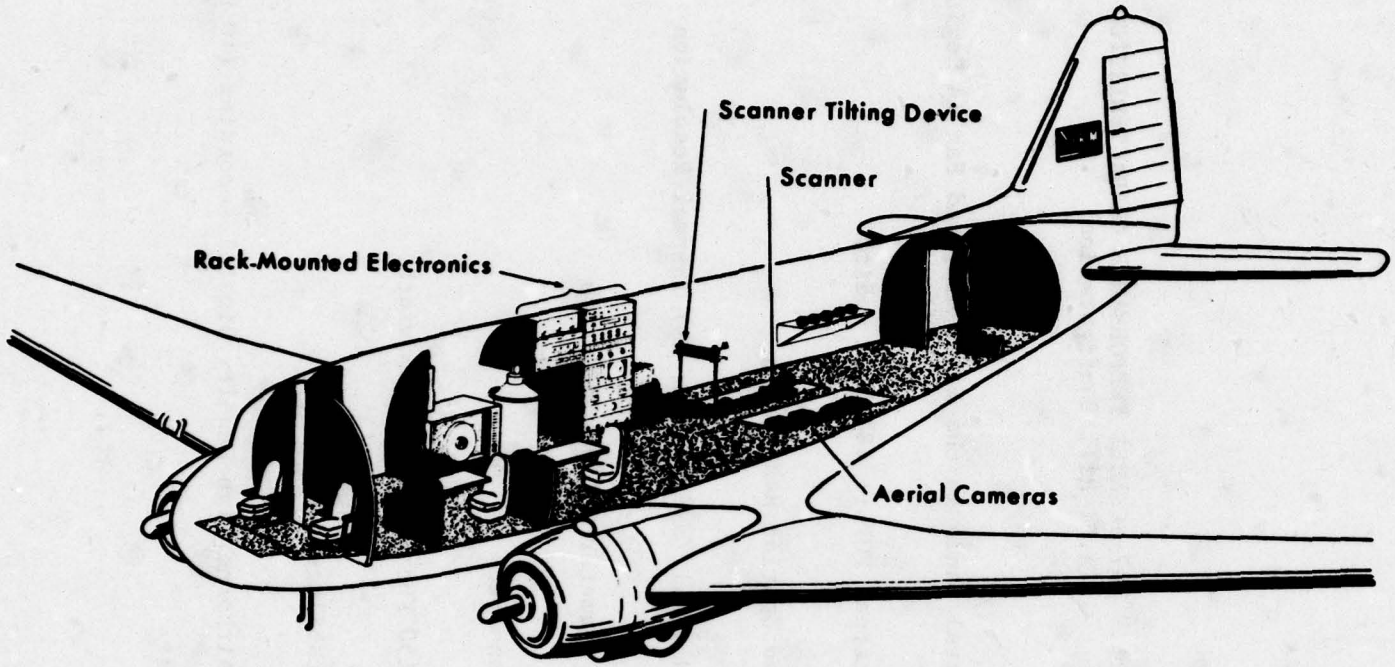

FIGURE 8. ISOMETRIC VIEW OF ERIM C-47 AIRCRAFT

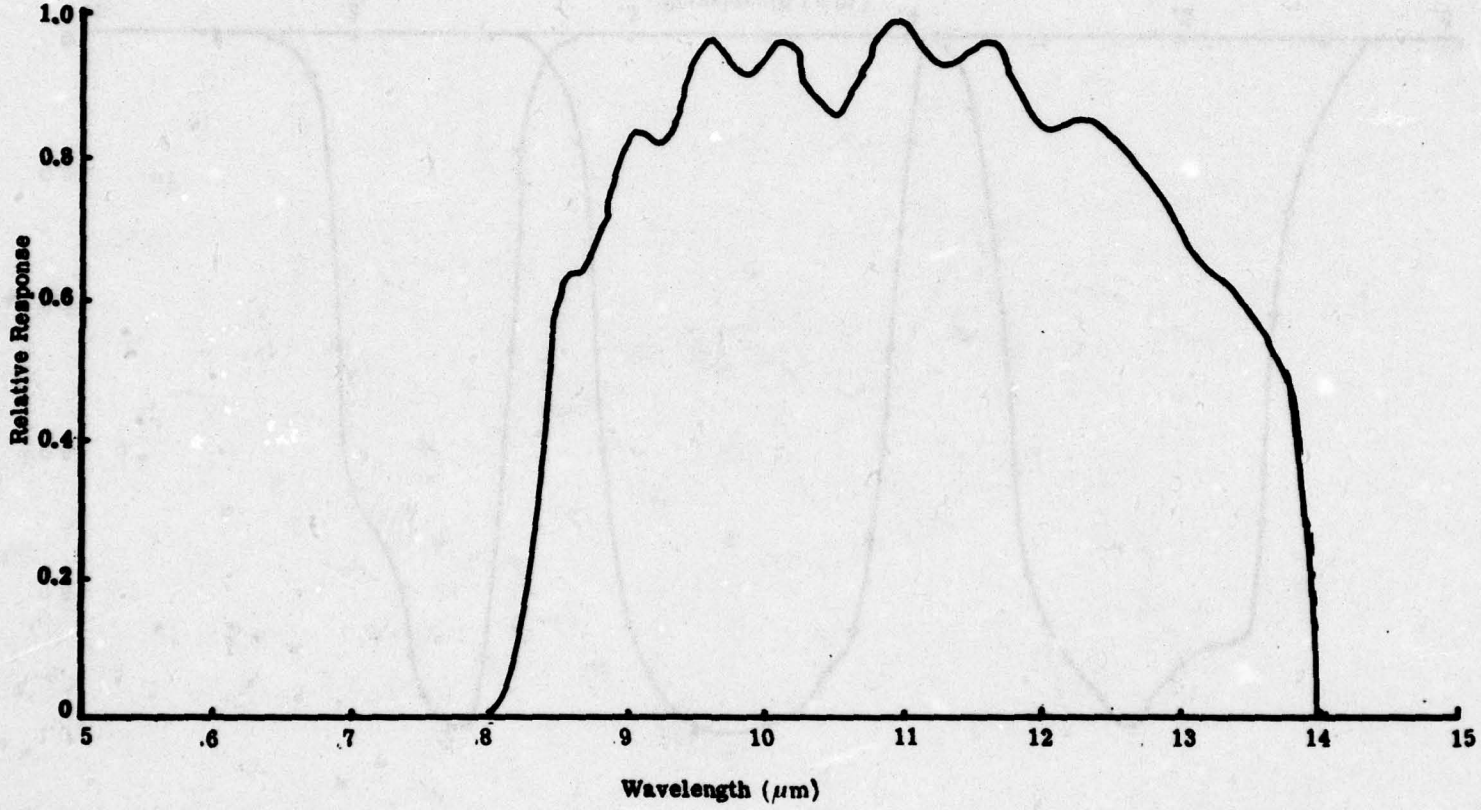

FIGURE 9. SPECTRAL RESPONSE OF LONG WAVE IR DETECTOR/FILTER COMBINATION (HgCdTe)

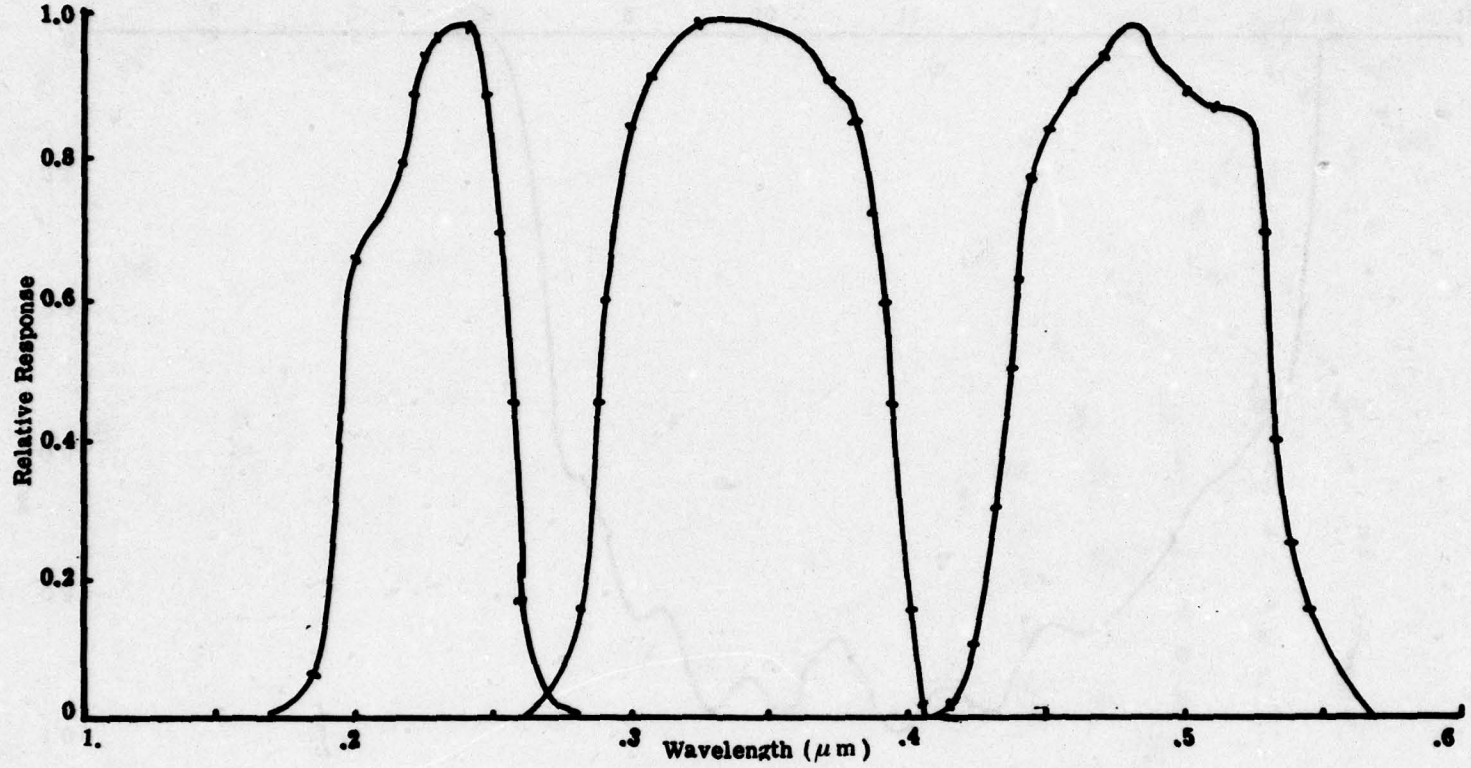

FIGURE 10. SPECTRAL RESPONSE OF MID-IR InSb DETECTOR ARRAY

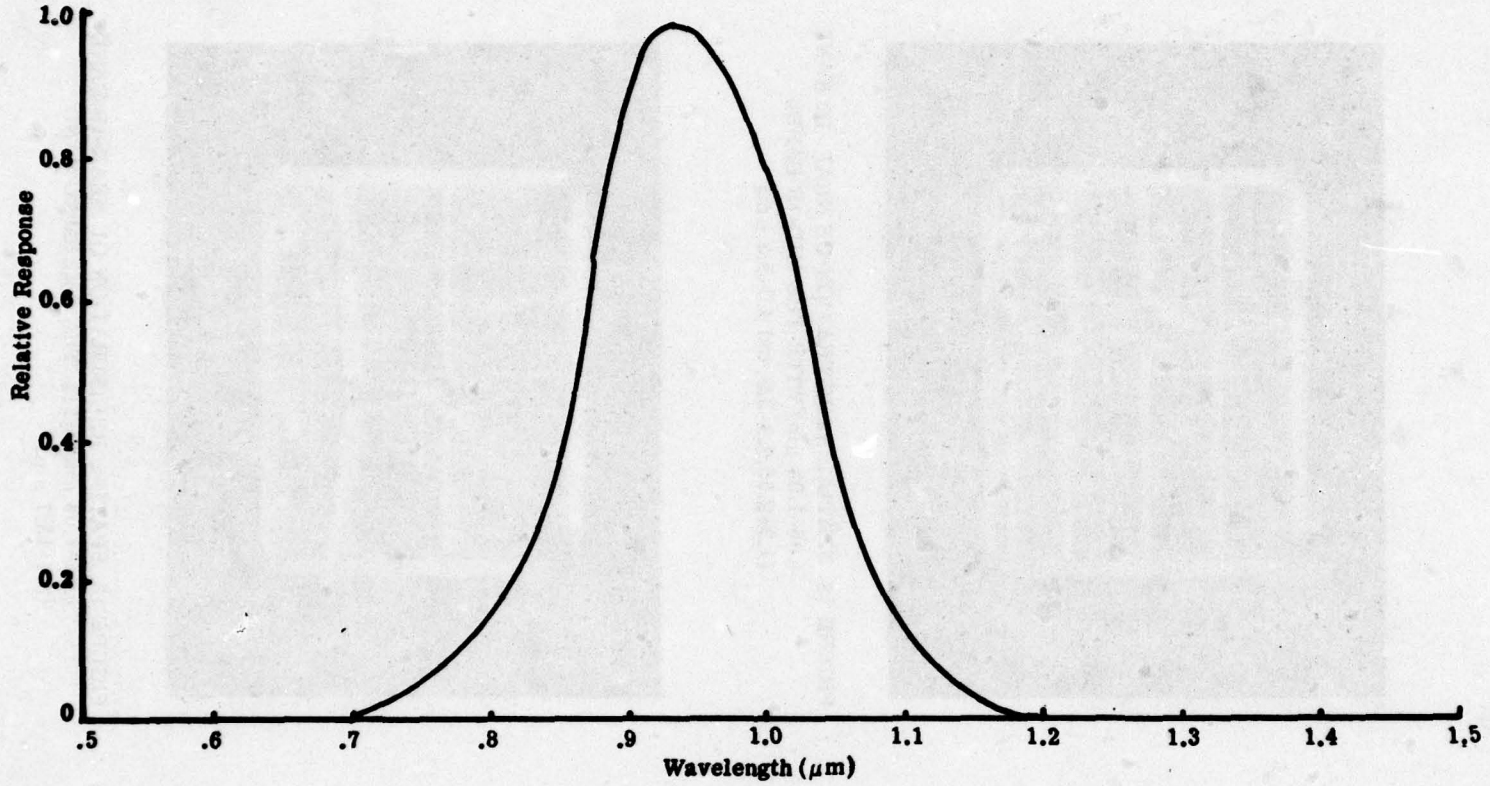

FIGURE 11. SPECTRAL RESPONSE OF NEAR IR PHOTOMULTIPLIER DETECTOR

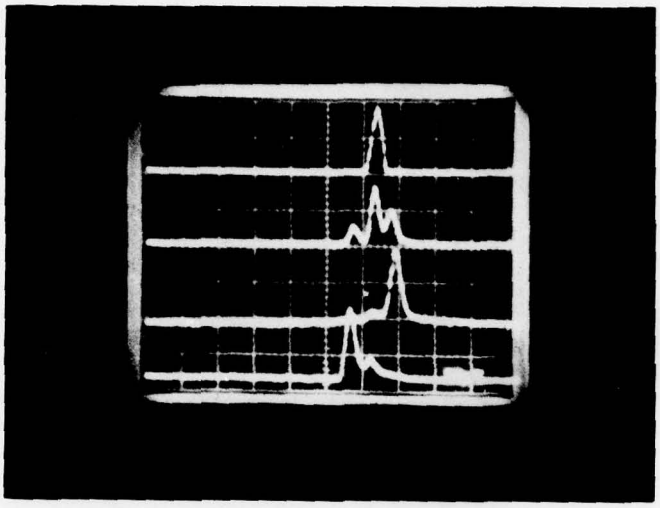

FIGURE 12. SPATIAL REGISTRATION OF NEAR-IR BAND (.86-1.04 μm) WITH THE MID-IR BANDS (1.9-2.55,2.9-3.9, and 4.3-5.3 μm)

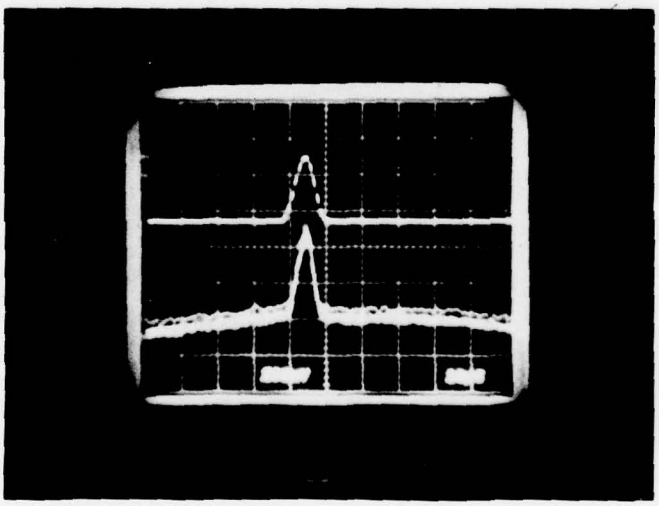

FIGURE 13. SPATIAL REGISTRATION OF NEAR-IR BAND (.86-1.04 μm) WITH THE THERMAL BAND (8.4-13.7 μm)

are two channels of the three-element InSb array and, because of the construction of the array, these channels are not expected to be in registration in this dimension. However, the two offset channels were brought into cross-track registration (within 1/2 pixel) with the other three channels by digital deskewing during the HDDT to CCT reformating process. The registration in the in-track dimension for all channels is within 1/4 pixel. All data produced in CCT format on this program is spatially registered to within one-half pixel.

3.4 INSTANTANEOUS FIELD-OF-VIEW

The instantaneous field-of-view or resolution of the M-7 system as configured for this data collection mission was calculated to be nominally 2.0 mr for all channels. However, the most useful measure of the resolution of an imaging system is the MTF (modulation transfer function) which represents the sine-wave spatial frequency amplitude response of the system. The prime utility of the MTF as a measure is that it permits the cascading of effects of several major components in determining the resolution of the overall system. At a given spatial frequency, the overall MTF is simply the product of the MTF's of all components. The MTF's presented in Figures 14, 15, 16, 17 and 18 represent the overall system MTF for each channel. The spatial frequency is given in cycles/milliradians.

Examination of these figures point out several important facts. First, it can be seen that in general the cross-track MTF is less than the in-track MTF*. This is to be expected to some degree since the response of signals at the higher spatial frequencies in the cross-track dimension is limited somewhat by detector time constant and amplifiying electronics bandwidth. The high spatial frequencies in the in-track dimension, being sampled at a much lower electronic frequency defined

---

*By cross-track we mean that dimension which is perpendicular to the flight line direction and in the direction of mirror rotation. The in-track dimension is <u>in</u> the direction of the aircraft flight line.

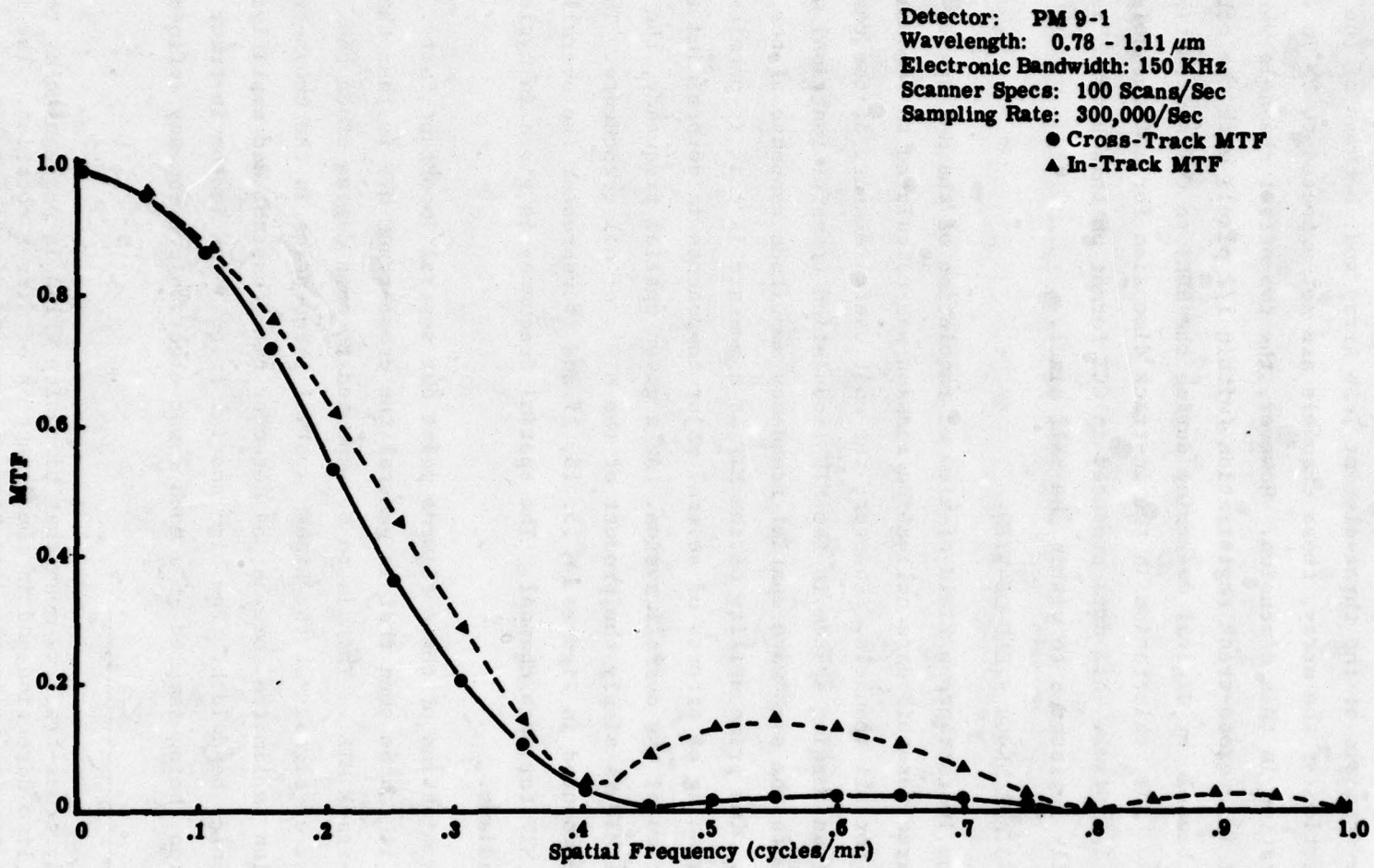

FIGURE 14. MTF VS SPATIAL FREQUENCY

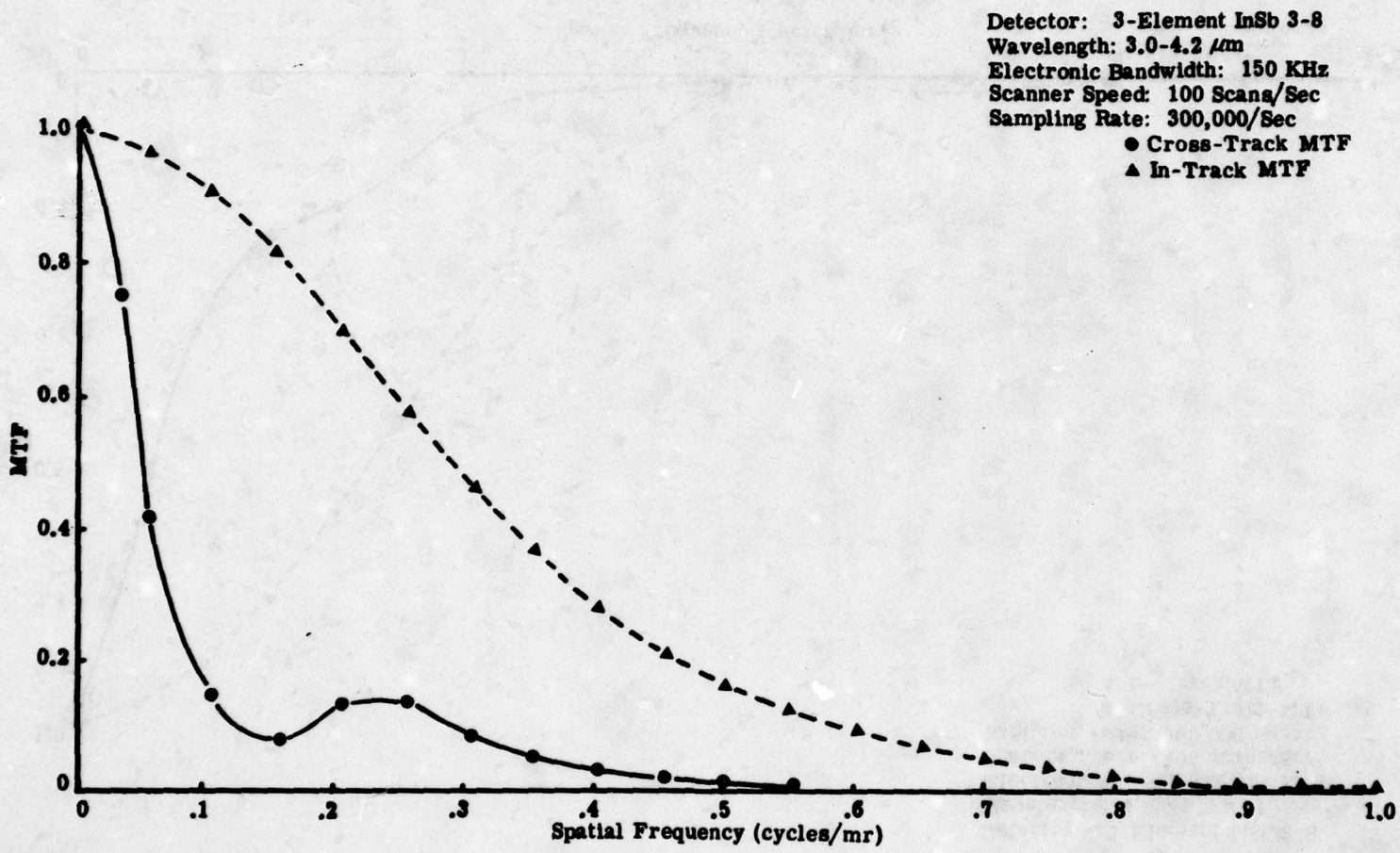

FIGURE 15. MTF VS SPATIAL FREQUENCY

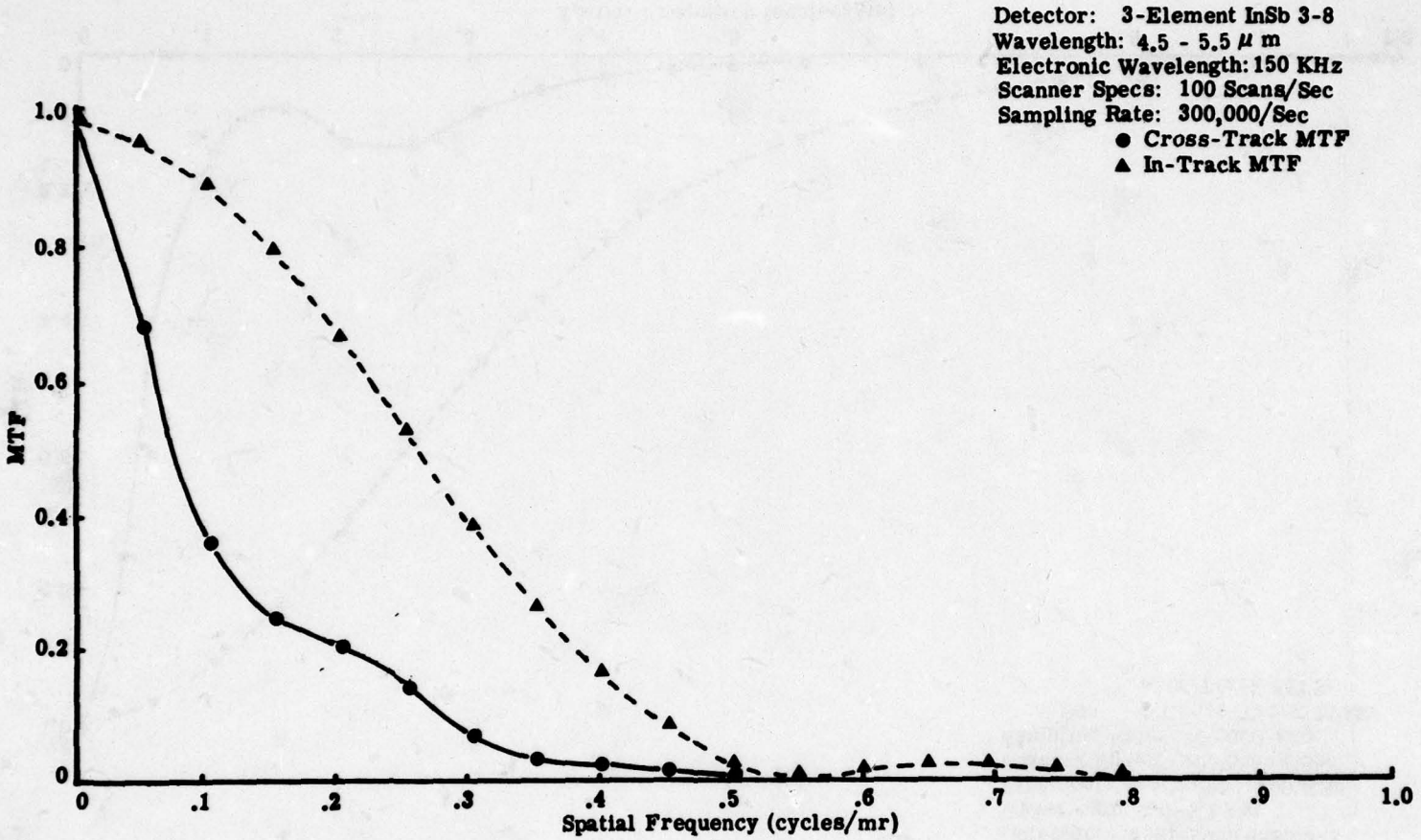

FIGURE 16. MTF VS SPATIAL FREQUENCY

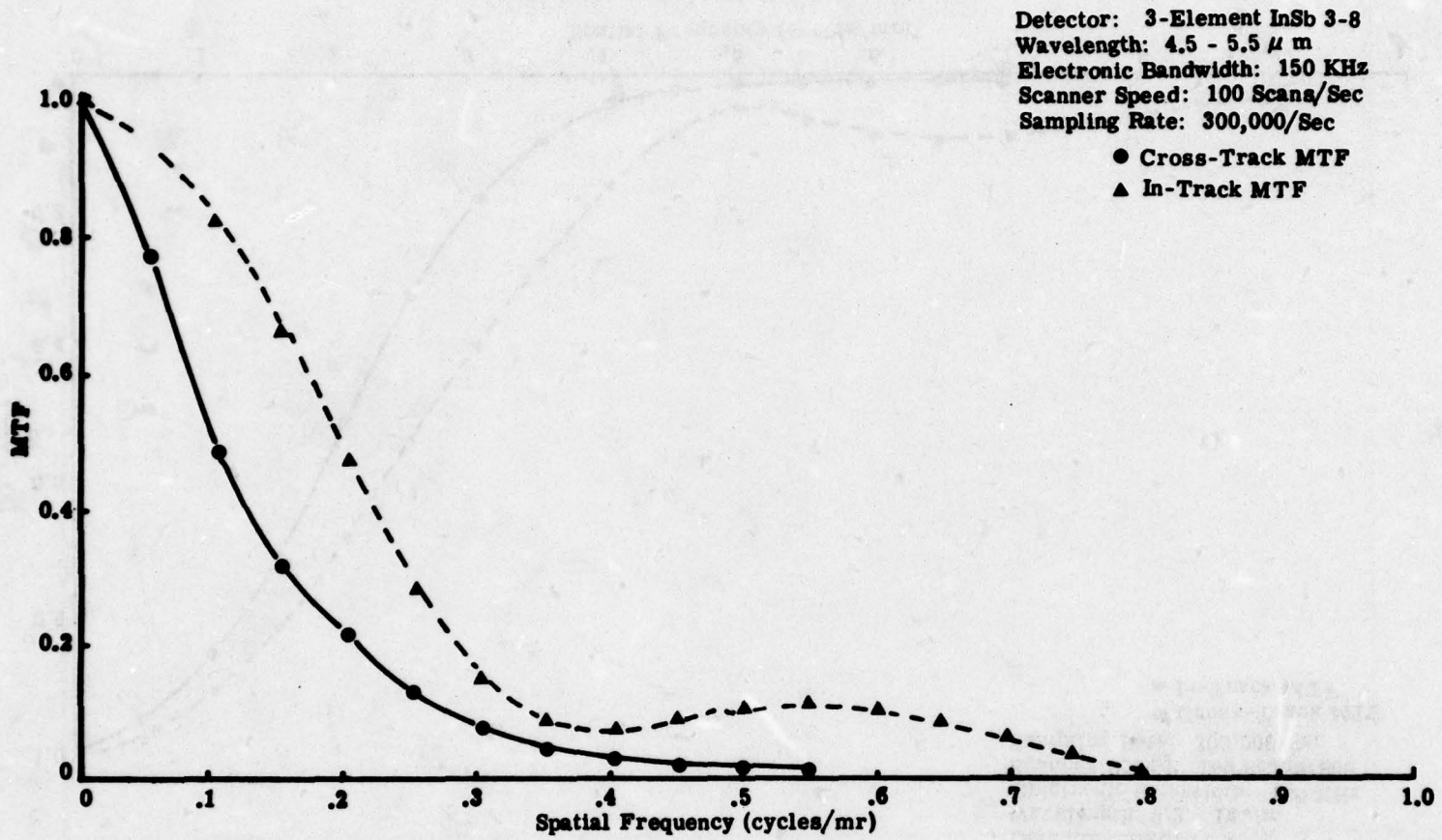

FIGURE 17. MTF VS SPATIAL FREQUENCY

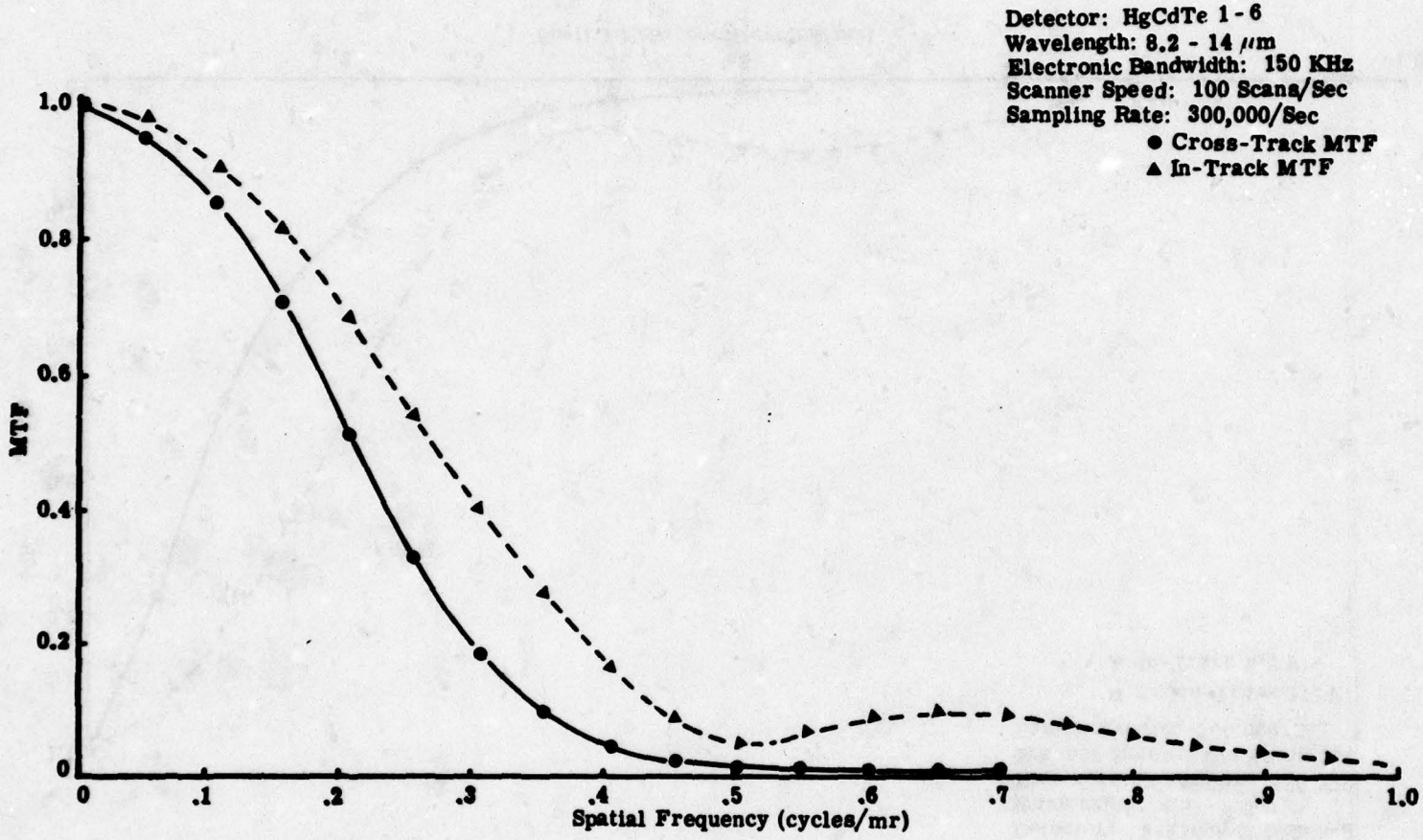

FIGURE 18. MTF VS SPATIAL FREQUENCY

by the mirror rotation rate, is not limited by these same factors. The general trend of Figures 9 through 13 is one in which the difference between cross-track and in-track MTF increases as the detectors go from photomultiplier tube (Figure 14) to HgCdTe (Figure 13) to Indium Antimonde (Figures 10, 11, and 12) is indicative of the detector response time influence on cross-track MTF. A photomultiplier tube has the fastest response time followed by the HgCdTe and finally the InSb detectors.

The "dip" in response at some mid-frequencies ($\sim$ 0.15 cycles/mr) in Figures 15, 16, and 17, however, is not related to any electronic frequency response problem. Rather, it is caused by undesirable surface reflections which occur because of manufacturing defects in the three-element InSb detector array. The reflections which can be seen in Figure 12 as extra pips to the sides of the main lobes, come from aluminized mylar baffles placed between the filter elements above each detector in the array. The problem is the greatest for the 2.0 - 2.6 μm center element which has these aluminum baffles on both sides. The result is to make each round detector appear as two or three detectors placed side by side. Thus, the "dip" that is observed in the figures is an optical problem and its magnitude is a function of the strength of the side-lobe reflection.

The data were sampled in the cross-track dimension at a constant rate supporting digital reconstruction of up to .25 cycles/mr. In the in-track dimension, several sample frequencies were employed depending upon altitude. These frequencies are shown below:

Altitude	In-Trace Sampling Frequency Limit
800	.25 cycles/mr
1600	.50 cycles/mr
3200	1.0 cycles/mr
6400	2.0 cycles/mr

It is important to know the digital sampling frequency with respect to the spatial frequency response curves to qualitatively evaluate the effect of aliasing. Aliasing can best be described as a folding of the spatial

frequency spectrum at the sampling frequency. This phenomenon, which is a result of the descrete time sampling of an analog time continuous signal, causes spatial frequencies higher than the sampling frequency to appear to be folded or "aliased" to lower spatial frequencies. If these aliased signals have large enough magnitudes, erroneous interpretation of the spatial information obtained from the imagery can occur.

The only way to avoid aliasing is to make the sampling rate at least twice as high as the highest expected spatial frequency in the analog video data. Thus, oversampling decreases chance for errors, caused by aliasing and the higher altitude data collected during this program can be assumed to be aliasing free in the in-track dimension. At the lower altitudes in the in-track dimension and at all altitudes in the cross-track dimension, the potential for some aliasing does exist as can be seen by examination of the MTF curves past the .25 cycle/mr sampling frequency limit. The potential for aliasing is stronger in the in-track dimension (at least at the lower altitudes) than the cross track. The existance of an aliasing potential is a problem only if the scene contains significant structure at the unsampled frequencies. Examination of the reconstructed imagery showed no noticeable artifacts indicative of such a condition.

3.5 RADIOMETRIC SENSITIVITY

Measurements were made to determine the radiometric sensitivity of the M-7 scanner in the spectral bands employed during the NVL data collection effort. The figure of merit commonly used to describe this detector/scanner sensitivity is the noise-equivalent radiance difference (NEΔL). This value is calculated by dividing the radiance difference producing signal by the detector peak voltage-to-rms noise ratio of that signal difference.

For the solar reflective bands in the region from 0.4 to 3.5 μm, the NEΔL is a function of the radiance level, L. Hence, a NEΔL value in this spectral region really has meaning only for a specified illumination condition. However, typical values representative of the illumination

levels encountered during the 1330 hours flight at A.P. Hill were obtained for the .8 to 1.1 and 2.0 to 2.6 μm bands. Shown in Table 12 is the digital reference source data obtained from the fifth pass during the 1330 hour mission for the above two bands. For a reference lamp radiance as shown, the NEΔL was calculated for each band and is shown in the table.

For the thermal emissive region from 4.0 to 14 μm, the sensitivity of the various bands can be more usefully presented as noise-equivalent temperature differences (NEΔT). However, it is important to realize that the rationship of radiance to temperature is non-linear; hence a given increment in temperature will result in various band radiance increments depending on the mean temperature and band involved. Shown in Figures 19, 20 and 21 are the radiance versus temperature curves for the 2.9 to 3.9, 4.3 to 5.3, and 8.4 to 13.2 μm bands. In Figure 19 it can be seen that a .02 $\mu m/cm^2$-ster increment in radiance centered around 31°6 results in a ΔT equal to 16°C while the same radiance increment centered around 64.5°C results in a temperature increment equal to 5°C. Hence, a given thermal band RMS noise figure expressed in radiance units of $\mu m/cm^2/sr$, will result in different NEΔT's for the system depending on the mean temperature of the measurement. For all of the NEΔT calculations obtained in the following tests, the mean temperature was assumed to be approximately 10°C to correspond with the surface scene temperatures observed during data collection.

The tests were made using blackbody reference plates internal to the M-7's scanner housing. There are three of these blackbody plates (two temperature-controlled, one ambient) which are viewed sequentially during each scan. The purpose of these plates is to provide known sources of emitted radiation by means of which the temperatures of objects viewed on the ground by the scanner can be calculated. In Table 13 are shown the digital values for the blackbody reference plates from the 1330 hour

TABLE 12. TYPICAL REFLECTIVE BAND SENSITIVITY

Band	Digital Lamp Value	Digital Offset (Dark Level)	Digital Difference	Digital RMS Noise	S/N Ratio
1.86 - 1.04 μm	45.78 counts	25.42 counts	20.36 counts	1.00 counts	20.36:1
1.9 - 2.55	129.52	43.52	86.00	3.10	27.74:1

Lamp Radiance (1.86 - 1.04) = 21,000 $\mu w/cm^2$-ster; NEΔL = 21,000/20.36 = 1031.43 $\mu w/cm^2$-ster

Lamp Radiance (1.9 - 2.55) = 420 $\mu w/cm^2$-ster; NEΔL = 420/27.74 = 15.14 $\mu w/cm^2$-ster

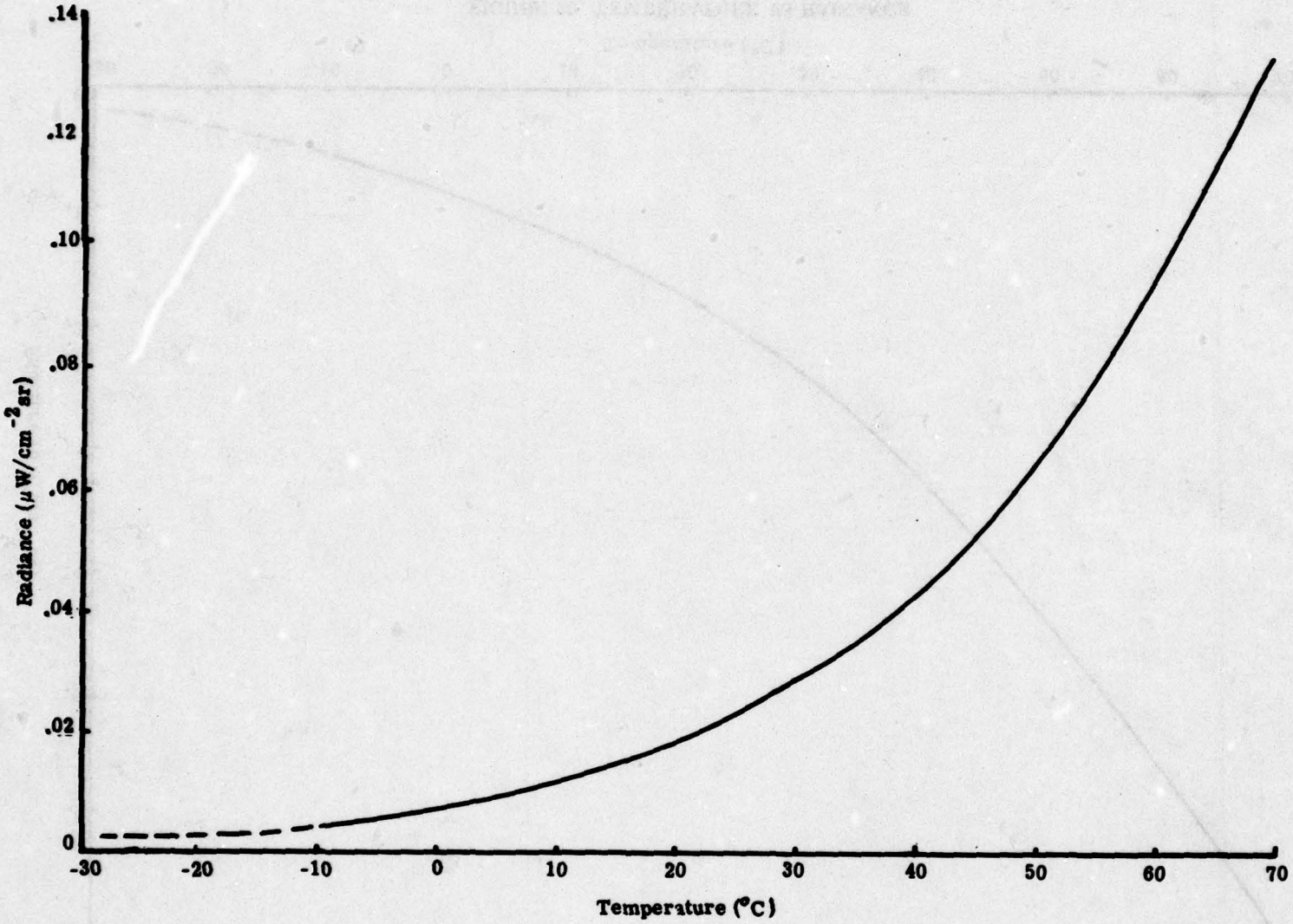

FIGURE 19. TEMPERATURE VS RADIANCE $\Delta\lambda$=2.85 - 3.95μm

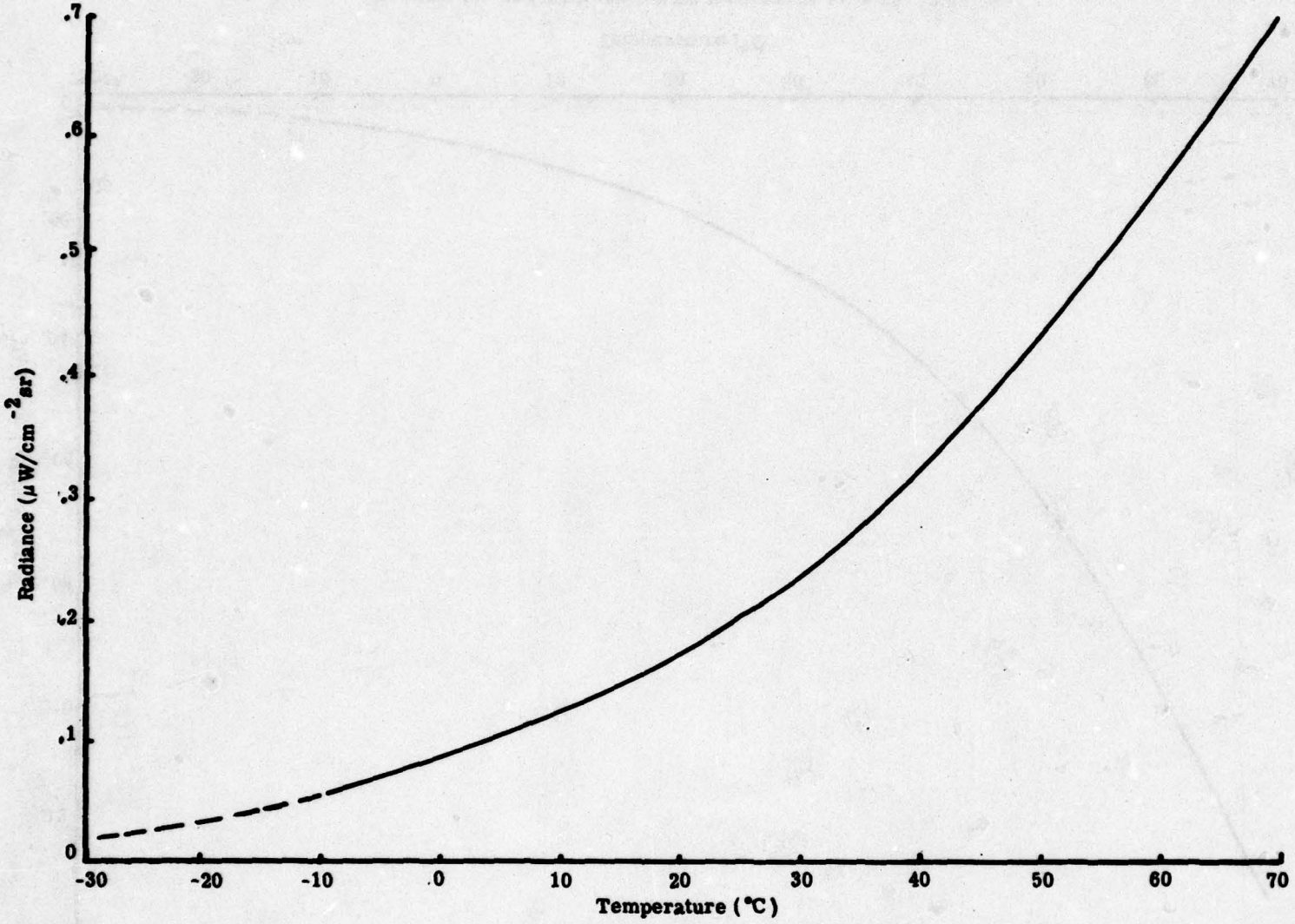

FIGURE 20. TEMPERATURE VS RADIANCE
$\Delta\lambda$=4.75-5.3μm

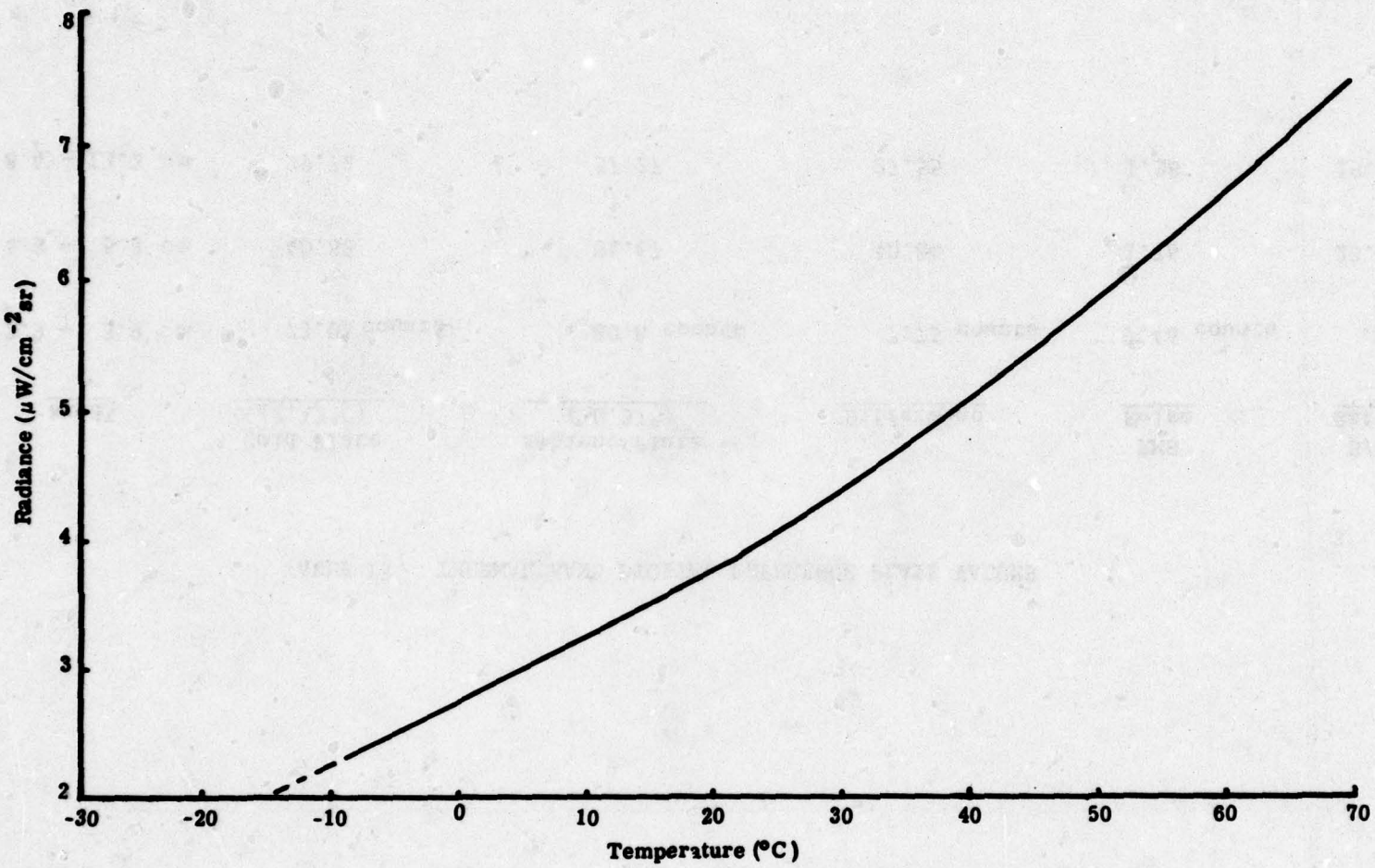

FIGURE 21. TEMPERATURE VS RADIANCE $\Delta\lambda$=8.4 - 13.7μm

TABLE 13. THERMAL BAND DIGITAL REFERENCE PLATE VALUES

Band	Cold Plate (2.12°C)	Ambient Plate (10.37°)	Difference	RMS Noise	S/N Ratio
2.9 - 3.9 µm	73.05 counts	80.8 counts	7.75 counts	9.46 counts	.82
4.3 - 5.3 µm	40.83	81.67	40.84	1.76	23.2
8.4 - 13.2 µm	29.72	57.27	27.55	1.38	19.96

flight and the fifth pass. Nominal plate temperatures for this pass were 2.12°C for the cold plate and 10.37°C for the ambient plate*.

Using Figures 19, 20, and 21 and the S/N ratios shown in Table 13, the NEΔT values for the three detector bands at 10°C are:

BAND	NEΔT (10°C)
2.9 - 3.9	8.70°C
4.3 - 5.3	0.30°C
8.4 - 13.7	0.27°C

The NEΔT of the 2.9 - 3.9 band should be worse than the other two thermal bands since there is much less energy emitted in this band at 10°C. However, the difference observed in these tests was larger than expected. Even under daylight conditions, where the detector was receiving significant solar reflected energy in addition to thermal emissive energy the overall image quality was much poorer than anticipated. The conclusion to be drawn is that this element of the array was not performing up to state-of-the-art potential, and the resultant data are probably of little use.

The above discussion describes the nominal sensitivity of the data collected. Techniques to extract quantitative thermal radiometric information from any of the data images are given in Appendix C.

---

*Due to digital hardware limitations, the hot plate was not reformatted onto CCTs. Since only two calibrated thermal reference plates are in fact required, this presented no calibration problems.

4.0
MULTISPECTRAL TARGET CUEING STUDY

The major activity of this program was the collection, preparation and documentation of a unique multitemporal and multispectral data base for a tactical military scenario. That activity was successfully accomplished. However, the second goal of providing significant initial evaluation of multispectral processing concepts was only partially achieved because of unforeseen diversion of resources to accomodate technical problems arising in the data base generation effort. This section describes the analyses conducted and the results achieved.

4.1 GENERAL CONSIDERATIONS

The multispectral data base collected for this program can be considered, in its fullest generality, to be an eight dimensional data set composed of five spectral dimensions, two spatial dimensions, and one temporal dimension. A full understanding of the total information content in this data would require a unified treatment of all dimensions, including second order statistical interactions.

Information in the temporal dimension is seldom considered in tactical military applications of remote sensing, the obvious exception being in change detection concepts. While temporal trends in spatial/spectral data characteristics may well provide definitive signature opportunities, the perceived need to support real-time operations negates the potential utility of such concepts. Rather, time is treated as a discrete ancillary condition and not as a true dimension of the information in the data.

The nature of the multispectral scanner image provides two independent spatial dimensions to the data set. The crudest use of such data involves the simple concept of a pulse length in either dimension. More complex spatial features such as area, shape or texture can be derived. Use of such derived features tends to recognize the fact that, while the <u>data</u> may be independent in an x,y coordinate system, the spatial <u>information content</u> of the scene may indeed be more uniquely perceived by use of a derived feature or alternative coordinate context.

The simplest use of the five spectral dimensions of the data is just to treat them as five independent information channels in processing. However, it is well known that correlation does exist between spectral bands in the infrared, so that the true dimensionality of the information is probably less than five. Further, the principal components of information in the five dimensional spectral space do not necessarily line up with any of the five axes (acquired bands) in that coordinate system. Finally, much of the information content is really not of interest (e.g. solar illumination level effects) so that by using derived features (e.g. band ratios) one may be able to differentially suppress that information not of use (i.e. clutter) in a specific application.

A preliminary evaluation of two different approaches to multispectral target cueing was accomplished. The first approach involved classical maximum likelihood classification using in-scene training. The second approach involved unsupervised spectral/spatial clustering followed by discrimination based upon size. The results of these efforts are presented in the following sections.

4.2 MAXIMUM LIKELIHOOD CLASSIFICATION WITH TRAINING

The most commonly used procedure for generalized multispectral recognition is that of maximum likelihood classification with in-scene training. In this procedure, the spectral values of each pixel in the scene are compared to the statistical distribution functions defining the characteristics of the candidate classes from which that pixel might have been drawn. The pixel is then assigned to that class from which it most likely <u>was</u> drawn. The candidate class distributions are empirically defined using samples from the scene which are somehow identified, usually, as in this case, using ground truth. A general description of this methodology is given in Appendix E.

Detailed procedures and results of the maximum likelihood classification are presented in Appendix F. The results are summarized in Table 14. It is obvious from these results that a significant lack of extendability exists for the target signature characteristics. For the daytime

TABLE 14. MAXIMUM LIKELIHOOD CLASSIFICATION

	Targets Present		Targets Cued	
Time	Training	Test	Training	Test
0930	7	5	7	0
1330	6	6	6	0
2330	3	9	3	6

data, the only targets detected were those from which the signature training statistics were established. At night, however, two-thirds of the test set (six out of nine targets) were detected in what amounted to a thermal hot spot evaluation.

The false alarm problems in the maximum likelihood classification were not quantitatively evaluated. However, reference to the classification results in the photos of Appendix F shows a qualitative trend quite similar to that for target detection: false alarms are a major problem during the daytime, but become significantly less so at night. Had the spatial dimensions of the data been utilized for additional size discrimination, the false alarms encountered at night might well have been reduced to a potentially tolerable, or at least promising, level. However, a spatial discrimination would not have led to such promising results on the daytime classification false alarms.

4.3 UNSUPERVISED SPECTRAL/SPATIAL CLUSTERING OF DERIVED FEATURES

The use of any multispectral recognition approach requiring training with in-scene ground truth is of obviously limited operational utility in a military reconnaissance application. Because of this fact, unsupervised approaches which attempt to partition the scene according to the natural spectral/spatial structure of the data have obvious appeal. The ultimate utility of such approaches depends upon the presence of recognizable structure to the data which can be associated with the presence of a target of interest.

A specific methodology for unsupervised spectral/spatial clustering was implemented in order to preliminarily assess the degree to which useful and recognizable data structure might be present in the Camp A.P. Hill data base. The technology utilized in this investigation has been successfully demonstrated by ERIM and others in civilian applications of multispectral remote sensing.

The approach taken involves a preprocessing of the raw spectral bands in order to create derived spectral features with which to work. This preprocessing allows for a more intuitively logical, physically-based understanding of the nature of the data variability present in the multispectral information. A detailed description of the methodology and results of current state-of-the-art spectral/spatial clustering applied to the 1330 hours Camp A.P. Hill data base is presented in Appendix G.

The primary intent of the unsupervised spectral/spatial clustering investigation was to ascertain whether there existed any coherent spectral structure to a tactical target which could separate it from its immediate background so as to produce a recognizable spatial shape. The results of this investigation, though admittedly limited in scope, suggest that such coherent spectral structure does not exist in general.

It was found that some targets clustered into recognizable spatial shapes, while others were completely inseparable from their backgrounds. However, in general, and for armor in particular, it was found that any combination of the physically-based spectral features produced several clusters for each target, so that no single recognizable spatial entity could be isolated. That is, within very broad tolerance limits, targets of interest do not have coherent or uniform spectral features for the spectral bands of the data base investigated.

5.0
CONCLUSIONS AND RECOMMENDATIONS

A multispectral infrared data base of tactical military vehicles has been created. Data were gathered at Camp A.P. Hill, Va. during typical springtime conditions prior to leafing of deciduous trees. The background constituents were typical of those found in undeveloped land in temperate regions. The data base has been documented, reformatted into computer compatible form, and delivered to the Sponsor.

A limited analysis of the data was accomplished in order to provide initial indications of the utility of multispectral target recognition concepts. The conclusions reached in this initial analysis, and the recommendations based upon them, are presented in the following sections.

5.1 CONCLUSIONS

The existence of a unique, passive infrared spectral signature for tactical military vehicles has not been verified. It appears that an extremely large amount of spectral variability exists, both between targets and, more importantly, even within a single target. Attempts to improve that situation by performing spectral transformations to isolate more stable and physically interpretable spectral features have not been successful.

The basic problem in the passive, spectral domain is that there appears to be no unique and fundamental cause and effect relationship between what a military vehicle is, and how it appears spectrally in the infrared portion of the electromagnetic spectrum. A modest caveat on this statement is that some degree of uniqueness, at least with respect to natural backgrounds, does exist for the thermal character of an operating vehicle at night. Otherwise, there may be no reason to expect unique spectra a priori, unless by human error some infrared equivalent to a Signal Flare Orange paint in a snow background is encountered.

The problem in the spatial domain is really a reflection of the extreme amount of spectral variability present within a given vehicle.

Even modestly sophisticated approaches to finding coherent spectral relationships generally fail to isolate a spatial entity which is recognizable by classical shape recognition concepts. The pattern recognition problem, after maximal use of the spectral information present, still appears to require the kind of complex spatial structure synthesizing capability typically provided by the eye/brain combination in human vision.

5.2 RECOMMENDATIONS

The generally negative conclusions concerning the existence of some useful spectral signature must be treated as preliminary. Further consideration of the problem may yield to some creative insight not presently available. It is recommended that any such investigations must recognize, and emphasize overcoming, the basic problems faced:

- "Tankness" does not uniquely translate to any particular region or feature of infrared spectral space
- Different spectral bands are not likely to resolve the problem, for they are generically measuring the same attributes
- Different attributes, such as polarization, may provide a key for they may be more closely dependent upon what a vehicle is (e.g., specular surfaces). Active techniques have been explored in other efforts [4]
- If spectral features are found, they are going to be subtle, so that one must concentrate on the real targets (e.g., Soviet armor in typical field paint and backgrounds), and not upon questionable analogs.

---

[4] M. Bair, et al., "Active Passive Cueing Techniques" (U), ERIM Report No. 112900-69-F, Air Force Avionics Laboratory, Contract No. F33615-75-C-1155 (In Publication, June 1979) (SECRET)

- The motivation for searching out spectral features should be driven by the need to isolate coherent spatial entities amenable to state-of-the-art spatial pattern recognition methodologies.

The apparent lack of unique spectral signatures, when coupled with the extreme within-target spectral variability found, suggests that the means for straightforward definition of characteristic shapes necessary for classical pattern recognition techniques may not be attainable. It is therefore recommended that emphasis be placed upon developing pattern recognition technology which holds the potential for emulating the eye/brain ability to synthesize gross spatial structure through recognizing the associations of the individual elements of that structure. The three-dimensional target classifier (3DTC) processing concept currently under development at ERIM has investigated that potential [5].

---

[5] S. Sternberg, et al., "3D Target Classifier" (U), ERIM Report No. 126200-36-F, Air Force Avionics Laboratory, Contract F33615-77-C-1010 (In Publication, June 1979) (CONFIDENTIAL)

APPENDIX A

M-7 OPTICAL-MECHANICAL SCANNER

The M-7 optical-mechanical scanner is an advanced type of airborne sensor capable of collecting and recording multiple channels of image data in either digital or analog form on magnetic tape for subsequent processing and analysis. The processing can take advantage of the information content of recorded spectral data in the ultraviolet, visible, and the thermal infrared for automatic terrain classification and identification. The M-7 scanner has successfully acquired high quality data for numerous applications, including the 1971 Corn Flight Watch Experiment, varied Landsat and Skylab investigations, and many others since 1971; its predecessor was first flown in the mid-1960's. The total system, including boresight cameras, can be operated in ERIM's C-47, C-46 or C-7 aircraft.

The M-7 scanner intercepts terrain radiation by means of a 5-inch diameter collection aperture. This radiation is redirected onto an optical telescope by a rotating flat mirror. The incoming radiation passes through a system of beamsplitters, dispersing optics, and spectral filters to a number of radiation detectors in the focal plate of the telescope which convert the focused beam of radiation to a set of electrical signals for recording on magnetic tape. Figure A-1 shows a schematic drawing of the M-7's optical system.

The rotating mirror causes the narrow instantaneous field-of-view of the telescope to scan in a plane perpendicular to the longitudinal axis of the aircraft through an opening in the bottom of the aircraft. Then before making the next ground scan, it scans radiation reference devices which are internal to the scanner. By the time the next scan begins, the aircraft has moved forward; thus, subsequent line scans are built upon one another to produce a continuous strip image of the terrain beneath the aircraft.

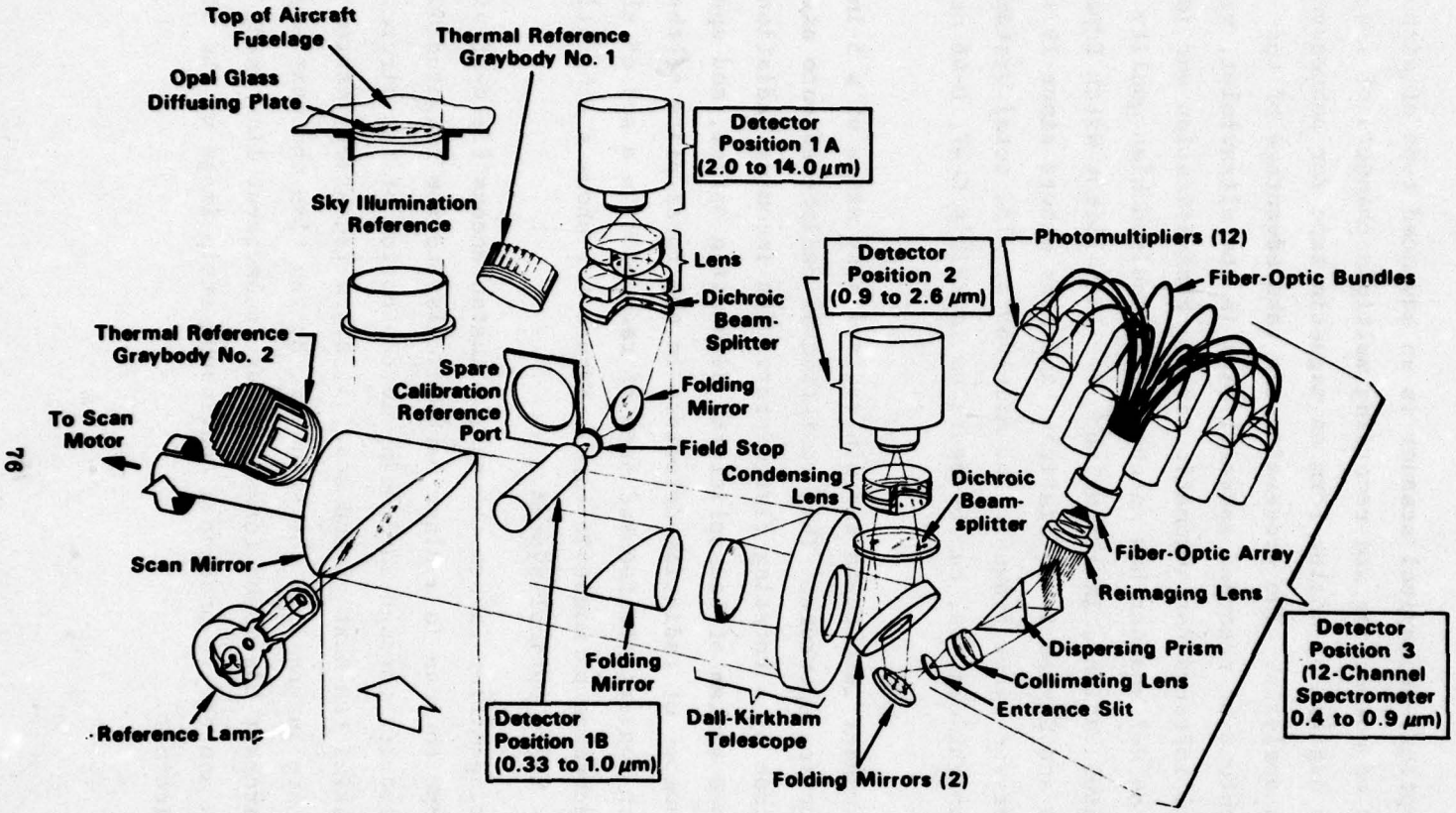

FIGURE A-1. OPTICAL SCHEMATIC OF ERIM EXPERIMENTAL M7 MULTISPECTRAL SCANNER

Covering a wavelength range from 0.33 to 14.0 micrometers, the M-7 scanner can operate in up to 19 different spectral bands through the use of various detector/filter combinations. Up to 12 spectral channels of image data can be recorded at any one time on either a high-density-digital or an analog 14-track magnetic tape recorder. The other two tape recorder tracks are used for housekeeping data purposes. A typical grouping of detectors provides a common spatial resolution of 2.5 milliradians. Other detectors have instantaneous fields-of-view (FOV) ranging from 2.0 to 20.0 mr.

The system has a nominal thermal resolution (NEΔT) of 0.1°C and a nominal reflectance resolution (NEΔT) of 1 percent.

The scanner views the terrain during 90° of its scan, providing an external field-of-view (FOV) covering the range from 45° left to 45° right of nadir. The scanner can be tilted for oblique scanning ahead of the aircraft at angles of up to 52° from nadir. The scanner imagery is roll-stabilized.

The system operates at either of two constant scan speeds -- 60 or 100 scans per second. Nominal electronics bandwidth is tape recorder limited to a range of dc to 150 kHz.

APPENDIX B

AIRBORNE SYSTEM PERFORMANCE

This section describes the various system performance tests, both optical and electrical, performed on the M-7 scanner. It was taken verbatum from Reference [6] and includes a discussion of overall data quality as well as system performance figures and general calibration procedures.

B.1 RADIATION CALIBRATION

B.1.1 Visible and Near-IR Radiance Calibration (0.4 - 2.6 μm)

The task of trying to provide absolute radiance calibration in the visible and near-IR regions for any line scanner is difficult, to say the least. Much has been wirtten about the theory behind such radiation calibrations, so no attempt will be made here to go into any great depth on the subject. This section provides, as background, a limited amount of theory on radiance calibration and describes the procedure and results of the tests.

Calibration Tests. The scanner calibration lamp signal, as described in Section 4.4, is used basically as a transfer standard to obtain the apparent spectral radiance of terrain objects. Its main purpose is to account for scanner system responsivity changes that, in general, are almost impossible to monitor conveniently. The scanner components themselves are designed to respond linearly with increased radiance from the ground terrain -- i.e., an increase in radiance gives a corresponding increase in detector signal. Hence the scanner detector voltage for each channel can be represented by the following general equation:

---

[6]. P.G. Hasell, Jr., et al., Michigan Experimental Multispectral Mapping System, A Description of the M7 Airborne Sensor and Its Performance, Report No. 190900-10-T, Environmental Research Institute of Michigan, Ann Arbor, Michigan, January 1974.

$$V_{T+p}(\lambda) = K\left[L_T(\lambda) + L_p(\lambda)\right] \qquad \text{(B-1)}$$

where

$$L_T(\lambda) = \frac{\rho_\tau E_T(\lambda)}{\pi}$$

and

$V_{T+p}(\lambda)$ = scanner signal voltages* recorded by aircraft recorder

K = a constant dependent on system factors such as responsivity of detectors and photomultipliers, system transmission losses, gains, etc.

$L_T(\lambda)$ = radiance of target*, assuming a Lambertian surface

$L_p(\lambda)$ = path radiance produced as a result of scattering of radiation by molecular and aerosol particles in the atmosphere*

ρ_τ = object directional reflectance

At present, the radiance qualtity $L_p(\lambda)$ is impractical to measure simultaneously with the airborne scanner imagery. But to make up for this, considerable effort is going into modeling the atmosphere so that the appropriate corrections can be made to the data during processing.

In terms of scanner radiance calibration, however, the individual terms of Eq. (1) are less important than the total radiance received at the scanner's aperture. Hence, the apparent target radiance (which includes the path radiance contribution) is a more appropriate quantity to measure. Simplifying Eq. (1), then, we get:

$$V_{T+p} = KL_{T+p}(\lambda) \qquad \text{(B-2)}$$

$L_{T+p}(\lambda)$ = apparent radiance of target, $L_T(\lambda) + L_p(\lambda)$

---

*In each scanner channel.

Were it not for the fact that the constant K in Eq. (2) actually varies somewhat because of changes in the detector and its responsivity, the radiance calibration of a scanner would be easy. A quick look at a known radiance source such as a reflectance standard illuminated by calibrated irradiance standards would suffice. Since this "constant" does vary, however, a means to remove K from Eq. (2) becomes necessary.

The prime purpose of the lamp reference source, as stated earlier, is to remote the factor K. The is done by dividing the voltage obtained from the target by the lamp voltage. Hence, if the target voltage is given by Eq. (2) and the lamp voltage is given by

$$V_\ell = KL_\ell(\lambda) \tag{B-3}$$

then by dividing Eq. (2) by Eq. (3) we get

$$V_{T+p} = \frac{V_\ell L_{T+p}(\lambda)}{L_\ell(\lambda)} \tag{B-4}$$

The radiance calibration is performed in a similar manner, except that the target, instead of being a terrain object, is an object of known radiance. If the calibration target is flame-sprayed aluminum (a well measured and stable reflectance standard) illuminated by quartz-iodine lamps, then the voltage generated by the radiance standard is

$$V_{A\ell}(\lambda) = K'L_{A\ell}(\lambda) \tag{B-5}$$

where $L_{A\ell}(\lambda) = \left[\rho_{A\ell}E_{QI}(\lambda)\ /\pi\right]$

E_{QI} = spectral irradiance of quartz-iodine lamps

$\rho_{A\ell}$ = directional reflectance of flame-sprayed aluminum

K' = system constant which has varied from K in previous equation

Dividing Eq. (5) by the lamp voltage

$$V_{\ell'}(\lambda) = K'L_\ell(\lambda) \tag{B-6}$$

we get

$$V_{A\ell} = \frac{V_{\ell'}\rho_{A\ell}E_{QI}(\lambda)}{L_{\ell}(\lambda)\pi} \tag{B-7}$$

Substituting Eq. (7) back into Eq. (4) and rearranging, we have

$$L_{T+p}(\lambda) = \left(\frac{V_T}{V_\ell}\right)\left(\frac{V_{\ell'}}{V_{A\ell}}\right)\left[\frac{\rho_{A\ell}E_{QI}(\lambda)}{\pi}\right] \tag{B-8}$$

Equation (8) gives the apparent radiance of the target in terms of known or measured quantities. It is obvious from Eq. (8) that the accuracy of radiance calibration depends upon two factors: first, how well $\rho_{A\ell}$ and E_{QI} are known; and second, $L_{\ell}(\lambda)$ remaining spectrally constant. A complete error analysis of M7 scanner signal calibration is planned. Also, a more detailed explanation of radiance calibration and uses of the sun sensor is given in Ref. [7].

Tests and Results. The calibration fixture used to calibrate the M7 scanner is shown in Figure B-1. The lamps used as irradiance standards are 200W General Electric 6.6A/T42/1CL quartz-iodine lamps traceable to similar NBS standards. The reflectance panel was a sheet of flame-sprayed aluminum painted with 3M white paint. To obtain maximal accuracy, the 3M panel was not assumed to be a Lambertian reflector but instead its bidirectional reflectance characteristics were measured and actually integrated over the scanner view angles of interest.

The dimensions shown in Figure B-1 were obtained by analytical methods to provide the maximum uniformity of illumination on the flame-sprayed aluminum panel, and also by the geometrical restraints imposed by the scanner.

---

[7] Hasell, P.G., and L.M. Larsen, Calibration of an Airborne Multispectral Optical Sensor, Report 6400-137-T, Willow Run Laboratories, Institute of Science and Technology, The University of Michigan, Ann Arbor, Sept., 1968.

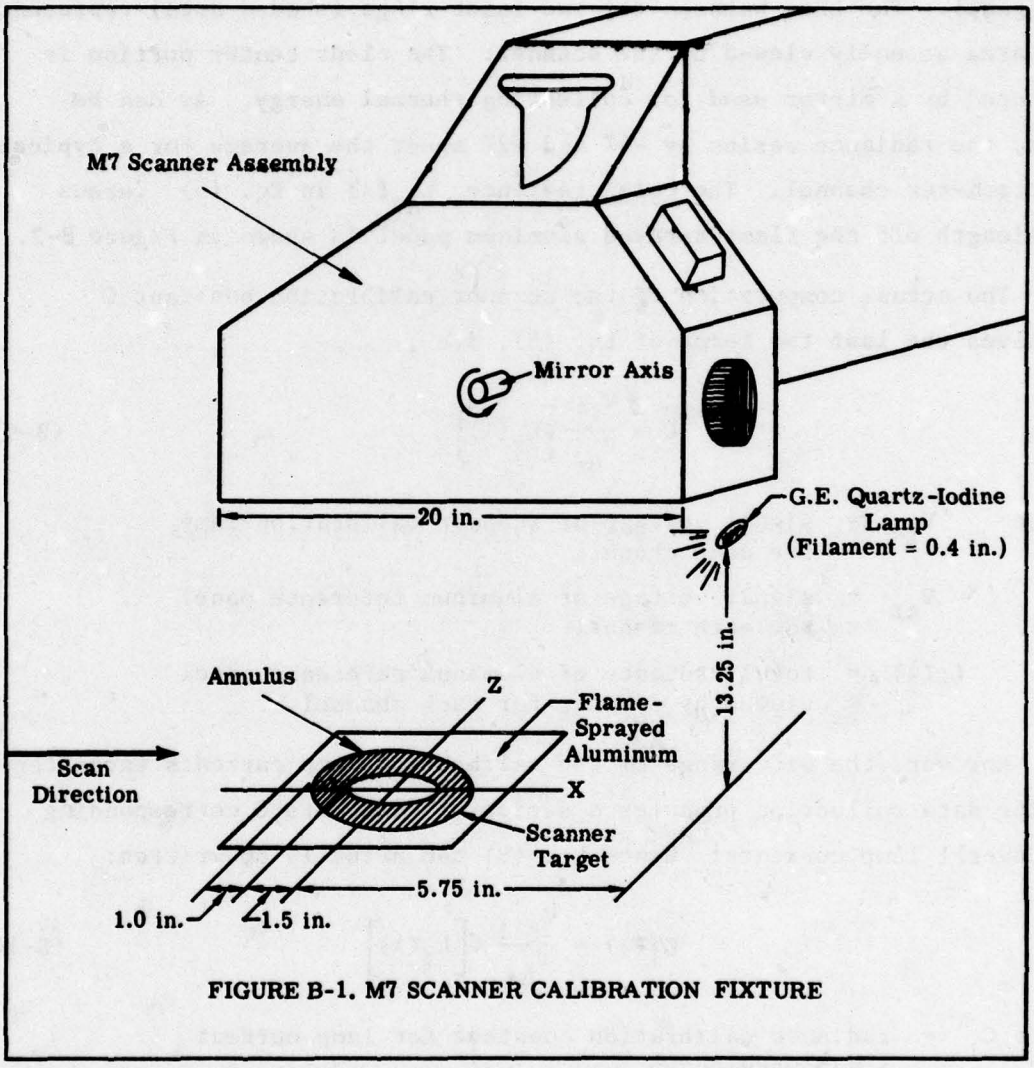

FIGURE B-1. M7 SCANNER CALIBRATION FIXTURE

Figure B-2 shows the result of the integration of the lamp irradiance and panel bidirectional reflectance to give uniform radiance from the panel. In this figure, the average radiance value viewed by the scanner looking perpendicular to the panel was assigned to a value of 100%, and contours of radiance differing by $\pm$1% were plotted over the rest of the panel. The area between the two inner rings (shaded area) represents the area actually viewed by the scanner. The clear center portion is obscured by a mirror used for collecting thermal energy. As can be seen, the radiance varies by -4% and +2% about the average for a typical spectrometer channel. The <u>total</u> radiance $L_{A\ell}(\lambda)$ in Eq. (5) versus wavelength off the flame-sprayed aluminum panel is shown in Figure B-2.

The actual computation of the scanner calibration constant C involves the last two terms of Eq. (8), i.e.,

$$C = \frac{V_{\ell'}}{V_{A\ell}} \left[L_{\ell}(\lambda) \right] \tag{B-9}$$

where $V_{\ell'}$ = signal voltage of scanner calibration lamp for each channel

$V_{A\ell}$ = signal voltage of aluminum reference panel for each channel

$L_{\ell}(\lambda)$ = total radiance of aluminum reference panel viewed by scanner for each channel.

However, the wide range of the calibration lamp currents encountered during data collection produces a series of constants C corresponding to several lamp currents. Hence Eq. (9) can actually be written:

$$C_i(\lambda) = \frac{V_{\ell' i}}{V_{A\ell}} \left[L_{\ell}(\lambda) \right] \tag{B-10}$$

where C_i = radiance calibration constant for lamp current i and wavelength λ.

To obtain the radiance of a terrain object in channel n, the appropriate $C_i(\lambda)$ for channel n at lamp current i is found and multiplied by V_T/V_{ℓ}, i.e.

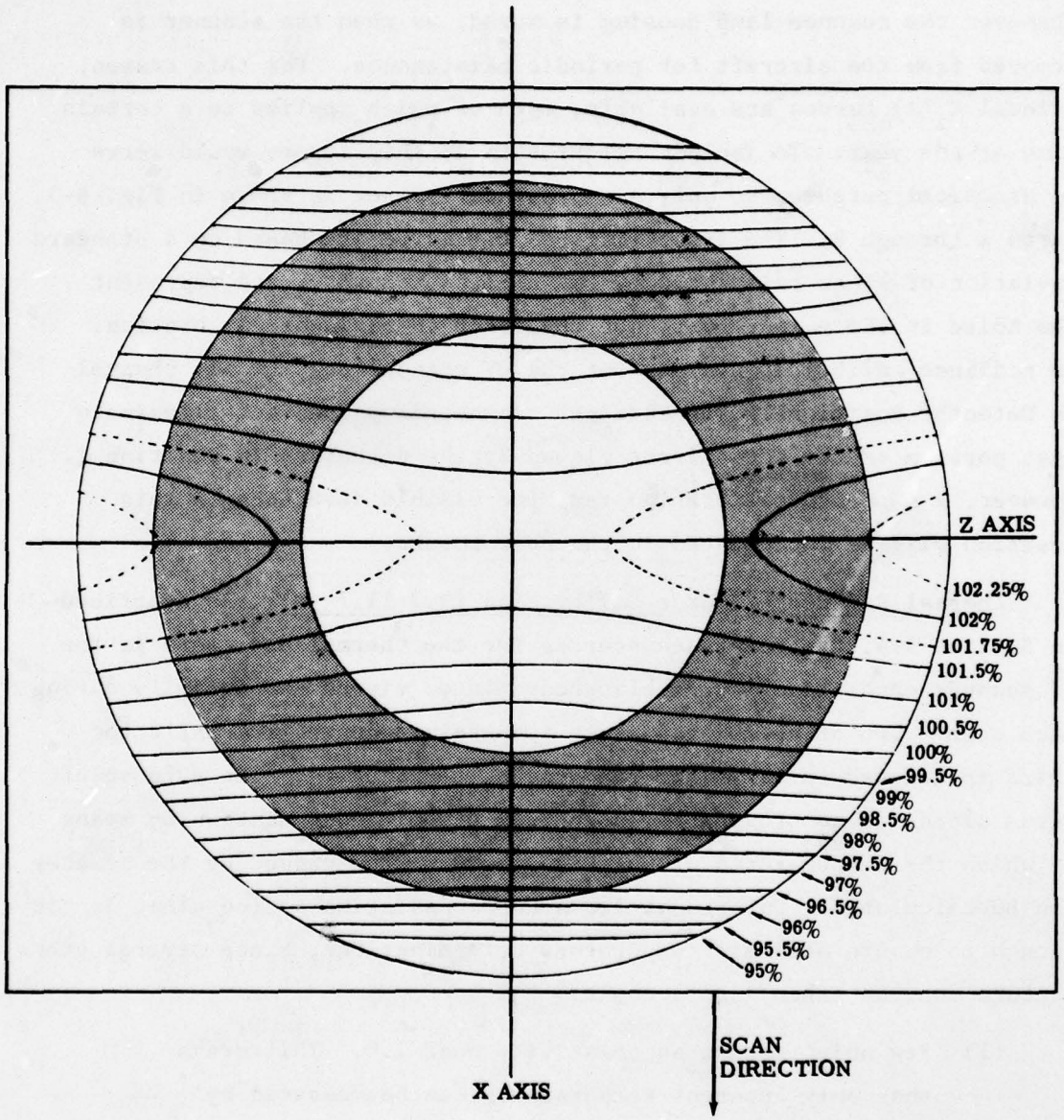

FIGURE B-2. RADIANCE CONTOURS ON M7 SCANNER CALIBRATION REFERENCE PANEL.
View normal to panel as seen by scanner.

$$L_T(\lambda) = C_i(\lambda)\left(\frac{V_T}{V_{\ell,i}}\right) \qquad \text{(B-11)}$$

Several measurements of this constant $C_i(\lambda)$ have shown it to change whenever the scanner lamp housing is moved, as when the scanner is removed from the aircraft for periodic maintenance. For this reason, several $C_i(\lambda)$ curves are available, each of which applies to a certain time of the year. To include all of them in this report would serve no practical purpose, so only a representative set is shown in Fig. B-3 parts a through k. The error flags on the curve are based on a standard deviation of ± 1 as calculated by the digital computer, and represent the noise in the measurement, not the error in radiance calibration. No radiance calibration exists for the UV channel nor for any channel in Detector Position 1B, because the scanner lamp does not illuminate that portion of the scan mirror viewed by the detectors in Position 1. However, a separate calibration lamp for visible detectors in this position will be implemented in the near future.

Thermal Reference Source Calibration (9.3-11.7 μm). As described in Section 4.4, the reference sources for the thermal detectors in the M7 scanner consists of three blackbody plates viewed sequentially during each scan. Two of these plates are temperature-controlled while the third is allowed to vary with the ambient temperature. The purpose of these plates is to provide known sources of emitted radiation by means of which the temperatures of objects viewed on the ground by the scanner can be calculated. Unfortunately, a known radiation source alone is not enough to ensure accurate temperature determinations, since several other factors must be taken into account.

(1) Few objects have an emissivity near 1.0. This means that only apparent temperatures can be measured by an airborne scanner.

(2) The atmosphere through which the radiation from the ground is received absorbs and re-emits some of this radiation. Hence, unless atmospheric corrections are

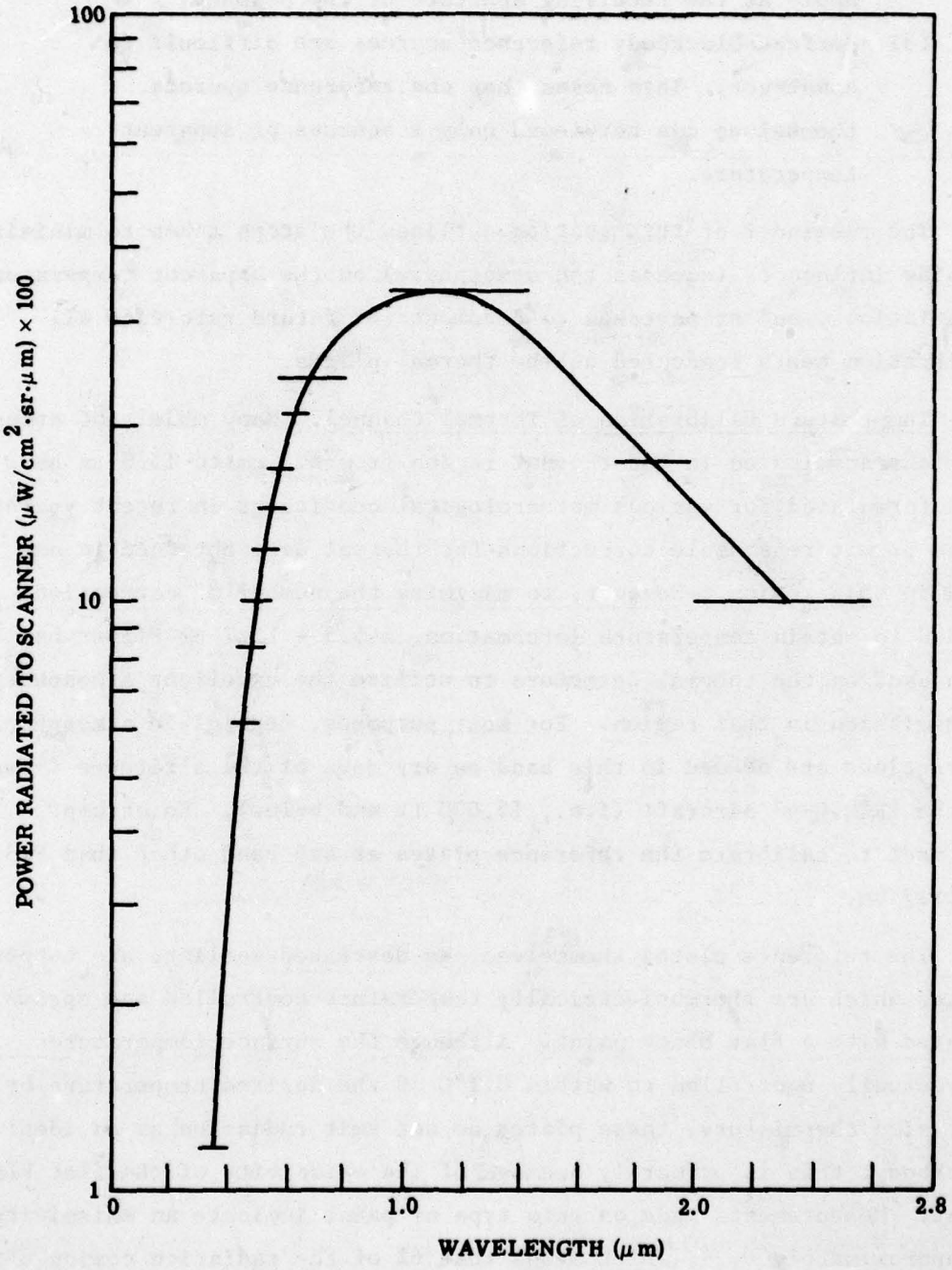

FIGURE B-3. POWER RADIATED TO SCANNER VERSUS WAVELENGTH BANDS

made, the apparent temperature measurements only apply at the receiving aperture of the scanner.

(3) Perfect blackbody reference sources are difficult to construct. This means that the reference sources themselves can be viewed only a sources of apparent temperature.

The remainder of this section outlines the steps taken to minimize outside influences (such as the atmosphere) on the apparent temperature calculations, and steps taken to document for future reference all calibration tests conducted on the thermal plates.

Temperature Calibration of Thermal Channel. Many models of atmospheric transmission in the thermal region from 4.0 μm to 15.0 μm have been formulated for various meteorological conditions in recent years. These permit reasonable corrections for thermal data obtained in any band in this region. However, to minimize the number of corrections needed to obtain temperature information, a 9.3 - 11.7 μm filter has been used on the thermal detectors to utilize the excellent atmospheric transmission in that region. For most purposes, negligible atmospheric corrections are needed in this band on dry days at the altitudes flown by the ERIM C-47 aircraft (i.e., 15,000 ft and below). No attempt was made to calibrate the reference plates at any band other than 9.3 to 11.7 μm.

The reference plates themselves, as described earlier, are copper plates which are thermoelectrically temperature controlled and spray-painted with a flat black paint. Although the surface temperatures are actually controlled to within 0.1°C of the desired temperature by precision thermistors, these plates do not emit radiation as an ideal blackbody; this is primarily because of the emissivity of the flat black paint. Measurements made on this type of paint indicate an emissivity of approximately 0.94, which means that 6% of the radiation coming off a plate is reflected energy. Hence, for any plate temperature other than the surrounding ambient, the apparent plate temperature as seen

by the scanner will be partly dependent on some reflected energy, and will not, in general, agree with the surface temperature as denoted by the thermistor.

Laboratory tests were made on the plates to measure the difference between surface temperatures and apparent temperatures. Strictly speaking, these measurements apply only to the ambient temperature conditions existing in the laboratory (approximately 22°-23°C) at the time of the measurements. However, the apparent temperature of the plates for any surface temperature can be calculated if the ambient temperature in the scanner housing is known. This is the prime reason for having an ambient plate as a reference.

Our measurements utilized YSI (Yellow Springs Instrument Company) precision thermistors imbedded in each plate to control the temperature through a feedback loop. These thermistors are calibrated to $\pm$ 0.1°C over the range -50°C to +100°C. Calibration data giving the temperature vs. resistance relationship is shown in Table B-1. The radiometric temperatures were obtained from a 20° FOV radiometer (Barnes PRT-5) calibrated against high emissivity (0.99) conical blackbodies. The result, shown in Figure B-4, is plotted as dial setting vs. plate temperature, where

$$\text{dial setting} = \frac{\text{thermistor resistance}}{100} \text{ (in ohms)}$$

The dashed curve is the surface temperature as calculated from the thermistors, and the solid and dotted black curves are the apparent temperatures of the two plates. As can be seen, the reference plates are not perfect blackbodies; some correction for their emissivity is needed. The surface temperature curve does not cross the apparent curve at the ambient temperature existing in the lab (~22°C), but instead crosses at approximately 35°C. This is because the radiometer head, being much warmer than the surrounding walls, increases the ambient temperature seen by the plates. The emissivity of the plates as indicated in Figure B-4 is approximately 0.95.

TABLE B-1. TEMPERATURE VERSUS RESISTANCE FOR YSI PRECISION THERMISTOR

TEMPERATURE VERSUS RESISTANCE -50° to +100°C									
TEMP (°C)	RES (Ohms)	TEMP (°C)	RES (Ohms)	TEMP (°C)	RES (Ohms)	TEMP (°C)	RES (Ohms)	TEMP (°C)	RES (Ohms)
-50	201.1K	-20	29.13K	+10	5971	+40	1598	+70	525.4
49	187.3K	19	27.49K	11	5692	41	1535	71	507.8
48	174.5K	18	25.95K	12	5427	42	1475	72	490.9
47	162.7K	17	24.51K	13	5177	43	1418	73	474.7
45	151.7K	16	23.16K	14	4939	44	1363	74	459.0
45	141.6K	15	21.89K	15	4714	45	1310	75	444.0
44	132.2K	14	20.70K	16	4500	46	1260	76	429.5
43	126.5K	13	19.58K	17	4297	47	1212	77	415.6
42	115.4K	12	18.52K	18	4105	48	1167	78	402.2
41	107.9K	11	17.53K	19	3922	49	1123	79	389.3
-40	101.0K	-10	16.60K	+20	3748	+50	1081	+80	376.9
39	94.48K	9	15.72K	21	3583	51	1040	81	364.9
38	88.46K	8	14.90K	22	3426	52	1002	82	353.4
37	82.87K	7	14.12K	23	3277	53	965.0	83	342.2
36	77.66K	6	13.39K	24	3135	54	929.6	84	331.5
35	72.81K	5	12.70K	25	3000	55	895.8	85	321.2
34	68.30K	4	12.05K	26	2872	56	863.3	86	311.3
33	64.09K	3	11.44K	27	2750	57	832.2	87	301.7
32	60.17K	2	10.86K	28	2633	58	802.3	88	292.4
31	56.51K	-1	10.31K	29	2523	59	773.7	89	283.5
-30	53.10K	0	9796	+30	2417	+60	746.3	+90	274.9
29	49.91K	+1	9310	31	2317	61	719.9	91	266.6
28	46.94K	2	8851	32	2221	62	694.7	92	258.6
27	44.16K	3	8417	33	2130	63	670.4	93	250.9
26	41.56K	4	8006	34	2042	64	647.1	94	243.4
25	39.13K	5	7618	35	1959	65	624.7	95	235.2
24	36.86K	6	7252	36	1880	66	603.3	96	229.3
23	34.73K	7	6905	37	1805	67	582.6	97	222.6
22	32.74K	8	6576	38	1733	68	562.8	98	216.1
21	30.87K	9	5265	39	1664	69	543.7	99	200.8
								100	203.8

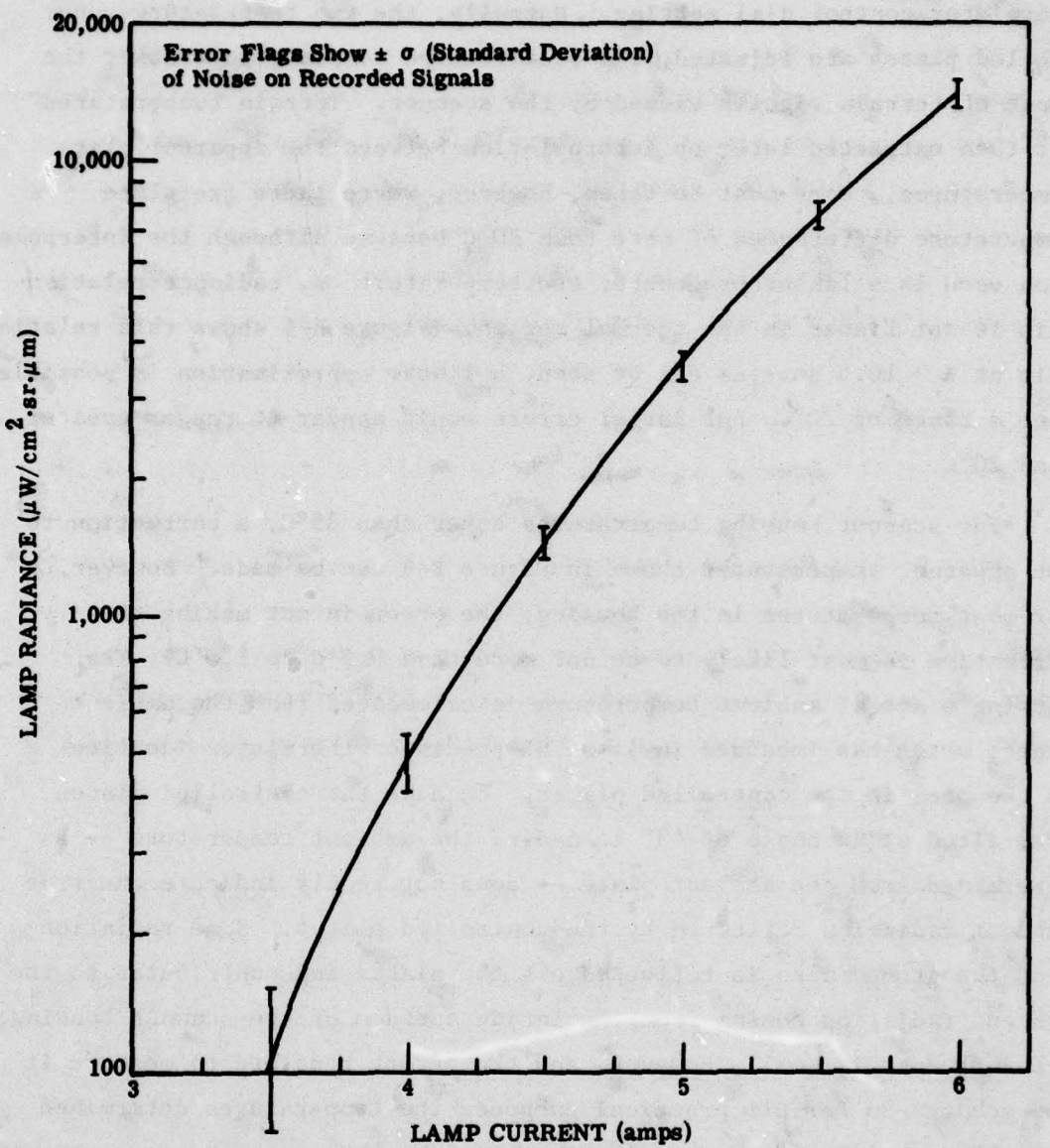

(a) Wavelength: 0.46 to 0.49 μm (C10)

FIGURE B-4. INTERNAL LAMP TRANSFER STANDARD CALIBRATION 1 JUNE TO 30 DECEMBER 1972

To a first approximation and, more exactly, for ambient housing temperatures around 35°C, the curve shown in Figure B-4 can be used to obtain the apparent plate temperature calibration points for any given thermistor control dial setting. Normally, the two temperature-controlled plates are adjusted, via oscilloscope display, to bracket the range of terrain signals viewed by the scanner. Terrain temperatures are then extracted later by interpolation between the apparent plate temperatures. Care must be taken, however, where there are plate temperature differences of more than 20°C because although the interpolation used is a linear procedure, the temperature vs. radiance relationship is not linear in the thermal region. Figure B-5 shows this relationship at X = 10.5 μm. As can be seen, a linear approximation is possible over a range of 20°C, but larger errors would appear at ranges greater than 20°C.

For scanner housing temperatures other than 35°C, a correction to the apparent temperatures shown in Figure B-4 can be made. However, for most temperatures in the housing, the error in not making this correction is most likely to be not more than 0.5°C to 1.0°C. The housing's actual ambient temperature is calculated from the ambient plate, which has imbedded in it a YSI precision thermistor identical to the ones in the controlled plates. Because the controlled plates are tilted at an angle of 45° to nadir, the ambient temperature -- as determined from the ambient plate -- does not really indicate the true ambient radiation reflected by the controlled plates. Some radiation from the ground also is reflected off the plates and contributes to the ambient radiation coming from the inside surface of the scanner housing; its influence is small, however, and the effort required to measure it too great. So far all practical purposes the temperatures determined from the ambient plate are sufficient to make the necessary corrections.

Accuracy Test of Plate Calibration Temperature. As a check on the plate calibration performed in the laboratory, a test utilizing hot and cold water baths was devised to measure the scanner's overall temperature sensitivity and accuracy. Separate plastic ice chests containing

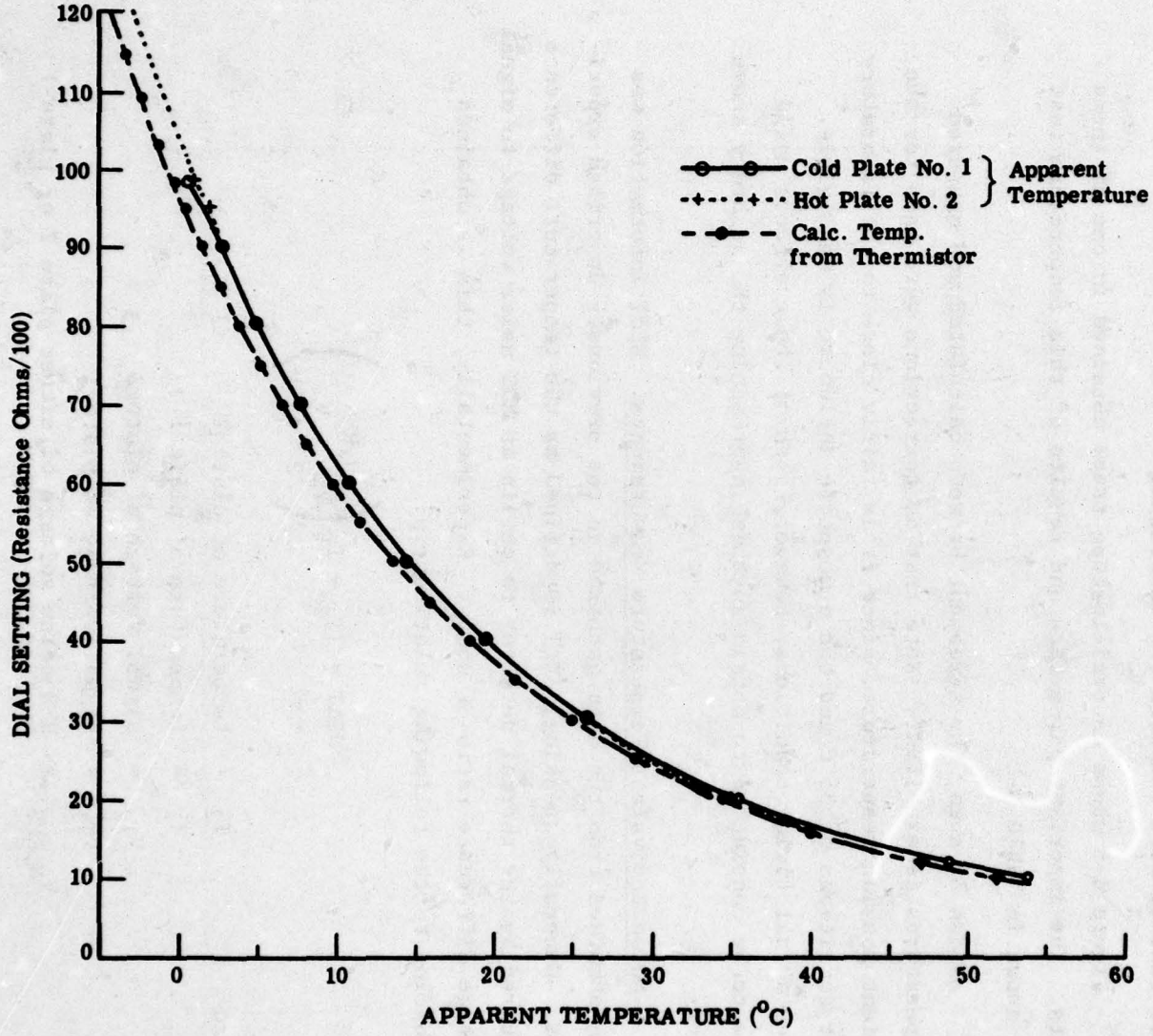

FIGURE B-5. CONTROL PANEL SETTING VERSUS APPARENT TEMPERATURE (JANUARY 1972)

heated and cooled water were placed side by side underneath the aircraft. The temperatures of these water baths were monitored constantly by both a thermometer and a PRT-5 radiometer. With the scanner running, water temperatures were also determined from the reference plates. These three results were compared for closeness.

Figure B-6 shows an oscilloscope trace obtained in one of these tests. The important parameters and results of this temperature test are shown in Table B-2.

As can be seen, the agreement between calculated and measured temperatures is excellent. Note that no corrections were made for the ambient housing temperature, since it is fairly close to the laboratory test conditions of 35°C and the atmosphere influence is negligible. Under actual flying conditions, however, both of these effects would have to be considered to obtain anything approaching the accuracy shown above.

Noise Equivalent Temperature Measurements. NEΔT information was also obtained from the data gathered in the previously described experiment. Generally speaking, NEΔT is defined as the temperature difference required by the thermal detector to obtain an RMS noise voltage to signal voltage difference ratio of unity. Experimentally, this is obtained according to the following relationship:

$$NE\Delta T = (T_2 - T_1)\left(\frac{V_{N,RMS}}{V_{T_2} - V_{T_1}}\right)$$

where
T_2 = temperature of plate 2
T_1 = temperature of plate 1
V_{T_2} = signal voltage of plate 2
V_{T_1} = signal voltage of plate 1
$V_{N,RMS}$ = RMS noise voltage of either plate 2 or plate 1

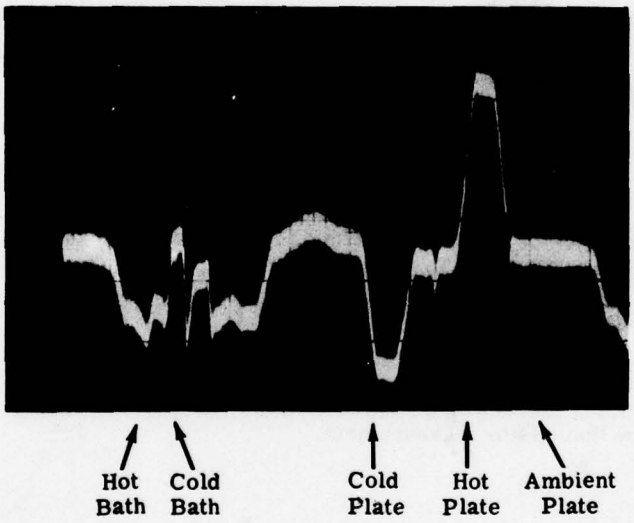

FIGURE B-6. OSCILLOSCOPE TRACE OF 9.3 to 11.7 μm BAND IN M7 SCANNER DURING THERMAL CALIBRATION

TABLE B-2. RESULTS OF THERMAL CALIBRATION TESTS IN 9.3-11.7 μm BAND

Cold plate ref. temp. = 24.1°C*
Hot plate ref. temp. = 33.7°C*
Ambient plate ref. temp. = 28.5°C*

	Thermometer	PRT-5	Scanner
Hot bath	28.3°C	28.3°C	28.4°C
Cold bath	27.2°C	26.9°C	27.2°C
Ambient plate	--		28.1°C

*Obtained by thermistor measurement.

The noise value $V_{N,RMS}$ is, of course, dependent on the electronic bandwidth of the system. More specifically, it varies inversely with the square root of the bandwidth for a flat spectral density condition. For the test case depicted in Figure B-7, the bandwidth was preamplifier-limited to approximately 240 kHz. However, in most cases the system is tape-recorder-limited to approximately 96 kHz. Hence, the actual NEΔT encountered in normal operation is found (from Fig. 38) to be

$$NE\Delta T = 9.6°C \times \frac{0.015\ V}{0.80\ V} \times \frac{\sqrt{96}}{\sqrt{240}}$$

$$NE\Delta T = 0.11°C$$

It should be mentioned that the noise voltage, $V_{N,RMS}$, was obtained from the peak-to-peak noise voltage by assuming a Gaussian noise distribution and a peak factor of 8 dB (which corresponds to peak/RMS ratios of 2.6).

Spectral Calibration. Any attempt to identify an object by its spectral characteristics obviously requires an accurate description of the spectral throughput of the measuring instrument. In the case of the M7 scanner, only the 12-channel spectrometer lends itself easily to this kind of measurement. The detectors used in the other two positions, i.e., near-IR and thermal, use bandpass filters which are an integral part of the detector. Once the filter-detector characteristics are determined (they are well-documented upon purchase), there is little need to measure the spectral characteristics unless, of course, some type of trouble is suspected, such as light leakage, etc. The 12-channel spectrometer, on the other hand, uses light pipes on the output of a dispersing prism to obtain the required bandpasses, and is considerably more subject to vibrations, misalignment, etc. Primarily for this reason, considerable effort is made to maintain an up-to-date spectral calibration.

The spectral calibration of the 12-channel spectrometer was accomplished by mounting the whole scanner assembly, including spectrometer, on a collimator (Figure B-8). The collimator consists of a large, 20-in.

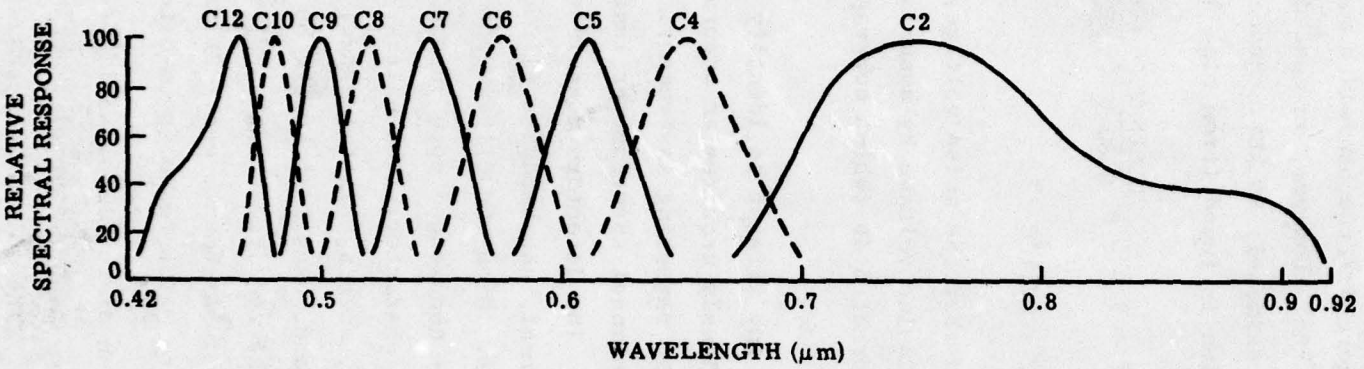

Relative Spectral Response of M7 Spectrometer

FIGURE B-7. COLLIMATOR FOR SPECTRAL CALIBRATION OF THE 12-CHANNEL SPECTROMETER

AD-A074 799 ENVIRONMENTAL RESEARCH INST OF MICHIGAN ANN ARBOR IN--ETC F/G 17/5
STUDY AND INVESTIGATION OF INFRARED MULTISPECTRAL TARGET CUEING--ETC(U)
JUN 79 S R STEWART, J L BEARD DAAK70-77-C-0203
UNCLASSIFIED ERIM-131500-9-F NL

2 OF 2
AD
AO 74 799

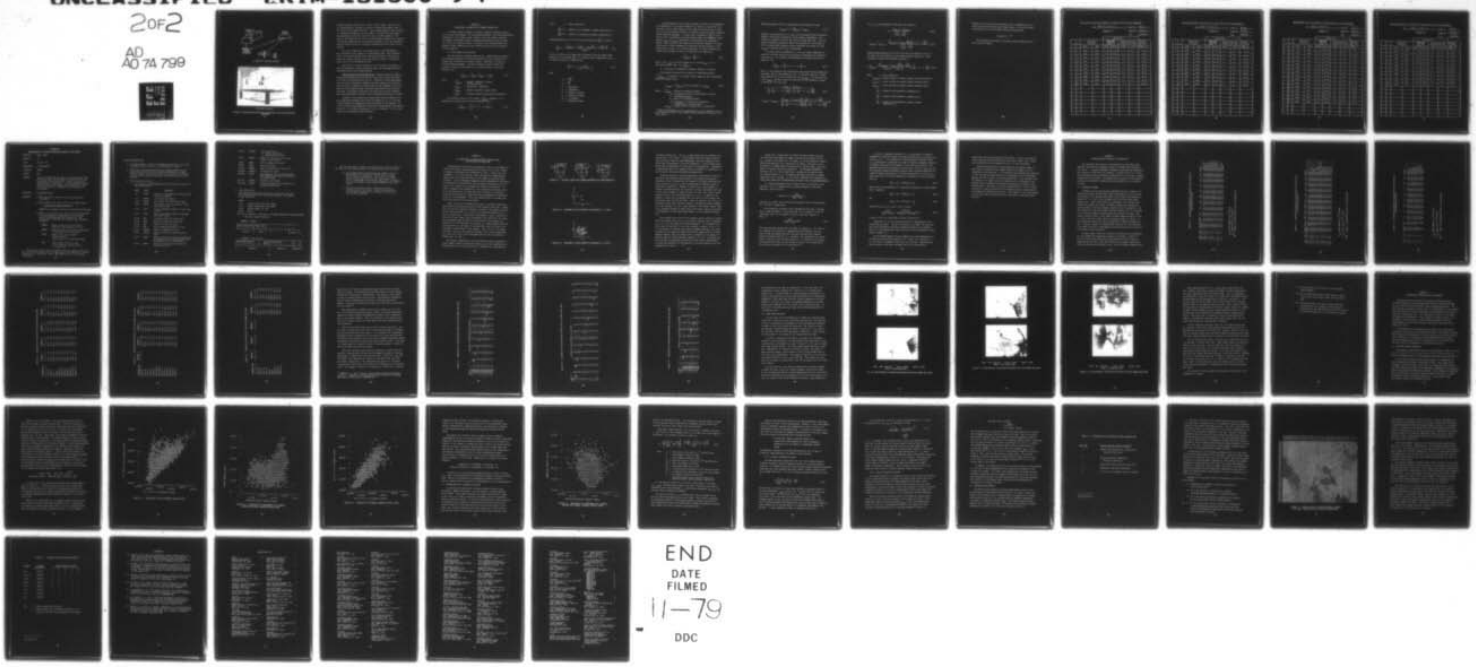

END
DATE FILMED
11-79
DDC

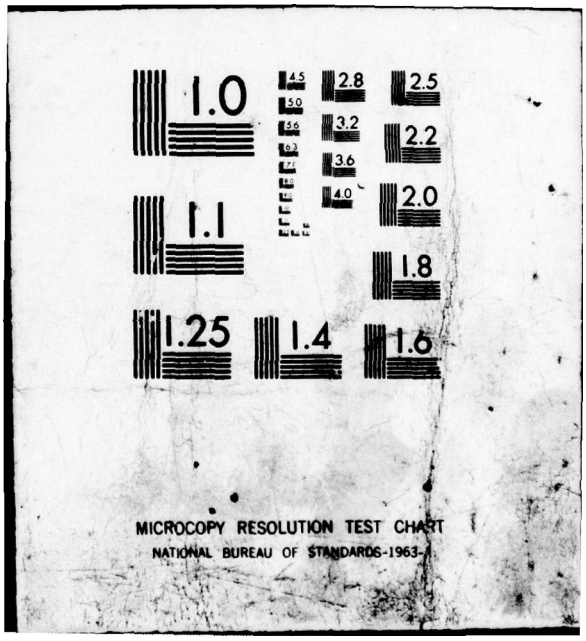
1.0
1.1
1.25
1.4
1.6
1.8
2.0
2.2
2.5
2.8
3.2
3.6
4.0
4.5
5.0
5.6
6.3
MICROCOPY RESOLUTION TEST CHART
NATIONAL BUREAU OF STANDARDS-1963-A

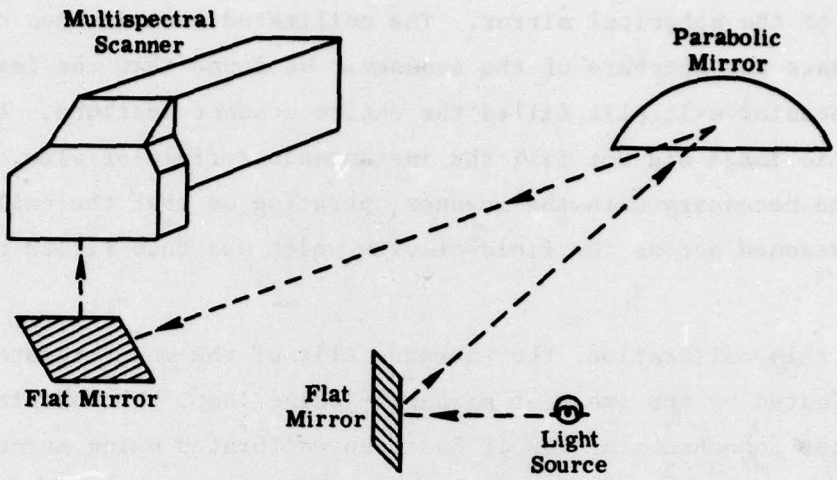

(a) Schematic of Collimator Assembly

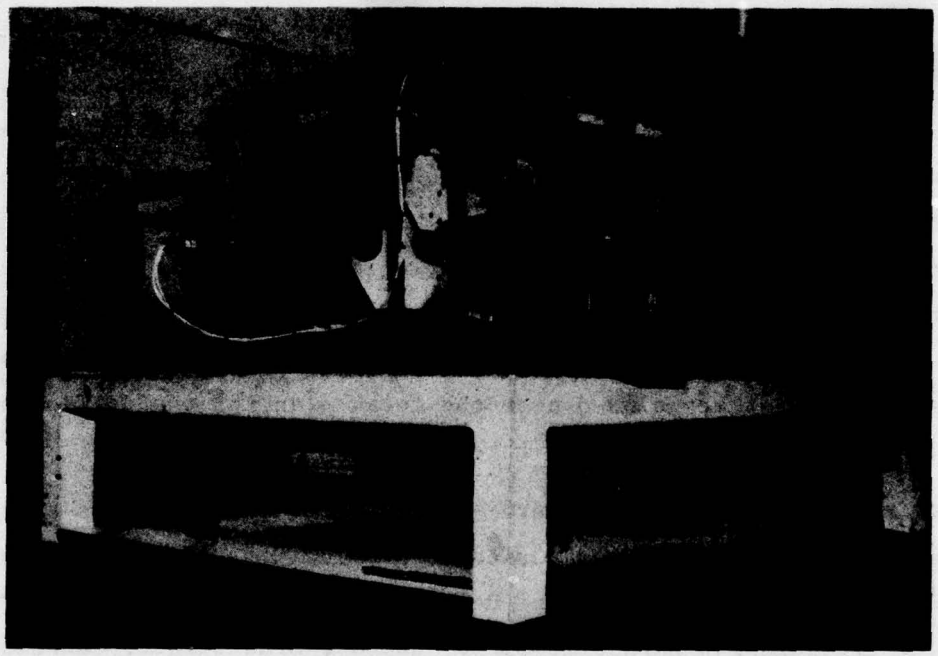

(b) Laboratory Collimator

FIGURE B-8. COLLIMATOR FOR SPECTRAL CALIBRATION OF THE 12-CHANNEL SPECTROMETER

diameter parabolic mirror with a 100-in. focal length. The exit slit of a monochromator, serving as a source of known wavelengths, sits at the focus of the spherical mirror. The collimated beam is then directed to illuminate the aperture of the scanner. We found that the image of the monochomator exit slit filled the entire scanner aperture. But because this image did not fill the instantaneous field-of-view, calibration became necessary with the scanner operating so that the collimated beam was scanned across the field-of-view which was thus filled on the average.

For this calibration, the entrance slit of the monochromator was illuminated by the image of a quartz-iodine lamp. The wavelength scale of the monochromator itself had been calibrated using mercury, potassium, sodium, cadmium, and cesium spectral lamps, a helium-neon laser, and various narrowband filters.

The relative spectral response of the 12-channel spectrometer is shown in Figure B-8. Unless otherwise noted, all wavelength bands are described by their 10% response points.

Spatial Resolution and Registration. Spatial resolution measurements were performed on the M7 scanner using the collimator described in Section 4.2 and pictured in Fig. 17. Purposes of these measurements were not only to verify the spatial resolution against its calculated value but also to provide an overall check on the alignment of the components in the optical system, including registration in all detector positions. The targets placed near the focal plane of the collimator were blackened panels, each with three rectangular holes near its center.

A number of such targets were constructed with the widths of the holes and spacing between them varied to provide 0.5, 1, 2, 4, 10 and 20 mrad targets for imaging in the detector plane of the scanner. For a 100-in. focal length parabolic mirror and a 2-mrad target, calculations show that a hole width and spacing of 0.2 in. is needed. All the other targets were dimensioned proportionately.

APPENDIX C

TEMPERATURE CALIBRATION OF THERMAL SCANNER DATA

A thermal scanner responds to radiance differences between objects in the scene being mapped. The intervening atmosphere and optical/mechanical components in the scanner itself, however, alter the signals received in a manner which makes absolute temperature calibration difficult without the aid of reference sources. Procedures for obtaining ground and apparent target temperatures using reference sources will be developed in this appendix.

A. Basic Radiation Principles

The raw electrical signals generated by a thermal detector mounted in an airborne scanner are linearly proportional to the radiance (not temperature) emitted by the observed target - modified, of course by an intervening atmosphere. The basic expression which relates the radiance received by the scanner to the target radiance is given in Equation (C-1).

$$L_{\text{scanner}}^{(\lambda)} = \tau_{\text{atmos}}^{(\lambda)} L_{\text{target}}^{(\lambda)} + L_{\text{path}}^{(\lambda)} \qquad \text{(C-1)}$$

where

$L_{\text{scanner}}^{(\lambda)}$ = apparent radiance at scanner entrance aperture

$L_{\text{atmos}}^{(\lambda)}$ = atmospheric transmission

$L_{\text{target}}^{(\lambda)}$ = radiance emitted by ground target

$L_{\text{path}}^{(\lambda)}$ = radiance emitted by intervening atmosphere

The radiance emitted by the target, $L_{\text{target}}^{(\ )}$, depends on its temperature and emissivity as shown in Equation (C-2).

$$L_{\text{target}}^{(\lambda)} = \varepsilon L_{BB}^{T_T}(\lambda) + (1 - \varepsilon) L_{BB}^{T_a}(\lambda) \qquad \text{(C-2)}$$

where ε = target emissivity

$L_{BB}^{T_T}(\lambda)$ = radiance of a blackbody at target temperature T_T

$L_{BB}^{T_a}(\lambda)$ = radiance of blackbody at ambient temperature T_a

Combining equations (C-1) and (C-2) and solving for $L_{BB}^{T_T}(\lambda)$ we get:

$$L_{BB}^{T_T}(\lambda) = \frac{L_{scanner}^{(\lambda)} - L_{path}^{(\lambda)} - \tau_{atmos}\left\{(1-\varepsilon)\, L_{BB}^{T_a}(\tau)\right\}}{\varepsilon\, \tau_{atmos}} \qquad \text{(C-3)}$$

If all the terms on the right side of Equation (C-3) are known (thus enabling us to determine $L_{BB}^{T_T}(\lambda)$), then the target temperature T_T can be found from Planck's radiation law.

$$L_{BB}^{T_T}(\lambda) = \frac{C_1}{\lambda^5 \left(C_2/(\lambda T_T) - 1\right)} \qquad \text{(C-4)}$$

where

$C_1 = \frac{2hc^2}{\Omega_o}$

$C_2 = \frac{hc}{k}$

λ = wavelength

T_T = temperature

h = Planck's constant

c = velocity of light

Ω_o = 1 steradian

k = Boltzman constant

Although Equation (C-3) gives an explicit solution for determining the temperature of any target viewed by the scanner, in practice it is not easy to solve since several of the terms on the right side of Equation (C-3) are extremely difficult to measure accurately without elaborate ground teams and equipment. In most cases, estimates of $L_{BB}^{T_a}(\lambda)$ and ϵ are all that is available for ground targets while the atmospheric parameters τ_{atmos} and L_{path} usually must be determined from atmospheric models. The accuracy of the temperature calculation depends, of course, on how many of these parameters are available and how accurately this information is known. For rough calculations, an ideal atmosphere and target can be assumed in which case Equation (C-3) reduces to:

$$L_{scanner}^{(\lambda)} = L_{BB}^{T_T}(\lambda) \qquad \text{(C-5)}$$

where ϵ and τ_{atmos} have been assumed to be 1.0 and $L_{path}(\lambda) = 0$. The final unknown, then, is $L_{scanner}^{(\lambda)}$.

B. Calculation of Radiance at Entrance Aperture of Scanner

The radiance received by the scanner's collecting aperture, $L_{scanner}^{(\lambda)}$, is related to the scanner output signal by the relationship given in Equation (C-6).

$$V_{target} = L_{scanner}^{(\lambda)} (\Omega^2)(\Delta\lambda)(A_c)(R)(\tau) + V_{offset} \qquad \text{(C-6)}$$

where $L_{scanner}^{(\lambda)}$ = radiance received by scanner

Ω = instantaneous field of view (IFOV) of scanner

$\Delta\lambda$ = wavelength bandpass

A_c = area of collecting aperture

R = responsivity of detection (volts/watt)

τ = transmission of scanner optics

V_{offset} = voltage offset in system due to electronics*

*Due to the preamplifiers and postamplifiers, power supplies, etc. in the scanner electronics, zero radiance input usually will not give zero volts output.

Rewriting Equation (C-6) by combining all the constants, we get:

$$V_{target} = k\, L^{(\lambda)}_{scanner} + V_{offset} \qquad \text{(C-7)}$$

Normally, the quantities Ω, $\Delta\lambda$, and A_c can be measured quite accurately. However, the detector resonsivity R and scanner transmission τ are difficult to measure and both can (and do) change with time. For this reason, blackbody calibration plates are inserted into the scanner's FOV to provide known radiance sources from which the values of k and V_{offset} in Equation (C-7) can be determined.

In truth, perfect blackbodies ($\varepsilon = 1.0$) are almost impossible to construct and what really are constructed are greybodies with emissivities near 1.0. The radiance from greybody has already been given by Equation (C-2).

$$L^{(\lambda)}_{target} = \varepsilon L^{T_T}_{BB}(\lambda) + (1 - \varepsilon)\, L^{T_a}_{BB}(\lambda) \qquad \text{(C-2)}$$

Hence, if the reference plat emissivities and scanner housing temperature are known, then by using Equation (C-2) and two known sources of radiation, Equation (C-7) can be solved for k and V_{offset}. The solutions for k and V_{offset} (obtained using two equations and two unknowns) is given in Equations (C-8) and (C-9).

$$k = \frac{V_{plate\ 1} - V_{plate\ 2}}{\left\{\varepsilon_1 L^{T_1}_{BB} + (1 - \varepsilon_1) L^{T_a}_{BB}\right\} - \left\{\varepsilon_2 L^{T_2}_{BB} + (1 - \varepsilon_2) L^{T_a}_{BB}\right\}} \qquad \text{(C-8)}$$

$$V_{offset} = V_{plate\ 1} - \frac{\left(V_{plate\ 1} - V_{plate\ 2}\right)\left(\varepsilon_1 L^{T_1}_{BB} + (1 - \varepsilon_1) L^{T_a}_{BB}\right)}{\left\{\varepsilon_1 L^{T_1}_{BB} + (1 - \varepsilon_1) L^{T_a}_{BB}\right\} - \left\{\varepsilon_2 L^{T_2}_{BB} + (1 - \varepsilon_2) L^{T_a}_{BB}\right\}} \qquad \text{(C-9)}$$

If $\varepsilon_1 = \varepsilon_2$, then Equations (C-8) and (C-9) reduce to

$$k = \frac{V_{plate\ 1} - V_{plate\ 2}}{\varepsilon\left(L_{BB}^{T_1} - L_{BB}^{T_2}\right)} \qquad \text{(C-10)}$$

$$V_{offset} = V_{plate\ 1} - \frac{\left(V_{plate\ 1} - V_{plate\ 2}\right)\left(\varepsilon\, L_{BB}^{T_1} + (1 - \varepsilon)\, L_{BB}^{T_a}\right)}{\varepsilon\left(L_{BB}^{T_1} - L_{BB}^{T_2}\right)} \qquad \text{(C-11)}$$

Substituting Equations (C-10) and (C-11) back into Equation (C-7), we can solve for the radiance at the scanner entrance aperture in terms of scanner voltages and blackbody radiances.

$$L_{scanner}^{(\lambda)} = \frac{\varepsilon\left(V_{scanner} - V_{plate\ 1}\right)\left(L_{BB}^{T_1} - L_{BB}^{T_2}\right)}{\left(V_{plate\ 1} - V_{plate\ 2}\right)} + \left(\varepsilon\, L_{BB}^{T_1} + (1 - \varepsilon)\, L_{BB}^{T_a}\right) \qquad \text{(C-12)}$$

where ε = plate emissivity

$V_{scanner}$ = output voltage of scanner viewing collecting aperture

$V_{plate\ 1}$ = output voltage of scanner viewing reference plate 1

$V_{plate\ 2}$ = output voltage of scanner viewing reference plate 2

$L_{BB}^{T_1}$ = radiance from blackbody at temperature T_1

$L_{BB}^{T_2}$ = radiance from blackbody at temperature T_2

$L_{BB}^{T_a}$ = radiance from blackbody at scanner housing temperature T_a

Equation (C-12) can be used in Equation (C-1) or Equation (C-5) to obtain the desired ground target temperatures. For the M7 scanner, the emissivity of the calibration plates is shown below:

$$\varepsilon_{emissivity} = .95$$

The following tables show the reference plate temperatures for all of the NVL images.

MULTISPECTRAL SCANNER CALIBRATION LOG FOR MISSION

Site Camp A.P. Hill, Va. Flight No. NVL #1

TABLE C-1

Flight Date 3/28/78

Time 2330 EST

Line	Run	Time, G.m.t., hr:min:sec		Scanner No. 1 Black Body Reference Temp.. °C		Radiation Reference Lamp Current, Amps		Ambient Blackbody Temp °C
		Start	Stop	Plate 1	Plate 2	Lamp 1	Lamp 2	Plate #3
1	1	0522	0523	4.02	9.90	2.4	3.0	15.48
	2	0534	0535	4.02	9.90	2.4	3.0	15.87
	3	0541	0542	4.02	9.90	2.4	3.0	17.46
	4	0547	0548	4.02	9.90	2.4	3.0	19.25
	5	0551	0552	4.02	9.90	2.4	3.0	20.54
	6	0555	0556	4.02	9.90	2.4	3.0	21.32
	7	0559	0600	4.02	9.90	2.4	3.0	21.70
	8	0608	0609	4.02	9.90	2.4	3.0	21.19
	9	0614	0615	4.02	9.90	2.4	3.0	21.10
	10	0620	0621	4.02	9.90	2.4	3.0	22.06

MULTISPECTRAL SCANNER CALIBRATION LOG FOR MISSION

Site Camp A.P. Hill, Va. Flight No. NVL #2

TABLE C-2 Flight Date 3/29/78

Time 1830 EST

Line	Run	Time, G.m.t., hr:min:sec		Scanner No. 1 Black Body Reference Temp.. °C		Radiation Reference Lamp Current, Amps		Ambient Blackbody Temp. °C
		Start	Stop	Plate 1	Plate 2	Lamp 1	Lamp 2	Plate 3
1	1	0009	0010	6.15	11.35	1.7	3.0	11.78
	2	0016	0017	6.15	11.35	1.7	3.0	11.51
	3	0022	0023	6.15	11.35	1.7	3.0	13.34
	4	0027	0028	6.15	11.35	1.7	3.0	14.94
	5	0032	0033	6.15	11.35	1.7	3.0	16.29
	6	0037	0038	6.15	11.35	1.7	3.0	17.67
	7	0042	0043	6.15	11.35	1.7	3.0	18.69
	8	0050	0051	6.15	11.35	1.7	3.0	18.33
	9	0057	0058	6.15	11.35	1.7	3.0	17.97
	10	0102	0103	6.15	11.35	1.7	3.0	18.45

MULTISPECTRAL SCANNER CALIBRATION LOG FOR MISSION

Site Camp A.P. Hill, Va. Flight No. NVL #3

TABLE C-3 Flight Date 3/30/78

Time 0930 EST

Line	Run	Time, G.m.t., hr:min:sec		Scanner No. 1 Black Body Reference Temp.. °C		Scanner No. 1 Radiation Reference Lamp Current, Amps		Ambient Blackbody Temp. °C
		Start	Stop	Plate 1	Plate 2	Lamp 1	Lamp 2	Plate 3
1	1	1525	1526	7.32	14.62	2.3	6.0	1.99
	2	1533	1534	7.32	14.62	2.2	6.0	2.38
	3	1540	1541	7.32	14.62	2.2	6.0	3.48
	4	1544	1545	7.32	14.62	2.2	6.0	4.49
	5	1548	1549	5.05	14.62	2.2	6.0	5.32
	6	1552	1553	4.02	18.57	2.2	6.0	6.14
	7	1556	1557	3.04	20.90	2.2	6.0	6.79
	8	1602	1603	3.04	20.90	2.2	6.0	7.24
	9	1608	1609	3.04	20.90	2.2	6.0	7.14
	10	1613	1614	3.04	20.90	2.2	6.0	7.75
	11	1620	1621	3.04	20.90	2.2	6.0	8.39
	12	1638	1639	3.04	20.90	2.2	6.0	8.00
	13	1642	1643	3.04	20.90	2.2	6.0	7.59
	14	1649	1650	3.04	20.90	2.0	6.0	7.43
	15	1657	1658	3.04	20.90	2.0	6.0	6.91

MULTISPECTRAL SCANNER CALIBRATION LOG FOR MISSION

Site Camp A.P. Hill, Va. Flight No. NVL #4

TABLE C-4 Flight Date 3/30/78

Time 1330 EST

Line	Run	Time, G.m.t., hr:min:sec		Scanner No. 1 Black Body Reference Temp., °C		Radiation Reference Lamp Current, Amps		Ambient Blackbody Temp. °C
		Start	Stop	Plate 1	Plate 2	Lamp 1	Lamp 2	Plate 3
1	1	1858	1859	2.12	23.54	2.2	6.0	6.07
	2	1904	1905	2.12	23.54	2.2	6.0	6.07
	3	1909	1910	2.12	23.54	2.2	6.0	6.91
	4	1913	1914	2.12	23.54	2.2	6.0	8.45
	5	1918	1919	2.12	23.54	2 2	6.0	10.37
	6	1922	1923	2.12	23.54	2.2	6.0	11.04
	7	1926	1927	2.12	23.54	2.2	6.0	11.78
	8	1931	1932	2.12	23.54	2.2	6.0	12.05
	9	1936	1937	2.12	23.54	2.2	6.0	11.63
	10	1940	1941	2.12	23.54	2.2	6.0	11.93

APPENDIX D

DOCUMENTATION OF COMPUTER COMPATIBLE MAGNETIC TAPE FORMAT

ROUTINES: IMSS; OMSS

VERSION: 1.0

DATE: May 23, 1977

PROGRAMMER: J. Morgenstern

LANGUAGE: XTRAN

SYSTEM: MTS

PURPOSE: Input and Output FSR to support multivariate data files on both mag tape and disc where the number of bits per data value is a multiple of 8: 8 bits, 16 bits and 32 bits/value are available. It also supports variable length ancillary data fields at the beginning of each scan line, as well as packing the data by pixels or by channels.

INTERFACE: 11LINE/QLINE System

COMMENTS:

1) IMSS can only be used to read data files written using OMSS.

2) The ancillary data is stored in a new common block:

```
COMMON/QANCIL/QHDNUM,QHEAD(200)
```

(QHDNUM is the number of bytes of ancillary information)

3) OMSS, at the present time, takes on the responsibility for ascertaining the parameters which define the manner in which the data are written out. The routine uses a NAMELIST I/O to request the following variables:

QOBYTE	:	Number of bytes to use to output each data value (may be 1, 2 or 4)
QOHEAD	:	Number of bytes of ancillary information at beginning of each scan line.
INTER	:	.TRUE. Write out as channel interleaved data .FALSE. Write out channel by channel
TAPE	:	.TRUE. Output will go on tape .FALSE. (default) output will go to disc file.

If the input data is read using I8BIT, then the default values for the first three parameters will be those used on the input data. If the input data is in some other format, the defaults are 1, 0, and TRUE, respectively.

SYSTEM CONSIDERATIONS

A. New common blocks: QANCIL and QIØPAR were defined. The values in QIØPAR should eventually be incorporated in QINCOM.

B. OMSS keeps track of the maximum line length available on the output device (32767 bytes to MTS disk, 3000 bytes to tape). When the output line is longer than this maximum, it is broken up into several pieces and multiple records per scan line are written.

C. File Definition (Format)

A. First record is TITLE/HEADER record (it largely follows the 7094 TITLE BLOCK).

Bytes	Name	Function
1-4	NSIZE	Number of bytes needed for input buffer (scan line length)
5-8	QREEL	(for multi-tape files)
9-12	QFILE	File number (for multi-file tapes)
13-16	DLINE	Digital data set line number of first scan line in file
17-20	QNSA	Sensor (permanent) number of first line in file
21-24	QNSB	Sensor (permanent) number of presumed last line in file
25-28	QKS	Line skip factor for stored data
29-32	QNSS	Number of pixels per scan line
33-36	QNA	Number of first scan point
37-40	QKP	Point numbering increment of data
41-44	QNCHAN	Number of channels of data
45-48	QBYTES	Number of bytes per individual data value
49-52	QHEAD	Number of bytes of ancillary information at beginning of scan line [multivariate data begins at byte (16+QHEAD)+1]
53-56	QRECS	Number of records used to store one scan line of data

57-60	QINTER	Interleaved flag: 0 channel interleaved 1 data stored by pixels
61-64	QUNITS	Number of individual data values stored in each record
65-68	DGEN	Data set generation number
69-76	DATE	Date of data set
77-140	SPARE	(Extra locations for future use)
141-260	QTITLE1	120 character title
481-600	QLIST	120 character list of modules which have modified this data (6 characters per module name)
601-720	TITLE2	Auxiliary title block
721-1440	TANCIL	Free-form ancillary data block to be further defined later

B. Scan Line Format

The remaining records in the file are scan lines, with each scan line written in QREC consecutive records. The format of any record is:

Bytes

1-4	Digital (data set) line number
5-8	Sensor (permanent) line number
9-12	Record number for this
13-16	Blank

[if this is record 1, then bytes 17 through (QHEAD+16) ancillary data]

The data follows from here.

QINTER = 0 means:

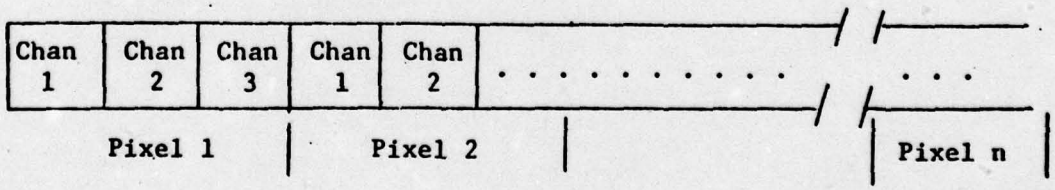

QINTER = 1 is the case:

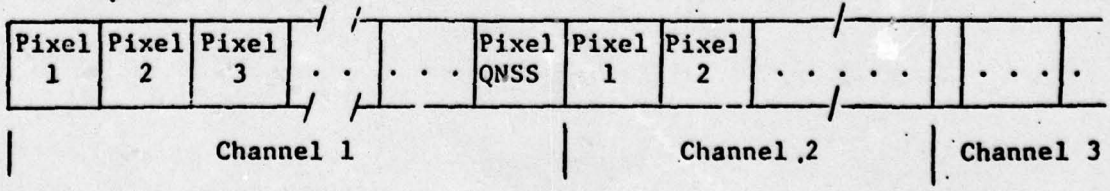

When the data must be written out using several physical records per scan line (a logical record), the following rules are observed:

a) All records written contain the same number of bytes, NSIZE (which is a multiple of 180 so that the tapes may be read on any machine). The records are padded with trailing zeros after the last data value on each record. The number of data units (one pixel, one channel) per record is given in the variable QUNITS in the title block.

b) The data are broken between successive records at a boundary between data units: pixels (if the data are stored channel interleaved) or channels (if the data are stored by channels).

APPENDIX E

AN INTRODUCTION TO MULTISPECTRAL CLASSIFICATION AND RECOGNITION PROCESSING

Multispectral classification essentially consists of deciding the class of the object being observed on the basis of its color. While the human eye utilizes three dimensions of color -- value, hue, and intensity -- for classification, other multispectral classification systems may use as many dimensions as the number of spectral bands observed. In the following paragraphs a brief discussion of the theory of multispectral classification and recognition processing, as it relates to the outputs of a multispectral scanner, is presented. In order to simplify the explanation of the recognition processing, much of the discussion will be presented first in terms of two spectral bands and the extension to many bands will be explained at appropriate points in the development. Also, for simplification, we assume that only three materials are being scanned.

First, then, let us consider the nature of two-band scanner data which would be obtained from each of three separate materials. Suppose that the spectral radiation intensity received at the scanner from each of the three materials, A, B, and C, is as shown by Figures E-1a, 1b, and 1c, respectively. The specific wavelengths λ_1 and λ_2 indicated on each of the three figure parts correspond to the centers of the respective wavelength bands covered by the two bands of the scanner, and therefore, for each material, the response of a given scanner band will be proportional to the height of the material's spectral curve at the wavelength corresponding to that channel. Thus, if u_1 is the signal from band 1 and u_2 is the signal from band 2, the relative magnitudes of u_1 and u_2 for each of the three materials will be as indicated in Figures E-1a, 1b, and 1c.

The scanner responses for the three materials may be presented in a more compact form by considering u_1 and u_2 as the two components of a two-dimensional vector and plotting the coordinates for each material

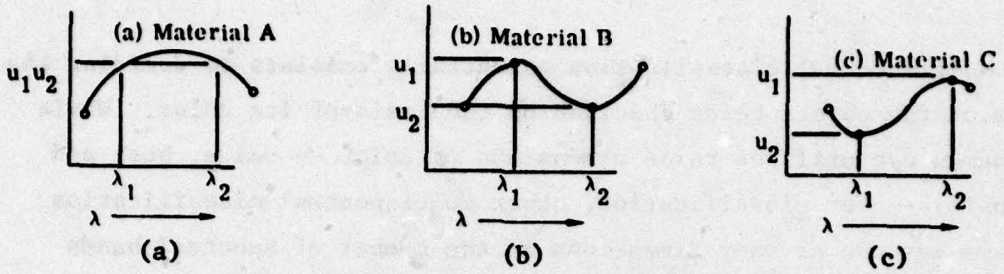

FIGURE E-1. SPECTRAL CURVES AND SCANNER RESPONSES FOR THREE MATERIALS

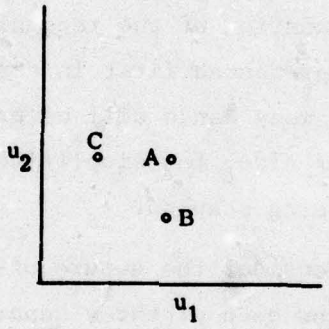

FIGURE E-2. RESPONSES OF TWO CHANNELS FOR MATERIALS A, B, AND C

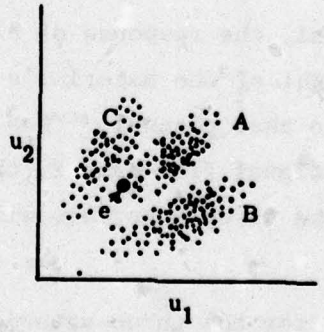

FIGURE E-3. RESPONSES TO MANY SAMPLES OF MATERIALS A, B, AND C

as shown in Figure E-2. The u_1, u_2 plane shown will be referred to as signal space or "u" space. If the scanner had three bands instead of two, this space would be three-dimensional, with the response of the third band corresponding to the third dimension. If the scanner had n bands, the corresponding "u" space would be n-dimensional. Although an n-dimensional space for n greater than 3 is difficult to visualize, it may be easily described and handled mathematically.

Actually, because of various statistical fluctuations in the properties of the materials being scanned, the intensity and spectral properties of the illumination, the scanner's look angle and other factors, the plot of u_1 vs. u_2 will not generally be distinct points as indicated in Figure E-2. Instead, if points for a large number of samples of these materials are plotted in u space, the points will tend to form three clusters as shown in Figure E-3 with each cluster corresponding to one of the three materials, A, B, or C. In general, the density of points will be greater near the center of each cluster and will become very low near the edge. Also, the clusters will tend to be elliptical rather than circular because of correlation between changes in u_1 and changes in u_2 for a given material. This means, simply, that if u_1 increases because of some natural occurrence, such as an increase of illumination on the scene being scanned, u_2 will probably increase also.

The problem to be solved by the processor may be stated as follows: "Given any sample point on the u_1, u_2 plane, from what type of material, A, B, or C, was the sample most likely obtained?" If the sample point falls near the centroid of one of the clusters of points for A, B, or C, the decision is obvious; the material probably belongs to the class indicated by the group near whose centroid the sample point is located. Suppose, however, that the sample point is located at e in Figure E-3 and thus does not clearly belong to either A, B, or C. A decision can still be made by comparing the densities (also called "likelihoods") of points from material A, from material B, and from material C in the neighborhood of point e.

Assume that a large strip of terrain has been scanned, and that the resulting large number of sample points has been plotted in the u_1, u_2 plane as in Figure E-3. Let $D_A(u_1, u_2)$ be the density of sample points from material A as a function of u_1 and u_2, let $D_B(u_1, u_2)$ be the density of sample points from material B, and let $D_C(u_1, u_2)$ be the density of sample points from material C. The "maximum likelihood" decision rule is to decide that point e belongs to the material with the largest density at e. The maximum likelihood principle is highly respected in its own right. It can also be justified as a Bayesian decision with equal prior probabilities and equal costs of misclassification.

In a target-background type of decision rule, the density of one material, say A, is compared with a composite density of the other materials, and the rule is

$$\text{decide on A if } \frac{K_A D_A}{K_B D_B + K_C D_C} > 1$$

where K_A, K_B, and K_C are the relative frequencies (prior probabilities) of A, B, and C, respectively.

The recognition processor can be implemented such that it decides that a sample belongs to a given material (A, for example) if the "A" likelihood ratio for the sample is greater than some constant, K. Thus, if

$$\frac{D_A(e)}{D_B(e) + D_C(e)} \geqq K \qquad \text{(E-1)}$$

then the processor decides that the sample is material A. The value of the constant K in equation E-1 depends upon the estimated costs for false alarms and missed detections and upon the particular optimal decision criterion which is to be employed. For recognition of various crops, a value of unity has been used for K. In this case, the identified material must have a point density at point e of at least 50% of the total point density for all materials at e.

In order to implement equation E-1, it is necessary to generate mathematical expressions which accurately describe $D_A(u_1, u_2)$, $D_B(u_1, u_2)$, and $D_C(u_1, u_2)$. It is assumed that these densities of points on the u_1, u_2 plane may be represented in terms of bivariate Gaussian probability density functions in this plane, if the latter are fitted to the measured statistical properties of actual data. Thus, if $f_A(u_1, u_2)$ is the bivariate Gaussian probability density function which represents the relative density distribution of points from material A in the u_1, u_2 plane (Fig. E-3), the actual density as a function of u_1 and u_2 will be given by

$$D_A(u_1, u_2) = P(A)f_A(u_1, u_2) \tag{E-2}$$

where P(A) is the probability of occurrence of material A in the scanned area. Similarly,

$$D_B(u_1, u_2) = P(B)f_B(u_1, u_2) \tag{E-3}$$

and

$$D_C(u_1, u_2) = P(C)f_C(u_1, u_2) \tag{E-4}$$

Substituting E-3, E-4, and E-5 into E-2 gives

$$\frac{D_A(e)}{D_B(e) + D_C(e)} = \frac{P(A)f_A(e)}{P(B)f_B(e) + P(C)f_C(e)} \geqq K \tag{E-5}$$

if point e is to be classified as belong to material A.

Inequality E-5 is the relationship which is implemented on the recognition processor. Instead of working on two bands, the processor can accept information from many channels and hence the recognition space is a multi-dimensional space instead of the two-dimensional plane shown in Figure E-3.

For processing signals from an unknown area, the probabilities of occurrence of the various materials (i.e., P(A), P(B), and P(C) in eq. E-5) must be estimated, since they are not known. Experience has shown, however, that these estimates can be very crude without

appreciably affecting the processor operation. In fact, the processor usually operates quite satisfactorily with P(A) = P(B) = P(C). Equal prior probabilities were assumed for the A. P. Hill processing.

Having determined which of many materials the unknown sample is most like, the question still remains whether the sample is to be classified as that material. It is possible that although the inequality E-5 for that material was satisfied, the magnitude of the probability density function at point "e" was extremely small. This indicates that the sample at "e" might better be classified as not belonging to any material whose probability distribution functions was included in the classification. Therefore, the final classification or lack of classification of a sample is based on its existence within a fixed region of the probability distribution function. This region is very often denied as that region which includes 99.9% of the points in the distribution function.

APPENDIX F

SUPERVISED MULTISPECTRAL CLASSIFICATION

The supervised multispectral classification was performed using standard algorithms and equipment available in ERIM's Earth Resources Data Center. A maximum likelihood recognition algorithm (see Appendix E) was utilized on a DEC PDP 11/70 computer. Selected runs of A. P. Hill data representing the best spatial resolution (1.6 ft) and nadir viewing conditions were processed. The methodology and results of the signature training and subsequent classification are described in the following sections.

F.1 SIGNATURE TRAINING

Training sets were selected by identifying the four corners of a quadrilateral which defined each target and background area to be used for training. The training areas used in this study are documented in Tables F-1, F-2, and F-3 for the 0930, 1330, and 2330 flight times, respectively. These tables show the coordinates of the corners that define the training set region, the name provided each training set and the number of picture elements (pixels) in each training set. The "X" coordinate is the pixel number location, whereas the "Y" coordinate is the scan line number location within the various data bases. The vehicle notation refers to the target location numbers defined for the A. P. Hill test site rather than to a specific target or vehicle. It was originally planned that the data gathered at 1830 be processed as well. However, because of limited target contrast for this data base, the targets could not be dependably located and this data set could not be included in the processing.

The mean signal values and covariance statistics were established for the targets and backgrounds selected for training. Tables F-4, F-5, and F-6 show the statistical characteristics of each training signature for the 0930, 1330, and 2330 hours data bases, respectively. For the 2330 data only Channels 4 and 5 (the two thermal channels) have

TABLE F-1. COORDINATE DEFINITION FOR TRAINING SETS FOR RUN 5, 0930 HOURS DATA BASE

DN	GN	COLOR	NOB	X1	Y1	X2	Y2	X3	Y3	X4	Y4	NAME
0	0	000										
1	1	070	113	558	337	566	344	567	350	547	341	TREES 1
2	2	700	36	529	336	534	336	534	346	529	346	VEHICLE
3	3	040	135	586	281	597	288	595	298	575	285	TREES 2
4	4	700	27	602	350	610	349	614	351	605	358	VEHICLE2
5	5	700	33	604	441	656	441	656	445	644	445	VEHICLE1
6	6	700	18	612	529	615	520	616	527	611	527	VEHICLE10
7	7	000	8	530	480	538	489	541	484	536	484	VEHICLE7
8	8	700	15	625	581	631	579	633	583	628	585	VEHICLE12
9	9	777	120	653	340	665	340	668	351	652	350	SOIL
10	10	000	10	602	240	606	241	604	248	601	247	VEHICLE3
11	11	474	90	616	256	624	261	609	269	605	262	FOREST

$X_{(i)}$ Pixel Number of i^{th} Corner

$T_{(i)}$ Scan Line of i^{th} Corner

NOB Number of Pixels*Scan lines in Training Set

TABLE F-2. COORDINATE DEFINITION FOR TRAINING SETS FOR RUN 5, 1330 HOURS DATA BASE

DN	GN	COLOR	NOB	X1	Y1	X2	Y2	X3	Y3	X4	Y4	NAME
0	0	000										
1	1	777	336	658	476	673	476	673	501	658	501	SOIL 1
2	2	777	294	640	544	655	544	655	566	640	566	SOIL 2
3	3	000	88	567	474	572	475	567	496	561	494	TREES 1
4	4	070	159	498	305	503	305	516	321	498	322	TREES 2
5	5	444	82	462	347	467	343	476	356	467	359	SOIL 3
6	6	474	77	425	260	439	259	439	268	430	268	OPEN WOOD 1
7	7	474	69	444	243	450	236	456	251	449	251	OPEN WOOD 2
8	8	700	30	503	429	507	429	507	440	503	440	VEHICLE7
9	9	700	20	452	340	455	336	461	343	458	345	VEHICLE5
10	10	700	12	450	386	460	386	458	389	452	389	VEHICLE6
11	11	700	16	608	385	613	385	613	390	608	390	VEHICLE1
12	12	700	24	487	274	491	274	492	282	487	282	VEHICLE4
13	13	700	8	522	186	528	185	528	190	522	191	VEHICLE3

$X_{(i)}$ Pixel Number of i^{th} Corner

$T_{(i)}$ Scan Line of i^{th} Corner

NOB Number of Pixels*Scan Lines in Training Set

TABLE F-3. COORDINATE DEFINITION FOR TRAINING SETS FOR RUN 5, 2330 HOURS DATA BASE

DN	GN	COLOR	NOB	X1	Y1	X2	Y2	X3	Y3	X4	Y4	NAME
0	0	000										
1	1	777	217	597	764	608	764	605	790	597	792	SOIL 1
2	2	070	179	502	751	513	749	524	764	513	769	TREES
3	3	777	141	511	684	520	684	533	697	527	704	SOIL 2
4	4	777	141	547	747	556	747	569	760	563	767	SOIL 3
5	5	433	152	585	487	594	487	599	512	593	512	SOIL 4
6	6	700	19	415	411	419	415	416	420	412	417	VEHICLE4
7	7	700	23	536	573	540	577	535	581	532	576	VEHICLE1
8	8	700	23	524	737	528	742	522	745	519	740	VEHICLE11
9	9	040	98	350	558	360	553	370	562	361	566	WOODS

$X_{(i)}$ Pixel Number of i^{th} Corner

$T_{(i)}$ Scan Line of i^{th} Corner

NOB Number of Pixels*Scan Lines in Training Set

TABLE F-4. TRAINING SET STATISTICS FOR 0930 HOURS DATA BASE

TRAINING SET	CHANNEL 1		CHANNEL 2		CHANNEL 3		CHANNEL 4		CHANNEL 5	
	μ	σ	μ	σ	μ	σ	μ	σ	μ	σ
Tree #1	89.7	7.5	60.2	2.6	61.8	15.0	59.9	2.6	85.5	1.9
Tree #2	48.4	4.0	57.0	3.0	51.1	15.9	47.6	2.7	74.3	2.6
Soil	122.9	8.9	120.3	6.8	107.7	17.7	103.4	3.8	103.1	3.3
Forest	52.2	5.5	61.9	3.9	58.8	17.3	67.0	1.8	89.9	1.3
Vehicle 1	63.0	6.6	76.6	6.8	93.2	24.6	107.1	18.8	150.4	11.2
Vehicle 2	55.2	7.0	65.2	4.5	81.1	11.8	91.7	16.7	103.6	9.8
Vehicle 3	59.5	6.9	63.5	3.4	60.4	9.7	111.9	10.9	117.9	7.9
Vehicle 4	128.1	5.0	111.1	4.0	116.7	26.3	184.9	15.6	159.9	16.1
Vehicle 7	77.4	5.0	84.9	2.2	113.8	19.5	116.0	13.8	150.4	7.9
Vehicle 10	59.6	6.4	64.8	2.3	76.7	15.4	117.9	12.4	119.1	9.4
Vehicle 12	66.1	10.2	71.6	7.1	93.9	15.9	55.7	4.4	79.8	3.1

TABLE F-5. TRAINING SET STATISTICS FOR 1330 HOURS DATA BASE

TRAINING SET	CHANNEL 1		CHANNEL 2		CHANNEL 3		CHANNEL 4		CHANNEL 5	
	μ	σ	μ	σ	μ	σ	μ	σ	μ	σ
Soil #1			127.9	7.9	127.7	8.5	104.3	3.6	72.3	3.7
Soil #2			126.9	5.1	130.9	8.5	124.1	4.2	87.6	4.5
Soil #3			91.5	4.7	106.0	8.0	103.9	2.9	73.6	2.5
Trees #1			53.5	3.9	80.1	6.6	74.7	3.5	56.1	2.7
Trees #2			56.9	3.8	83.1	7.2	85.1	3.2	63.3	2.5
Open Wood 1			71.2	4.2	89.2	7.8	86.7	3.4	63.3	3.4
Open Wood 2			86.9	3.8	102.7	7.6	104.4	3.7	78.3	3.5
Vehicle 1			79.4	5.9	127.3	8.8	171.2	11.2	113.6	8.3
Vehicle 3			72.8	1.9	110.5	11.5	184.6	20.1	121.1	10.7
Vehicle 4			82.6	6.0	121.7	12.8	171.0	18.1	122.5	12.6
Vehicle 5			75.3	8.6	118.3	11.0	168.1	33.0	110.4	22.5
Vehicle 6			93.9	8.1	115.8	9.8	141.4	10.8	111.8	4.2
Vehicle 7			120.8	5.3	132.8	14.7	178.5	11.4	135.6	5.4

TABLE F-6. TRAINING SET STATISTICS FOR 2330 HOURS DATA BASE

TRAINING SET	CHANNEL 1		CHANNEL 2		CHANNEL 3		CHANNEL 4		CHANNEL 5	
	μ	σ	μ	σ	μ	σ	μ	σ	μ	σ
Soil #1							106.7	3.3	63.8	3.8
Soil #2							107.2	3.6	84.3	1.9
Soil #3							101.8	3.5	75.8	2.0
Soil #4							78.3	3.6	53.0	3.0
Trees							116.1	3.6	105.9	3.9
Woods							126.0	3.8	120.9	2.0
Vehicle 1							160.4	21.7	150.0	23.3
Vehicle 4							138.2	20.9	135.4	11.1
Vehicle 11							223.5	40.6	225.4	41.9

useful data since there was inadequate signal available in the other spectral regions. For the 0930 and 1330 data bases, all four infrared channels are available for consideration. The values in these tables are the raw scanner digital output values. Multispectral recognition using in-scene training does not require a calibrated data base. However, calibration information for these data bases has been developed and is available.*

Upon examining the signature statistics in Tables F-4, F-5, and F-6, two interesting points are noted. First, the largest separations begween the target classes and background classes occur for Channels 4 and 5, the thermal channels. Also, the variation in the signals attributed to the target classes are much larger than those associated with the backgrounds.

There are two factors that may account for this latter fact. The first has to do with the difficulty of accurately defining the training set area associated with each target. It is probable that considerable background signal contamination occurs within the target training sets. The second factor relates to the fact that the targets themselves exhibit considerable variation in radiance over their spatial extent. This leads to a large amount of variance in vehicle training signals, at least for the fairly high resolutions processed.

After the training process had been completed, an upper bound for potential classification accuracy was determined by using the training signatures to classify the training data itself. Tables F-7, F-8, and F-9 present the classification results for the 0930, 1330, and 2330 data bases, respectively. The tables show the percent of a specific training set's pixels that are classified as belonging to each signature class. For example, in Table F-7, training set 3 (Trees 2) is correctly

*Beard, J. L. and R. Horvath, "Sensor/Seeker Subsystems Modeling," Report No. 112900-64-F, Environmental Research Institute of Michigan, Ann Arbor [in publication] (CONFIDENTIAL).

TABLE F-7. TRAINING SET CLASSIFICATION RESULTS FOR 0930 HOURS DATA BASE

TNG SET NO.	PERCENT CATEGORIZED AS GROUP											
	0	1	2	3	4	5	6	7	8	9	10	11
1 Bkg.	0.	100.	0.	0.	0.	0.	0.	0.	0.	0.	0.	0.
2 Tar.	0.	0.	100.	0.	0.	0.	0.	0.	0.	0.	0.	0.
3 Bkg.	0.	0.	0.	98.	1.	0.	0.	0.	1.	0.	0.	0.
4 Tar.	0.	0.	0.	0.	96.	0.	0.	0.	0.	0.	0.	4.
5 Tar.	0.	0.	0.	0.	0.	94.	0.	6.	0.	0.	0.	0.
6 Tar.	0.	0.	0.	0.	6.	0.	83.	0.	0.	0.	11.	0.
7 Tar.	0.	0.	0.	0.	0.	0.	0.	100.	0.	0.	0.	0.
8 Tar.	0.	0.	0.	0.	0.	0.	0.	0.	100.	0.	0.	0.
9 Bkg.	0.	0.	0.	0.	0.	0.	0.	0.	0.	100.	0.	0.
10 Tar.	0.	0.	0.	0.	7.	0.	7.	0.	0.	0.	86.	0.
11 Bkg.	0.	0.	0.	0.	1.	0.	0.	0.	0.	0.	0.	99.

TABLE F-8. TRAINING SET CLASSIFICATION RESULTS FOR 1330 HOURS DATA BASE

TNG SET	PERCENT CATEGORIZED AS GROUP													
	0	1	2	3	4	5	6	7	8	9	10	11	12	13
1 Bkg.	0.	92.	0.	0.	0.	1.	0.	0.	0.	0.	0.	0.	0.	0.
2	0.	0.	100.	0.	0.	0.	0.	0.	0.	0.	0.	0.	0.	0.
3	0.	0.	0.	95.	5.	0.	0.	0.	0.	0.	0.	0.	0.	0.
4	0.	0.	0.	3.	95.	0.	3.	0.	0.	0.	0.	0.	0.	0.
5	0.	0.	0.	0.	0.	98.	0.	2.	0.	0.	0.	0.	0.	0.
6	0.	0.	0.	0.	1.	0.	99.	0.	0.	0.	0.	0.	0.	0.
7	0.	0.	0.	0.	0.	14.	0.	86.	0.	0.	0.	0.	0.	0.
8	0.	0.	0.	0.	0.	0.	0.	0.	100.	0.	0.	0.	0.	0.
9	0.	0.	0.	0.	0.	0.	0.	0.	0.	75.	0.	10.	5.	10.
10	0.	0.	0.	0.	0.	0.	0.	0.	0.	0.	100.	0.	0.	0.
11	0.	0.	0.	0.	0.	0.	0.	0.	0.	0.	0.	100.	0.	0.
12	0.	0.	0.	0.	0.	0.	0.	0.	0.	8.	0.	12.	67.	12.
13	0.	0.	0.	0.	0.	0.	0.	0.	0.	0.	0.	0.	0.	100.

TABLE F-9. TRAINING SET CLASSIFICATION RESULTS FOR 2330 DATA BASE

TNG	PERCENT CATEGORIZED AS GROUP									
SET	0	1	2	3	4	5	6	7	8	9
1 Bkg.	0.	100.	0.	0.	0.	0.	0.	0.	0.	0.
2 Bkg.	0.	0.	100.	0.	0.	0.	0.	0.	0.	0.
3 Bkg.	0.	0.	0.	99.	1.	0.	0.	0.	0.	0.
4 Bkg.	0.	0.	0.	1.	99.	0.	0.	0.	0.	0.
5 Bkg.	0.	0.	0.	0.	0.	100.	0.	0.	0.	0.
6 Tar.	0.	0.	0.	0.	0.	0.	84.	11.	0.	5.
7 Tar.	0.	0.	0.	0.	0.	0.	40.	55.	0.	5.
8 Tar.	0.	0.	0.	0.	0.	0.	13.	9.	78.	0.
9 Bkg.	0.	0.	0.	0.	0.	0.	0.	0.	0.	100.

classified 98% of the time as training set 3, 1% of the time it is classified as either training set 4 (Vehicle 2) or training set 8 (Vehicle 12). In other words, the tables provide the probability of correct classification and false alarm rates within the training sets themselves. These data show that the training signatures are fairly distinct. For this set of data, the maximum confusion rate between targets and background is 5% and occurs for the 2330 hours data. An error rate of 5% represents one target pixel being misclassified as a background pixel.

F.2 SCENE CLASSIFICATION

The next step in the processing was to apply the training signatures from a particular run to the entire data base for that same run in order to determine the performance of this multispectral technique in terms of both false alarms and detection. The results of these multispectral classifications are shown in Figures F-1, F-2, and F-3 for the 0930, 1330, and 2330 data bases, respectively. These figures are photographs of the display of the classification results.

In order to interpret these photos, one needs the information related to their generation. The associated color codes used for each classification are provided as a part of Tables F-1, F-2, and F-3 under the column labeled "COLOR". The three digits shown under this column are, respectively, the amount of red (first column), the amount of green (second column), and the amount of blue (third volumn) used in the false color presentation. For example in Table F-1, the training set labeled "Vehicle 4" has a color code 700. The display has seven levels of intensity for each color, thus 700 is bright red in the false color display.

For the most part, the vehicle training sets have been assigned a bright red color, trees are a shade of green, and soils are white. In the classification photos, pixels appearing as black are those which have been classified as not belonging to any of the training sets (i.e., they lay outside of the 99.9% probability contours of <u>all</u> signatures).

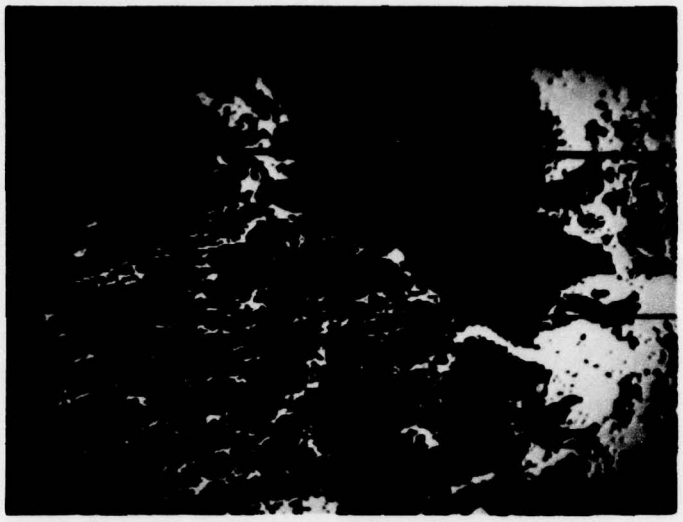

Code: Red = Vehicle Green = Woods White = Soil
Black = Everything Else

RE F-1. MULTISPECTRAL CLASSIFICATION RESULTS FOR 0930 HOURS DATA BASE

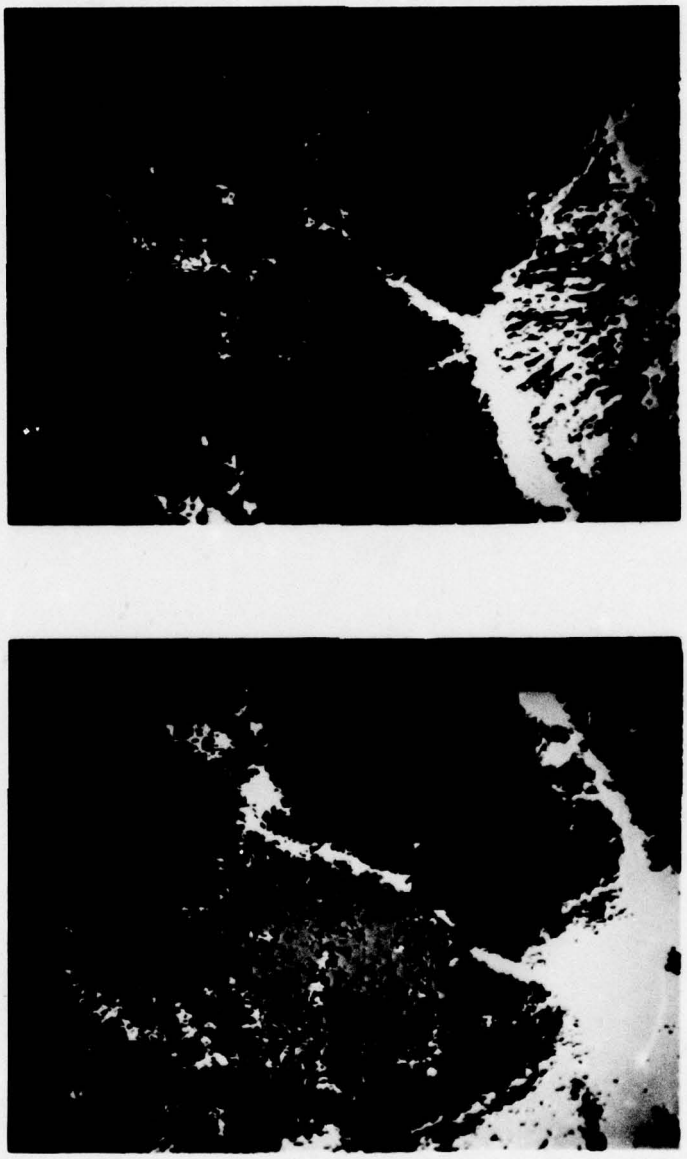

Code: Red = Vehicle Green = Woods White = Soil
Black = Everything Else

FIGURE F-2. MULTISPECTRAL CLASSIFICATION RESULTS FOR 1330 HOURS DATA BASE

Code: Red = Vehicle Green = Woods White = Soil
Black = Everything Else

FIGURE F-3. MULTISPECTRAL CLASSIFICATION RESULTS FOR 2330 HOURS DATA BASE

Upon examining Figure F-1, it is seen that seven vehicles are cued. However, there are a significant number of false alarms within the frame, especially within the wooded areas. This is explained by referring back to Table F-7, where it is shown that a misclassification occurred between the categories Forest, Vehicle 2, and Trees 2. For the most part, the false alarms that occurred did not have as large a spatial extent as the vehicles that were cued. Thus, a spatial filter could be used to eliminate some of the false alarms. There are, however, a number of false alarms that have spatial extents equivalent to the vehicles and as such would not be eliminated using a simple spatial filter. Even given such a capability for false alarm suppression, however, a significant detection problem still exists since only the seven vehicles used for training were identified.

For the 1330 hours data base (Fig. F-2), six vehicles were used for training. There were no misclassifications between vehicle and non-vehicle training sets (see Table F-8). However, again in this case only the trained targets were cued and in addition there were more large area false alarms produced than are apparent in the 0930 hours data base.

For the 2330 data base (Fig. F-3) where only 3 vehicles were used for training, 9 vehicles were cued. False alarms tended to be spatially small for this data base. The red lines that cross the images are a result of line drop outs in the original data base, thus, should be ignored when interpreting the results. It is also interesting to note that while the ambient M-60 tank (Position 12) was not used for training, it is one of the targets detected. Further, it should be noted that for this data base only the 4.5 to 5.5 and 8 to 14.0 μm bands are being used. Thus, for this data base, where the targets tend to be much hotter than the background, a two-channel hot spot detection performs quite well.

The results of this preliminary multispectral cueing study can be summarized as follows:

(1) The false alarm rate is high for the three data bases examined.

(2) For the 0930 and 2330 hours data bases, a spatial filter could significantly lower the false alarm rate.

(3) For the most part, only those targets which were included within the training set were detected (exception was the 2330 data base for which 9 targets were detected while only 3 were used for training).

APPENDIX G

UNSUPERVISED SPECTRAL/SPATIAL CLUSTERING

Unsupervised spectral/spatial clustering was performed using standard methodology and algorithms which have been developed by ERIM for earth resource and agricultural remote sensing applications. The basic approach consisted of three steps: 1) transformation of the original spectral channels into derived channels which (hopefully) more uniquely represent interpretable and stable information features of the scene; 2) unsupervised clustering of these features to produce "blobs" (i.e. contiguous localized groups of pixels exhibiting similar spectral characteristics); and 3) discrimination among blobs based upon their target-like size.

The methodology for implementing this approach was intentionally constrained to use only such information as might be anticipated a priori based upon physical principles, or which might be derived from a statistical treatment of the image data without knowledge of ground truth. Detailed methodology and results of application to the 1330 hours A.P. Hill data (Run 5) are presented in the following sections.

G.1 SPECTRAL FEATURE EXTRACTION

Four spectral bands were utilized in this procedure: 0.86 to 1.04 μm, 1.9 to 2.55 μm, 4.3 to 5.3 μm, and 8.4 to 13.7 μm. The 2.9 to 3.9 μm band was excluded because of noise problems previously cited (Section 3.5).

The two near-infrared spectral bands respond to a combination of solar illumination and object reflectance factors. The former factor is highly correlated between these bands (e.g. shadowing effects) while the latter factor may or may not be correlated, depending upon the material type of the particular objects being viewed. It was decided to transform these two bands into two derived spectral bands which would, as nearly as possible, isolate illumination effects (a clutter factor) from reflectance effects (an information factor).

Figure G-1 is a scatterplot of the near-infrared data values of 1548 pixels randomly selected from the scene. The values plotted indicate the number of pixels having the particular data value represented (a "+" equals one, an "x" ten or more). The data form a fan-shaped pattern whose apparent vertex, or origin, lies just off the scale at position (x,y = 45, 26). Physically, this origin corresponds to the zero radiance level in both channels. The radial distance of any data point from this origin is descriptive of its average albedo (average reflectance times local illumination for both spectral bands). For any given material, the effect of variable illumination (e.g. shadows) can be expected to produce data variability along such a radial. Conversely, materials whose spectral reflectance ratios for the two bands are different can be expected to lie along different radials (i.e. along different straight lines passing through the apparent origin at different angles). In order to isolate, as much as possible, the shadow effects (clutter) from the reflectance effects (information) the data values of the two near infrared bands, B1 and B2, were transformed to define two new data bands called "Albedo" and "Reflectance Ratio", vis.

$$\text{Albedo} = \left[(B1 - 26)^2 + (B2 - 45)^2\right]^{1/2}$$

$$\text{Reflectance Ratio} = 80*\arctan\left[(B1 - 26)/(B2 - 45)\right]$$

A scatter plot of the resulting transformed near infrared bands is shown in Figure G-2. It will be noted that most of the rather high degree of correlation seen in Figure G-1 is missing from Figure G-2, thus implying that we have at least approximately achieved our objective of isolating independent information effects by means of the transformation used.

Figure G-3 is a scatterplot of the thermal infrared spectral band data values for the same 1548 pixels previously used. A high degree of correlation is seen between these bands, as is to be expected based upon the dominance of target temperature in each. For the limited

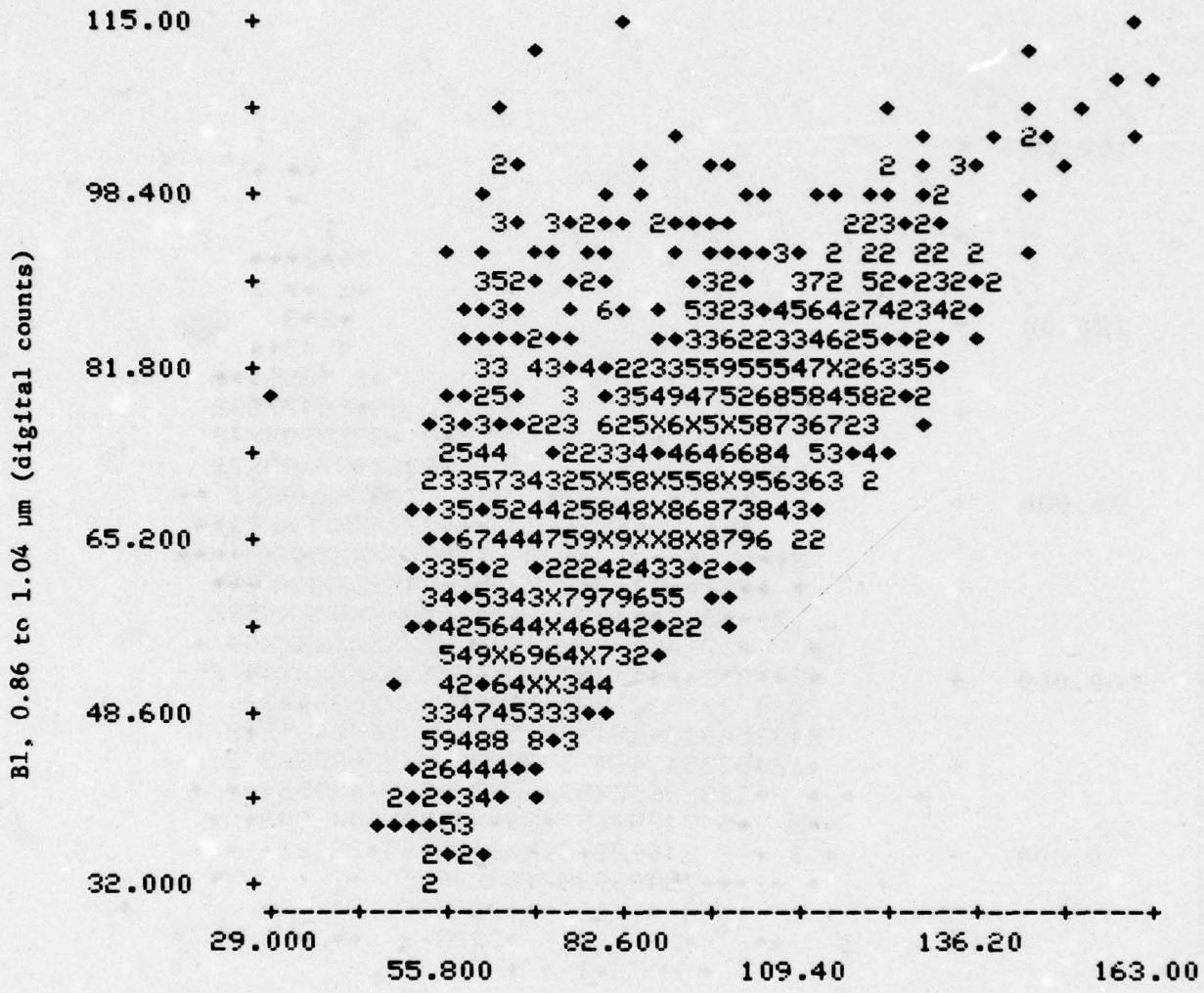

FIGURE G-1. SCATTERPLOT OF NEAR INFRARED SPECTRAL BANDS

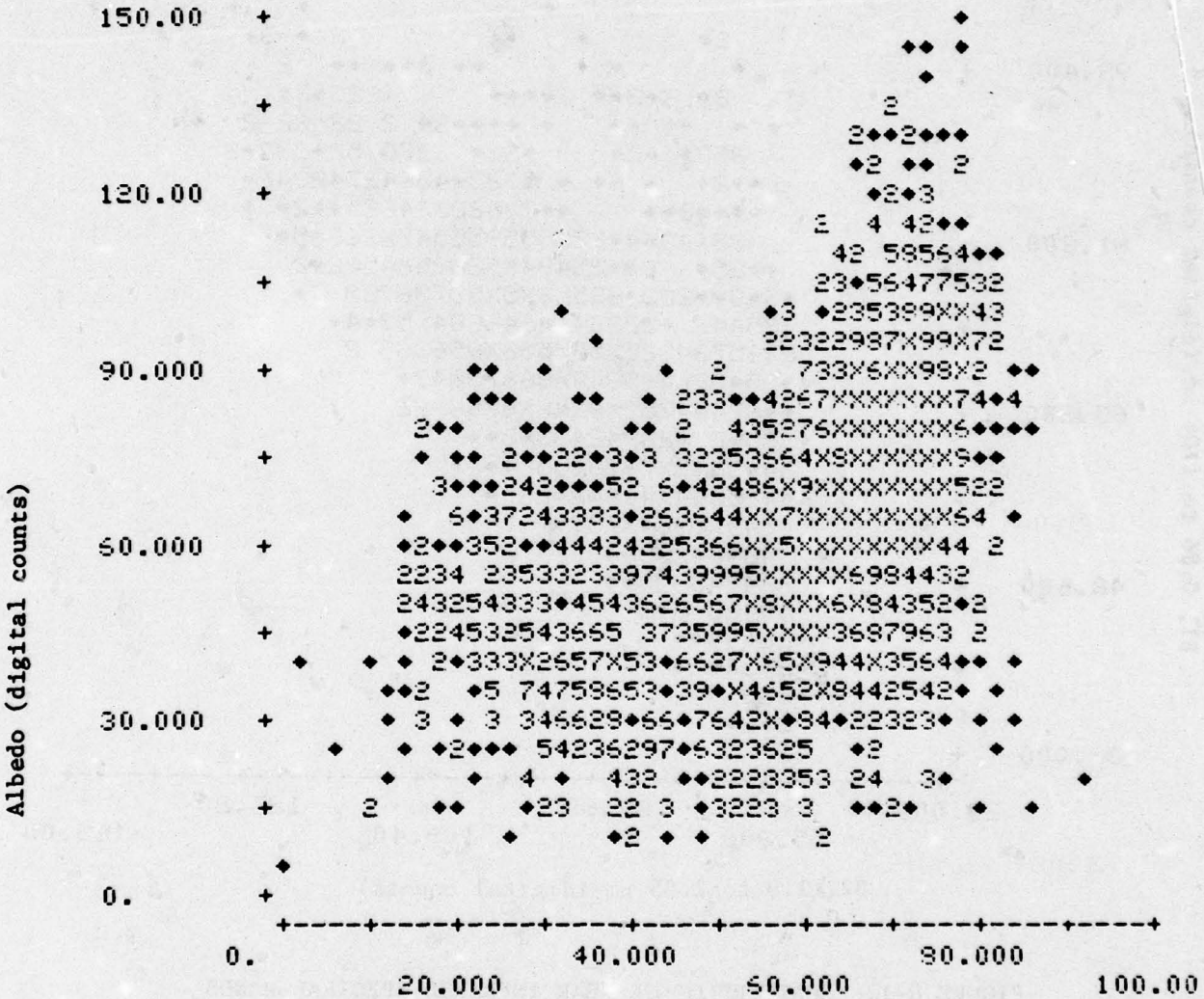

FIGURE G-2. SCATTERPLOT OF TRANSFORMED DATA CHANNELS DERIVED FROM NEAR INFRARED SPECTRAL BANDS

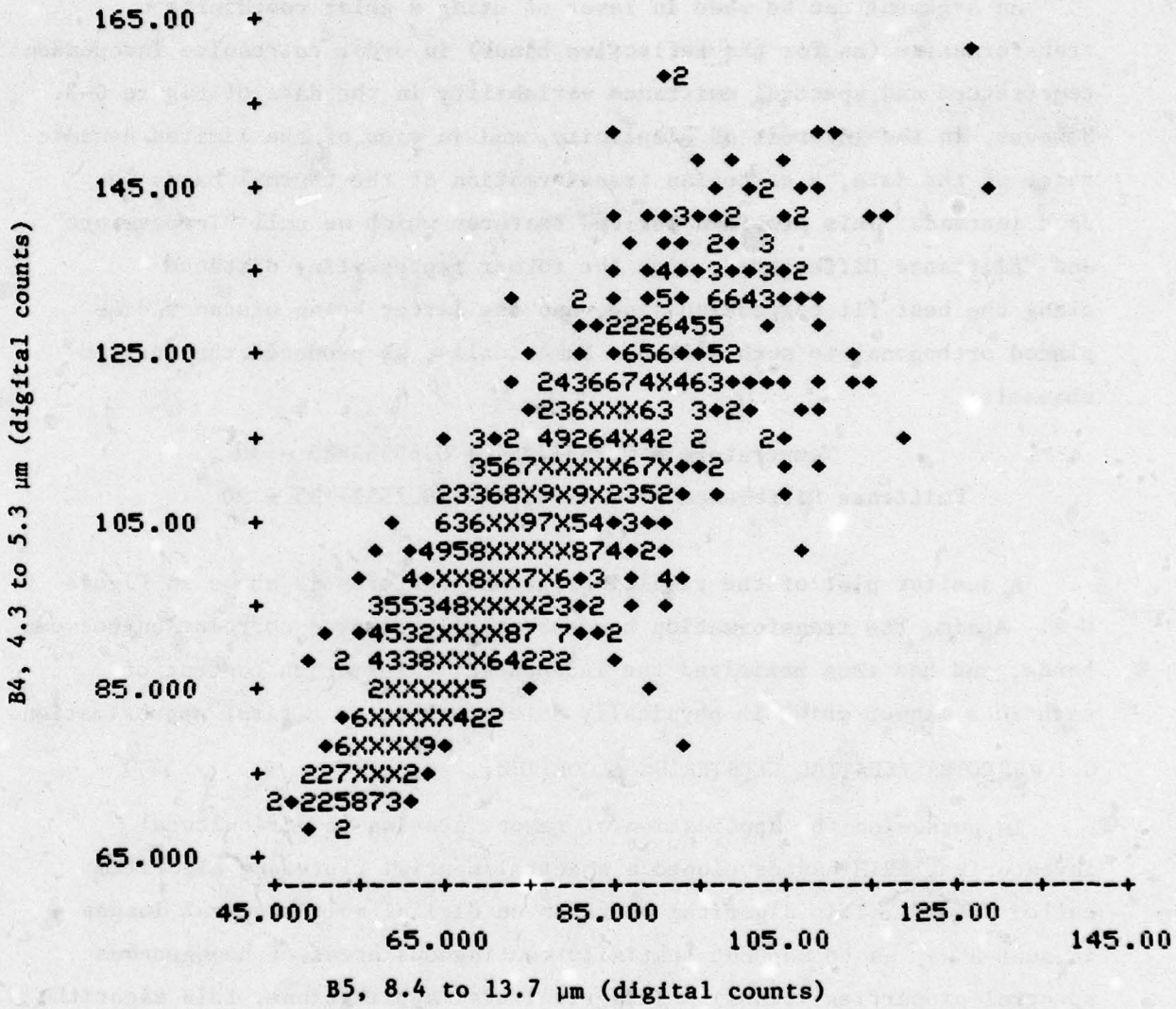

FIGURE G-3. SCATTERPLOT OF THERMAL INFRARED SPECTRAL BANDS

temperature range involved, the correlation present is essentially linear, with variations along the major axis of the distribution representing (substantially) temperature effects, and variations orthogonal to this representing spectral emittance differences between the two bands.

An argument can be made in favor of using a polar coordinate transformation (as for the reflective bands) in order to resolve independent temperature and spectral emittance variability in the data of Figure G-3. However, in the interest of simplicity, and in view of the limited dynamic range of the data, a cartesian transformation of the thermal bands was used instead. This provided derived features which we call "Temperature" and "Emittance Difference", with the former representing distance along the best fit regression line, and the latter being distance displaced orthogonal to such a line. Numerically, we produced the derived channels:

$$\text{Temperature} = 0.75517*B4 + 0.65553*B5 - 30$$
$$\text{Emittance Difference} = -0.65553*B4 + 0.75517*B5 + 90$$

A scatter plot of the resulting thermal features is shown in Figure G-4. Again, the transformation has essentially removed correlation between bands, and has thus maximized the independent information content of each in a manner which is physically interpretable to a first approximation.

G.2 SPECTRAL/SPATIAL CLUSTERING ALGORITHM

In pursueing the application of remote sensing to agricultural inventories, ERIM has developed a spectral/spatial clutering algorithm called "BLOB". This algorithm operates on digital multispectral images in such a way as to map out spatially continguous areas of homogeneous spectral properties (blobs). In agricultural applications, this algorithm is especially useful because the resultant blob structure defined very closely matches the actual agricultural field structure present in the image, thus allowing subsequent processing operations to deal with the mean spectral values of all pixels within a field rather than with each

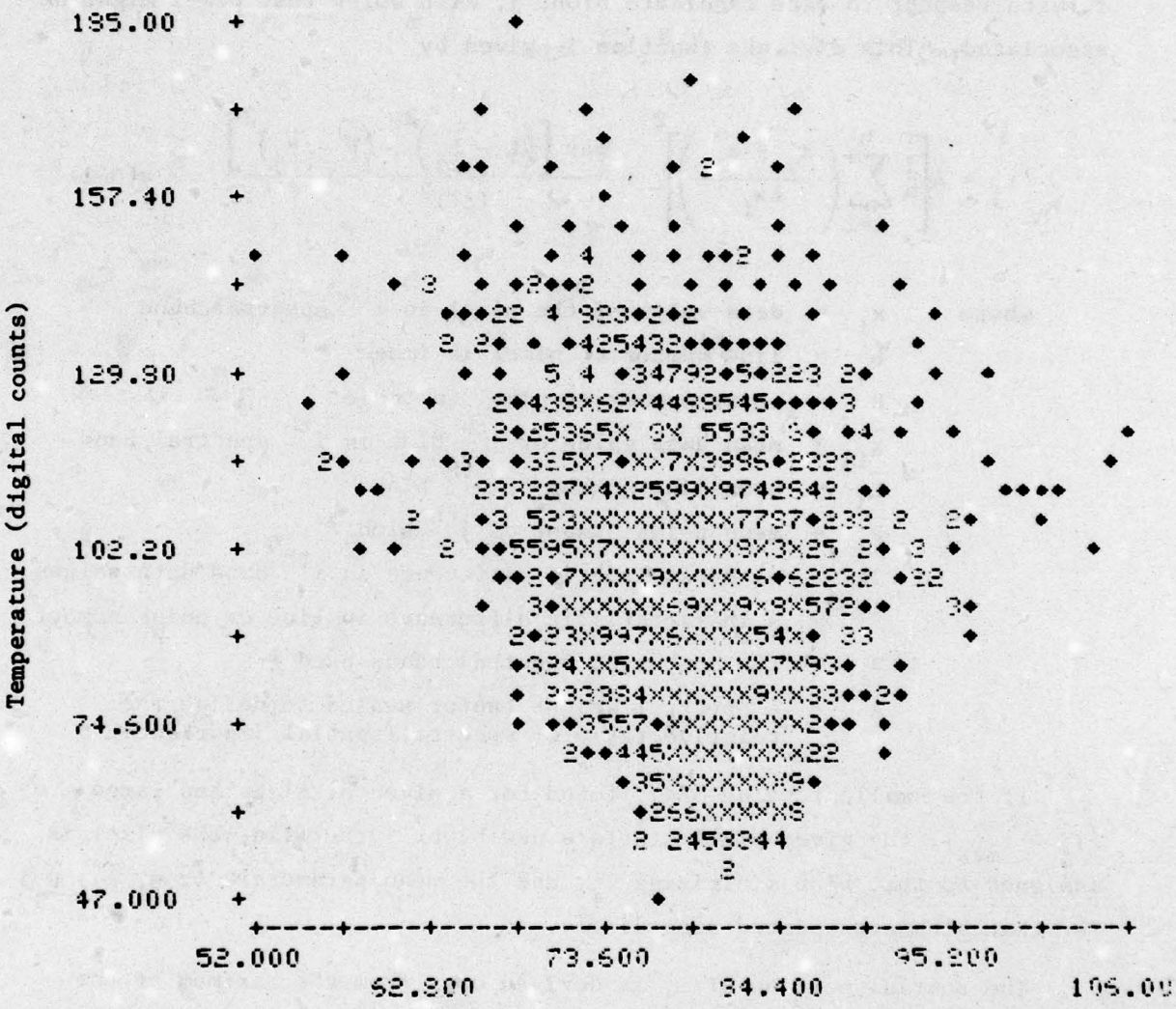

FIGURE G-4. SCATTERPLOT OF TRANSFORMED DATA CHANNELS DERIVED FROM THERMAL INFRARED SPECTRAL BANDS

pixel as an individual entity. This process has obvious benefit in terms of both precision (noise reduction in averaging) and data volume (one spectral vector per field rather than one per pixel).

Generically, BLOB computes, for a given pixel, a distance function, τ, with respect to each candidate blob, j, with which that pixel might be associated. This distance function is given by

$$\tau_j = A\left[\frac{1}{n}\sum_{i=1}^{n}\left(\frac{x_i - \bar{x}_{ij}}{\Delta x_i}\right)\right]^2 + \frac{\max\left[\left(L - \bar{L}_j\right)^2, \left(P - \bar{P}_j\right)^2\right]}{(\Delta \ell)^2} \qquad (G\text{-}1)$$

where
- x_i = data value of the pixel in i^{th} spectral band
- L = line number of pixel in image
- P = point number of pixel in image
- $\bar{x}_{ij}$ = mean data value of j^{th} blob in i^{th} spectral band
- $\bar{L}_j$ = mean line number of j^{th} blob
- $\bar{P}_j$ = mean point number of j^{th} blob
- Δx_i = a characteristic difference in i^{th} band data values
- $\Delta \ell$ = a characteristic difference in line or point number
- n = the number of spectral bands used
- A = a spectral weight factor scaled to define the relative ratio of spectral/spatial importance.

If the smallest value of τ_j found for a given pixel is too large $(\tau_j > \tau_{max})$, the given pixel starts a new blob. Otherwise, the pixel is assigned to that blob minimizing τ_j, and the mean parameters $(\bar{x}_{ij}, \bar{L}_j, \bar{P}_j)$ for that blob are updated accordingly.

The spatial portion of τ_j is derived only from the maximum of the line or point displacements from a blob center. This feature recognizes the expected orientation relationships between rectangular agricultural field boundaries and scan line directions in Landsat Multispectral Scanner (MSS) images, and tends to produce rectangular blobs.

Specific and detailed tailoring of the spectral/spatial clustering was beyond the scope of this investigation. However, a first order modification of parameter settings was implemented in order to reflect the investigative intent of the present work. It was felt that insight into the nature of multispectral signature characteristics of tactical targets would be achieved by addressing the following question:

- Is there any coherent spectral feature of a target which could separate it from its immediate background so as to produce a recognizable spatial shape?

The parameter settings for the BLOB algorithm were set in order to develop an understanding of the answer to this question.

G.2.1 Spectral Parameter Settings

The BLOB algorithm of Equation (G-1) is a total distance measure produced by adding a spectral distance function to a spatial distance function. If we ignore the latter term, we have a purely spectral clustering algorithm that joins together spectrally similar things no matter where in the image they occur. In such a situation, spectral similarity occurs if

$$\frac{1}{n}\sum_{i=1}^{n}\left(\frac{x_i - \bar{x}_{ij}}{\Delta x_i}\right) \leq \frac{\tau_{max}}{A} \qquad \text{(G-2)}$$

Since ratios are involved, we have some freedom is assigning values to the three parameters τ_{max}, A and Δx_i (x_i, $\bar{x}_{ij}$ and n are, of course, set by the data used). We arbitrarily set $\tau_{max} = 30.9$ for convenience since that is the value used in our agricultural applications. For similar reasons, we set Δx_i equal to 1/20 of the nominal data range in the i^{th} spectral channel (the nominal data range is that range of digital values between the 5% and 95% points on a cumulative histogram of the channel). It then remained to select a reasonable value for A.

If we rewrite Eq. (G-2) for a single spectral band (n = 1), insert the values for Δx and τ_{max} and rearrange, we have

$$\frac{x - \bar{x}_j}{\text{Data Range}} < \left(\frac{1}{20}\right)\left(\frac{30.9}{A}\right)^{1/2} \qquad \text{(G-3)}$$

$$< \frac{0.278}{\sqrt{A}}$$

If A = 1, then Eq. (G-3) indicates that a pixel will automatically be rejected from the cluster if its data value, x, differs from the cluster mean, $\bar{x}_j$, by more than the fraction 0.278 of the data dynamic range. This is a rather generous range for calling things "similar". Conversely, if A is made very large, then very small differences of $x - \bar{x}_j$ cause rejection and data noise can be the dominant feature driving the clustering. After some investigation, a value of A = 4 was chosen. This means that in the single channel rendition of Eq. (G-3), a difference from the cluster mean of $0.278/\sqrt{4} = 0.139$, or about one-seventh the dynamic range, will define "similarity". This is about a factor of four to six above the noise level of a typical spectral channel evaluated.

G.2.2 Spatial Parameter Settings

The primary purpose of the spatial portion of the clustering algorithm in this investigation was to prevent spectrally similar pixels which are widely separated spatially from being grouped into the same cluster. Otherwise, the hope of seeing a vehicle-shaped cluster would have been compromised. On the other hand, it was also necessary to choose the spatial parameters carefully so as not to inadvertantly carve up the image into vehicle-sized blobs in the absence of any spectrally defined boundaries.

Both of the above criteria were met by choosing the characteristic length, $\Delta\ell$, in Eq. (G-1) to be equal to 2.12 pixels (or lines). This means that, for the previously defined $\tau_{max} = 30.9$, the maximum half-width of a blob (i.e. the maximum halfwidth of the region over which spectrally similar pixels will be clustered together) is equal to

$$\text{max half width} = \Delta\ell\sqrt{\tau_{max}}$$
$$= 2.12\sqrt{30.9}$$
$$= 11.8 \text{ pixels (lines)}$$

At the data scale of 1.6 feet per pixel (line) this means that no cluster can be bigger than about 38 feet in length or width. Thus, if a vehicle has spectral features that are different from any background within 38 feet of it, it will be isolated out as a separate spatial entity. Conversely, over the spatial extent of a vehicle (half-length = 12 feet = 7.5 pixels) the maximum effect of the arbitrary spatial cut-off characteristic is no more than $\left(\frac{7.5}{2.12}\right)^2$, or 12.5 out of the total allowable $\tau_{max} = 30.9$. This leaves 30.9 - 12.5 = 18.4 units of our distance measure for spectral effects. Thus, over the area of even a large vehicle, the relative weighting of spectral information changes little, from a value of unity at the center, to a value of no less than $(18.4/30.9)^{1/2} = 0.77$ at the extreme edge of the vehicle.

In summary, the effective result of the spatial portion of the algorithm is to create a local neighborhood of less than 40 feet diameter in the vicinity of a target. If, within this neighborhood, the target has some internally consistent spectral signature which differs from that of the local backgrounds present, the BLOB spatial/spectral clustering algorithm will isolate a target shaped entity (blob) which may subsequently be recognized by its spatial features.

G.3 PROCESSING AND RESULTS

The BLOB spectral/spatial clustering algorithm was used with the derived spectral features defined in Section G.1 in order to assess the extent to which there exists a coherent spectral signature for a target vehicle which allows it to be isolated from its immediate background to produce a recognizable spatial shape. The derived spectral feature channels for the 1330 hours Camp A.P. Hill data were utilized in various combinations as shown in the test cases defined in Table G-1.

TABLE G-1. SPECTRAL/SPATIAL CLUSTERING CHANNEL COMBINATIONS

Test Case	Derived Spectral Feature Channels*
1	Albedo, Reflectance Ratio, Temperature, Emittance Difference
2	Reflectance Ratio, Temperature, Emittance Difference
3	Reflectance Ratio, Emittance Difference
4	Temperature, Emittance Difference
5	8.4 to 13.7 μm (original spectral channel)

*See Section G.1.

Test Case 1 used all of the derived spectral features available and represented the maximal use of all independent spectral information present in the original multispectral data. Test Case 2 dispensed with the albedo feature, thus providing for a first order elimination of the clutter effects caused by shadowing. Test Case 3 further eliminated temperature and thus used only those features associated most directly with the intrinsic optical properties of the scene materials present. Test Case 4 included only the independent thermal information features provided by the two thermal infrared spectral bands originally collected. Finally, Test Case 5 utilized only a single thermal infrared spectral band, one of the original spectral bands collected.

Spectral/spatial clustering was performed on the five test cases using the 1330 hours Camp A.P. Hill data base. Figure G-5 shows a small portion of an output map for one of the test cases. Each blob isolated is keyed by a different symbol combination. Since there are literally thousands of blobs produced in each test case, a map-like display is somewhat of a problem in terms of coding. We have not very effectively solved that problem, and any display more comprehensive than that of Figure G-5 rapidly becomes unintelligable in terms of presentation in a report such as this.

Analysis of the processed results was designed to proceed in four serial steps:

1) Determination of whether a target was isolated as a vehicle shaped blob;

2) If 1) was successful, definition of a spatial filtering algorithm/approach to cueing those blobs;

3) If 1) and 2) were successful, assessment of the number of non-target blobs also cued (false alarms);

and 4) If false alarms from 3) were substantial, investigation to determine whether additional false alarm rejection could be accomplished by some spectral selection criterion following spatial detection.

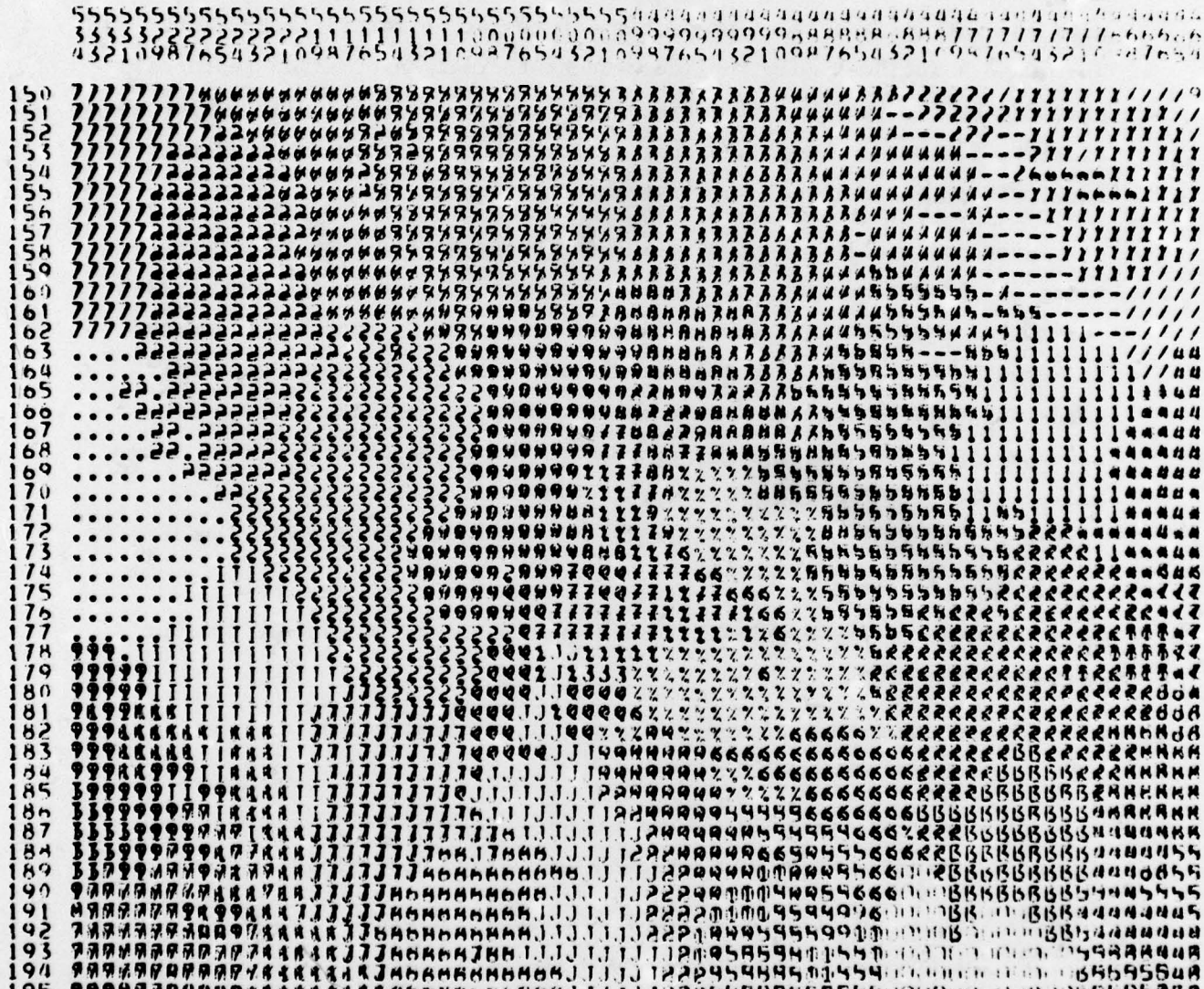

FIGURE G-5. EXAMPLE DISPLAY OF SPECTRAL/SPATIAL CLUSTERS, TEST CASE 1 INDIVIDUAL BLOB PIXELS ARE SYMBOL-KEYED

Unfortunately, the analysis results from Step 1 quickly highlighted the fact that serious problems existed in the basic concept that there might be something coherent about the spectral signatures within an individual target. In general, it was found that most of the targets present were actually represented by several very small blobs. Apparently, the within-target variance of all feature combinations tried was just too great in general to create a single major spatial feature possessing, by itself, any useful shape information.

Table G-2 provides a summary of the analysis results partitioned by test case and by target. Some exceptions to the general negative result can be seen. In particular, the 3/4 ton truck and the 5 ton truck generally were isolated out of their backgrounds by virtue of creating vehicle-sized rectangular blobs. On the other hand, one of the APC's and the 2-1/2 ton truck were never isolated from their immediate backgrounds, not even as a grouping of small blobs.

The results obtained do identify some relative utility to the derived spectral features utilized. The best results, both overall and for each target, were obtained in Test Case 2. This supports the original hypothesis by the shadowing effects represented by the albedo feature which was eliminated in Test Case 2. On the other hand, the worst results were found in Test Case 3. Apparently, there is not a large amount of discriminative power in the surface optical properties alone, at least as represented by the specific feature transformations used on the data set processed.

The implications of the results achieved are significant. We have taken one approach to transforming the raw spectral data into derived features which should be more stable, and certainly are more intuitively understandable. We have asked whether there is any uniformity of those features on a tactical target, under conditions where the term "uniformity" represents a rather substantial allowance for variance with respect to the dynamic range of the data. And we have found in general, and in every instance for armored vehicles, that the answer to that question, at least for this limited data set, is negative.

TABLE G-2. SPECTRAL/SPATIAL CLUSTERING RESULTS

Target	Location (Line/Point)	Spectral/Spatial Cases*				
		1	2	3	4	5
APC	187/443	P	P	P	P	P
2 1/2 T	228/481	-	-	-	-	-
M-60	303/414	P	P	-	-	-
M-60	343/511	P	P	-	P	P
3/4 T	388/513	P	✓	-	✓	✓
APC	406/422	-	?	-	-	-
5 T	435/463	✓	✓	✓	✓	✓
APC	445/430	-	-	-	-	-

Key: ✓ = vehicle shaped blob isolated
P = several small blobs isolated which add up to a ✓
- = target not isolated from background in any manner

*See Table G-1.

REFERENCES

[1] Stewart, Steve, MS Cueing Techniques Program, Mission Report for Night Vision Laboratory Program, Camp A.P. Hill Virginia Test Site, March 28, 29, 30, 1978, Environmental Research Institute of Michigan, Ann Arbor, Mi. Report No. 131500-8-P, May 1978.

[2] Spectral and Polarization Characteristics of Selected Targets and Backgrounds: Instrumentation and Measured Results 93.3-14.0 μm), D. Faulkner, R. Horvath, J.P. Ulrich, E. Work, Willow Run Laboratories, The University of Michigan, Technical Report No. AFAL-TR-71-199, August 1971.

[3] Handbook of Military Infrared Technology, William L. Wolfe, Editor, The University of Michigan, 1965, Sponsored by Office of Naval Research, Department of the Navy, Washington, D.C.

[4] M. Bair, et al., "Active Passive Cueing Techniques" (U), ERIM Report No. 112900-69-F, Air Force Avionics Laboratory, Contract No. F33615-75-C-1155, (In Publication June 1979) (SECRET).

[5] S. Sternberg, et al., "3D Target Classifier" (U), ERIM Report No. 126200-36-F, Air Force Avionics Laboratory, Contract No. F33615-77-C-1010 (In Publication June 1979) (CONFIDENTIAL)

[6] P.G. Hasell, Jr., et al., "Michigan Experimental Multispectral Mapping System, A Description of the M7 Airborne Sensor and Its Performance," Report No. 190900-10-T, Environmental Research Institute of Michigan, Ann Arbor, Michigan, January 1974.

[7] Hasell, P. G., and L. M. Larsen, "Calibration of an Airborne Multispectral Optical Sensor, Report 6400-137-T, Willow Run Laboratories, Institute of Science and Technology, The University of Michigan, Ann Arbor, Michigan, September 1968.

DISTRIBUTION LIST

W26P70 — 10
Night Vision Laboratory
USAECOM, DRSEL-NV-VI
Fort Belvoir, VA 22060

Defense Documentation Center — 14
ATTN: DDC-TCA
Cameron Station (Bldg 5)
Alexandria, VA 22314

Director — 1
National Security Agency
ATTN: TDL
Fort George G. Meade, MD 20755

Advanced Research Projects Agency — 1
1400 Wilson Blvd
Arlington, VA 22209

Commander, Naval Ship Systems Cmd — 1
Technical Library, Rm 3 S08
National Center No. 3
Washington, DC 20360

Department of the Navy — 1
Chief, Office of Naval Research
Washington, DC 20350

Director — 1
Naval Research Laboratory
Code 2627
Washington, DC 20390

Commander — 1
Naval Electronics Laboratory Ctr
ATTN: Library
San Diego, CA 92152

Commander — 1
U.S. Naval Ordnance Lab
ATTN: Technical Library
White Oak, Silver Spring, MD 20910

Commander — 2
Naval Electronic Systems Cmd Hq
ATTN: Code 0563
Washington, DC 20360

Commandant, Marine Corps — 1
Hq., U.S. Marine Corps
ATTN: Code A04C
Washington, DC 20380

Communications Electronics Div. — 1
Development Center
Marine Corps Dev & Educ Cmd
Quantico, VA 22134

Marine Corps Ln Officer — 1
Bay 2C214A, Hex Bldg
ATTN: John W. Everett
China Lake, CA 93555

Naval Weapons Center — 1
Code 5525
ATTN: Henry Blazak
China Lake, CA 93555

Rome Air Development Center — 1
ATTN: Documents Lib (TDLD)
Griffiss AFB, NY 13440

Hq. ESD (TRI) — 1
L.G. Hanscom Field
Bedford, MA 01730

Air Force Avionics Laboratory — 2
ATTN: AFAL/DOT, STINFO
Wright-Patterson AFB, OH 45433

Recon Central/RSA — 1
Air Force Avionics Laboratory
Wright-Patterson AFB, OH 45433

Air Force Avionics Laboratory — 1
ATTN: AVRO
Wright-Patterson AFB, OH 45433

Armament Dev & Test Center — 1
ATTN: SSLT
Eglin Air Force Base, FL 32542

Hq. Air Force Systems Cmd — 1
ATTN: DLTE
Andrews Air Force Base
Washington, DC 20331

Tactical Air Reconnaissance Ctr — 1
Army Liaison Office
Shaw AFB, SC 29152

HQDA (DAMI-ZA) — 2
Washington, DC 20310

Commander — 1
U.S. Army Training & Doctrine Cmd
ATTN: ATTS-X
Fort Monroe, VA 23651

HQDA (DACE-ED) — 1
Washington, DC 20314

Commander — 1
U.S. Army Training & Doctrine Cmd
ATTN: ATCD-SI
Fort Monroe, VA 23651

HQDA (DARD-DDC) 1
Washington, DC 20310

Commander
U.S. Army Training & Doctrine Cmd 1
ATTN: ATCD-C
Fort Monroe, VA 23651

HQDA (DARD-ARP/Dr. R. B. Watson) 1
Washington, DC 20315

Commanding General 1
U.S. Army Materiel Command
ATTN: AMCMA-EE
Washington, DC 20315

Commanding General 1
U.S. Army Materiel Command
ATTN: AMCRD-FW
Washington, DC 20315

Commander 1
U.S. Army Training & Doctrine Cmd
ATTN: ATCD-F
Fort Monroe, VA 23651

Commanding General 1
U.S. Army Materiel Command
ATTN: AMCRD-H
Washington, DC 20315

Commanding General 1
U.S. Army Missile Command
ATTN: AMCMI-RR, Dr. J.P. Hallowes
Redstone Arsenal, AL 35809

Commanding General 2
U.S. Army Missile Command
Redstone Scientific Info Center
ATTN: Chief, Document Sec
Redstone Arsenal, AL 35809

Commander 1
U.S. Army Training & Doctrine Cmd
ATTN: ATCE
Fort Monroe, VA 23651

Commanding General 1
U.S. Army Weapons Command
ATTN: AMSWE-REF
Rock Island, IL 61201

Commanding General 1
U.S. Army Weapons Command
ATTN: AMSWE-RER-L
Rock Island, IL 61201

Commander 1
U.S. Army Combined Arms Combat
Developments Activity
ATTN: ATCAIC
Fort Leavenworth, KS 66027

Commander 1
U.S. Army Training & Doctrine Cmd
ATTN: ATCD-CI
Fort Monroe, VA 23651

Commander 1
U.S. Army Logistics Center
ATTN: ATCL-MC
Fort Lee, VA 23801

Commandant 1
U.S. Army Ordnance School
ATTN: ATSOR-CTD
Aberdeen Proving Ground, MD 21005

Commander 1
U.S. Army Intelligence School
ATTN: ATSIT-CTD
Fort Huachuca, AZ 85613

Commandant 1
U.S. Army Field Artillery School
ATTN: ATSFA-CTD
Fort Sill, OK 73503

Commandant 1
U.S. Army Air Defense School
ATTN: ATSAD-CTD
Fort Bliss, TX 79916

Commandant 1
U.S. Army Engineer School
ATTN: ATSEN-CTD
Fort Belvoir, VA 22060

Commanding Officer 1
Harry Diamond Laboratories
ATTN: Library
Washington, DC 20438

CO, USA Foreign Science & Tech Ctr 2
ATTN: AMXST-ISI
220 Seventh St, NE
Charlottesville, VA 22901

CO, USA Foreign Science Div 1
ATTN: AMXST CE Division
220 Seventh St, NE
Charlottesville, VA 22901

CO, US Army Picatinny Arsenal 1
ATTN: SMUPA-VC5 (Mr. P. Kisatsky)
Bldg 350
Dover, NJ 07801

CO, US Army Picatinny Arsenal 2
ATTN: SMUPA-RT-S
Bldg 59
Dover, NJ 07801

Commanding Officer 1
Frankford Arsenal
ATTN: Library, H1300, B1.51-2
Philadelphia, PA 19137

Commanding Officer 1
Frankford Arsenal
ATTN: W1000-65-1 (Mr. Helfrich)
Philadelphia, PA 19137

Commanding Officer 1
Frankford Arsenal
ATTN: SMUFA-W-1000 (Mr. Kerensky)
Philadelphia, PA 19137

Commanding General 1
White Sands Missile Range
ATTN: STEWS-ID-S Hq
White Sands Missile Range, NM 88002

Commanding Officer 1
Edgewood Arsenal
ATTN: SMUEA-TSTI-TL
Edgewood Arsenal, MD 21010

Commanding Officer 1
U.S. Army Mtls & Mech Rsch Center
ATTN: AMXMR-ATL, Tech Lib Br
Watertown, MA 02172

President 1
U.S. Army Artillery Board
Fort Sill, OK 73503

Commanding Officer 1
Aberdeen Proving Ground
ATTN: STEAP-TL
Aberdeen Proving Ground, MD 21005

Commanding Officer 1
Aberdeen Proving Ground
ATTN: STEAP-MT-TF, Bldg 436
Aberdeen Proving Ground, MD 21005

Director, Ballistic Rsch Labs 1
U.S. Army Aberdeen R&D Center
ATTN: AMXRD-BTL (Mr. F. J. Allen)
Aberdeen Proving Ground, MD 21005

Commanding Officer 1
U.S. Army Ballistic Rsch Labs
ATTN: AMXRD-BSP (Dr. D. Reuyl)
Aberdeen Proving Ground, MD 21005

Commanding Officer 1
U.S. Army Land Warfare Lab
ATTN: CRDLWL-1A
Aberdeen Proving Ground, MD 21005

Commanding Officer 1
U.S. Army Limited Warfare Lab
ATTN: CRDLWL-7C
Aberdeen Proving Ground, MD 21005

Commanding Officer 1
U.S. Army Land Warfare Lab
ATTN: Mr. David Samuels
Aberdeen Proving Ground, MD 21005

Commanding Officer 2
U.S. Army Electronic Proving Grd
ATTN: STEEP-MT
Fort Huachuca, AZ 85613

Chief, USAECOM Field Engr Ofc 1
U.S. Army Electronic Proving Grd
ATTN: STEEP-LN-F (Mr. H.A. Ide)
Fort Huachuca, AZ 85613

Commanding Officer 1
USASA Test & Evaluation Center
Fort Huachuca, AZ 85613

U.S. Army Research Ofc-Durham 1
ATTN: CRDARD-IP
Box CM, Duke Station
Durham, NC 27706

U.S. Army Research Ofc-Durham 1
ATTN: Dr. Robert J. Lontz
Box CM, Duke Station
Durham, NC 27706

USA Security Agcy Combat Dev Act. 1
ATTN: IACDA-EW
Arlington Hall Station, Bldg 420
Arlington, VA 22212

Commandant 1
U.S. Army Air Defense School
ATTN: C&S Dep MSL Sci Div
Fort Bliss, TX 79916

Commander 1
U.S. Army Combined Arms Combat
Developments Activity
ATTN: ATCACC
Fort Leavenworth, KS 66027

Commanding Officer 1
U.S. Army Dugway Proving
Ground Lib
ATTN: STEDP-TL, Tech Lib
Dugway, UT 84022

Commanding Officer 1
U.S. Army Cold Regions R&E Lab
ATTN: CRREL-RP (Dr. Yin Chao Yen)
Hanover, NH 03755

Commanding Officer 1
Yuma Proving Ground
ATTN: STEYP-AD (Tech Lib)
Yuma, AZ 85364

Director 1
U.S. Army Advanced Mtl Concepts Agcy
ATTN: AMXAM
Washington, DC 20315

Commanding Officer 1
U.S. Army Materiel Command
ATTN: AMCRD-R (H. Cohen)
Washington, DC 20315

Commandant 1
U.S. Army Infantry School
ATTN: ATSIN-CTD
Fort Benning, GA 31905

Commander 1
U.S. Army Logistics Center
ATTN: ATCL-X
Aberdeen Proving Ground, MD 21005

Commandant 1
U.S. Army Armor School
ATTN: ATSAR-CTD
Fort Knox, KY 40121

Commandant 1
U.S. Army Aviation School
ATTN: ATSAV-CTD
Fort Rucker, AL 36360

Commandant 1
U.S. Army Institute for Mil Assistance
ATTN: ATSMA-CTD
Fort Bragg, NC 28307

Commandant 2
U.S. Army Field Artillery School
ATTN: Target Acquisition Dept
Fort Sill, OK 73503

Commanding General 1
U.S. Army Missile Command
ATTN: AMSMI-RFG (Mr. N. Bell)
Redstone Arsenal, AL 35809

Commanding Officer 1
Harry Diamond Laboratories
ATTN: AMXDO-RCB (Mr. J. Nemarich)
Washington, DC 20438

Commanding Officer 1
U.S. Army Systems Analysis Agcy
ATTN: AMSRD-AMB (Mr. A. Reid)
Aberdeen Proving Ground, MD 21005

Commanding Officer 1
Frankford Arsenal
Joint Laser Safety Team
ATTN: SMUFA-W1000
Philadelphia, PA 19137

Commanding General 1
Project MASSTER
Fort Hood, TX 76544

U.S. Army Liaison Office 1
MIT-Lincoln Lab, Rm A-210
P.O. Box 73
Lexington, MA 02173

Chief 1
Missile Electronic Warfare Tech Area
EW Lab, USA Electronics Command
White Sands Missile Range, NM 88002

CG, U.S. Army Electronics Cmd 1
ATTN: AMSEL-PP/P-IED
(Mr. C. Mogavero)
225 South 18th St
Philadelphia, PA 19103

Chief, Intelligence Materiel 1
Development Office
Electronic Warfare Lab,
USAECOM
Fort Holabird, MD 21219

Commanding General
U.S. Army Electronics Command
Fort Monmouth, NJ 07703
AMSEL-WL-D 1
AMSEL-NL-D 1
AMSEL-TL-D 1
AMSEL-VL-D 1
AMSEL-BL-D 1
AMSEL-CB 1
AMSEL-SI-CB 1
AMSEL-MA-MP 1
AMSEL-MS-TI 2
AMSEL-GG-TD 1
CSCS-FM 1
AMSEL-RD 1
TRADOC-LNO 1

Director
Night Vision Laboratory
Fort Belvoir, VA 22060
AMSEL-NV-D 1
AMSEL-NV-VI 1
AMSEL-NV-PA/RA 1

Commanding General 1
U.S. Army Strategic Communications
Command
ATTN: SCC-FM-D
Fort Huachuca, AZ 85613

Sylvania Electronic Systems 1
Western Division
ATTN: Tech Reports Library
P. O. Box 205
Mountain View, CA 94040

NASA Scientific & Tech Info Facility 2
ATTN: Acquisitions Br (S-AK/DL)
P. O. Box 33
College Park, MD 20740

Advisory Group on Electron Devices 2
ATTN: Secy, SP Gr on Optical Masers
201 Varick St
New York, NY 10014

Electronic Properties Info Ctr 1
Hughes Aircraft Company
Centinela and Teale Streets
Culver City, CA 90230

Remote Area Conflict Info Ctr 1
Battelle Memorial Institute
505 King Avenue
Columbus, OH 43201